Deciphering the effect of mutant *STUB1* on the heat shock response in SCAR16 patient-derived cells

Dissertation

Zur Erlangung des Grades eines
Doktors der Naturwissenschaften

der Mathematisch-Naturwissenschaftlichen Fakultät
und
der Medizinischen Fakultät
der Eberhard-Karls-Universität Tübingen

vorgelegt
von

Stefanie Alexandra Schuster
aus Baden-Baden, Deutschland

Februar 2020

Tag der mündlichen Prüfung:	20.05.2020
Dekan der Mathematisch-Naturwissenschaftlichen Fakultät:	Prof. Dr. Wolfgang Rosenstiel
Dekan der Medizinischen Fakultät:	Prof. Dr. Ingo Autenrieth
1. Berichterstatter:	Prof. Dr. Ludger Schöls
2. Berichterstatter:	Prof. Dr. Peter Heutink
Prüfungskommission:	Prof. Dr. Ludger Schöls
	Prof. Dr. Peter Heutink
	Prof. Dr. Tassula Proikas – Cezanne
	Prof. Dr. Stefan Liebau

I hereby declare that I have produced the work entitled 'Deciphering the effect of mutant *STUB1* on the heat shock response in SCAR16 patient-derived cells', submitted for the award of a doctorate, on my own (without external help), have used only the sources and aids indicated and have marked passages included from other works, whether verbatim or in content, as such. I swear upon oath that these statements are true and that I have not concealed anything. I am aware that making a false declaration under oath is punishable by a term of imprisonment of up to three years or by a fine.

Tübingen, _____ _____

Date Signature

TABLE OF CONTENTS

SUMMARY

CHIP, encoded by the gene *STUB1*, is a central component of cellular protein homeostasis. It acts as a co-chaperone of HSC/HSP70 and HSP90 to modulate their activity and as an E3 ligase, tagging chaperone-bound misfolded proteins with ubiquitin and thereby leading to their degradation. Mutations in *STUB1* cause the neurological disorder autosomal recessive cerebellar ataxia type 16 (SCAR16), characterized by atrophy of the cerebellum, brain stem and spinal cord, but patients also show widespread neurodegeneration with symptoms of epilepsy, cognitive impairment and hypogonadism.

CHIP$^{-/-}$ mice present with cerebellar atrophy manifesting in distinct motor but also cognitive impairment phenotypes and aging-induced cardiac hypertrophy. 20% of CHIP$^{-/-}$ mice die post-natally and 100% die upon thermal challenge. Furthermore, they present with decreased stress tolerance, increased oxidative damage and increased insoluble protein aggregate levels. *In vitro* data supports this line of evidence by showing a higher vulnerability to stress and an impaired heat shock response (HSR) in *STUB1*$^{-/-}$ cells.

To further understand the pathophysiology of SCAR16 and the effect of mutant *STUB1* on the HSR, we first analyzed HSR induction and recovery in patient-derived fibroblasts. In accordance with previously published results from mesodermal cell lines, we saw a trend towards lower nuclear HSF1 levels after heat shock in patient cells compared to control cells which translated into lower HSP transcript levels upon induction. Furthermore, we detected an impaired HSR recovery on protein level, indicated by remaining high levels of HSP70. Interestingly, mutant CHIP did not alter cell viability of fibroblasts upon prolonged heat stress, but a CHIP-independent high susceptibility of fibroblasts to heat-inducible cell death was observed in all lines.

As SCAR16 primarily affects the central nervous system, we next attempted to determine the relevance of CHIP in the HSR of cortical neurons. For this purpose and for ideal *in vitro* disease

modeling, we generated induced pluripotent stem cells from fibroblasts of 3 SCAR16 patients and 3 healthy controls. Furthermore, we generated a homozygous knockout by CRISPR/Cas9-mediated genome editing from one isogenic control line by dual cleavage of DNA and deletion of 155 base pairs, thereby generating a premature stop codon at amino acid position 99. The homozygous knockout state was verified on transcript and protein level. All generated iPSC lines were validated for genomic integrity by exclusion of plasmid integration, SNP array analysis, resequencing of the mutation site and STR analysis. To verify the pluripotency of iPSCs, we assessed the expression of pluripotency-related intra- and extracellular proteins and the transcript levels of pluripotency-related genes and examined the potential of iPSCs to spontaneously differentiate into cells of all three germ layers. The generated iPSCs of 3 SCAR16 patients, 3 healthy controls and the STUB1(-/-) line were differentiated into cortical neurons specific for layer V of the neocortex with high homogeneity of CTIP2/TUJ-positive cells. In contrast to our findings in patient-derived fibroblasts, we did not see any distinctive (dys)functional CHIP-related effect on HSF1 translocation from the cytoplasm to the nucleus upon heat shock, as shown by cellular fractionation analysis. Yet, we observed an increased HSR induction on transcript level that, surprisingly, did not translate into any changes on HSP70 protein level. However, unstressed neurons of both patients and controls already expressed high levels of HSP70 compared to fibroblasts. Analyzing cell viability of cortical neurons upon prolonged heat stress, we saw a surprising resistance of neurons to this stress stimulus compared to fibroblasts, again regardless of CHIP mutations.

To gain more insights into the effect of dysfunctional CHIP in cortical neurons, we next performed proteomic analysis and observed dysfunctional protein (re)folding and a higher basal oxidative stress level in patients.

Our results question the role of impaired HSR in SCAR16 neuropathology and highlight cell-specific differences of the HSR, emphasizing the need of careful selection of proper disease models.

SYNOPSIS

1. Rare neurological disorders

Cerebellar ataxias (CAs) and hereditary spastic paraplegias (HSPs) are rare neurological disorders with a prevalence of 1-5 or 1-10 per 100.000 individuals, respectively (Ruano *et al.*, 2014). Both are monogenic disorders with huge genetic heterogeneity: more than 100 genes have been identified to cause CAs and more than 80 for HSP with an autosomal dominant, recessive, X-linked and mitochondrial trait of inheritance in both diseases (Hedera, 2018; Bird, 2019).

Apart from genetic heterogeneity, CAs are also clinically diverse neurological disorders characterized by a loss of coordination (ataxia) leading to unsteadiness of gait and stance, impaired fine motor skills, slurred speech and diplopia due to cerebellar deficits. Apart from the cerebellum, degeneration may also occur in the brainstem, the corticospinal and spinocerebellar tracts as well as the dorsal columns of the spinal cord, the peripheral nerves but also the cerebral cortex. This extends the phenotypic spectrum to extracerebellar symptoms such as spasticity, weakness, sensory deficits or cortical symptoms like seizures and cognitive impairment. Some subtypes of CA affect other organs as well, leading to cataract, cardiomyopathy or hypogonadism. Age of onset ranges from childhood to adulthood (reviewed by Kuo, 2019; Manto *et al.*, 2019). Pathophysiological mechanisms involved in CAs include *inter alia* proteotoxicity, RNA toxicity, impaired bioenergetics, ion channel dysfunction and metabolic defects (reviewed by Klockgether *et al.*, 2019). Apart from a few metabolic CAs, no causative treatment is available so the current therapy is focused on physiotherapy, occupational therapy and speech therapy (reviewed by Kuo, 2019; Manto *et al.*, 2019).

Hereditary spastic paraplegia is characterized by the axonal degeneration of upper motor neurons with highly variable severity and age of onset, ranging from early childhood to late adulthood. Patients with pure HSP present with progressive lower limb spasticity and weakness leading to gait impairment while complicated forms can also include *inter alia* cognitive

impairment, optic atrophy, cerebellar ataxia, peripheral neuropathy or seizures. Pathophysiological mechanisms range from intracellular axonal trafficking defects and mitochondrial dysfunctions to impaired endoplasmic reticulum (ER) shaping and function and alterations of membrane shaping and trafficking (Blackstone *et al.*, 2011; Schule *et al.*, 2011; Lo Giudice *et al.*, 2014). With rare exceptions, treatment is also limited to physiotherapy and symptomatic reduction of muscle spasticity only (Schule *et al.*, 2016).

Both diseases share many symptoms and mechanisms: many complex forms of HSP also present with ataxia (e.g. SPG5, SPG7, SPG11, SPG46) and many ataxias go along with spasticity as well (e.g. ARSACS, SCA1, SCA3, SCA7)(reviewed by Manto *et al.*, 2019). Understanding the disease mechanisms is the key to finding a treatment or cure for the disease.

2. Disease modeling of neurological and neurodegenerative diseases

Studying neurological disorders remains a challenge due to the inaccessibility of the diseased brain for analysis. Patient-derived brain tissue can only be analyzed *post mortem* which poses problems with preservation of DNA, RNA, proteins and lipids but also precludes the study of the disease onset and the attributed early damages. To understand the pathology of these diseases therefore requires an appropriate disease model *in vitro* or *in vivo*. Both systems have their advantages and disadvantages.

While *in vitro* models allow faster data acquisition and easier reproducibility of results, they are often based on overexpression or knockdown of genes in immortalized cell lines which are cheap, readily accessible and easy to manipulate genetically. Those cell lines, though, are often derived from cancers and therefore contain numerous genomic aberrations and are usually highly proliferative which does not provide an adequate model for non-proliferating post-mitotic neurons. In addition to that, overexpression of pathogenic genes may lead to an artificial cell signaling. While primary cells isolated from rodents do show cell specificity, they are usually difficult to be maintained and expanded, limiting the accessibility and scalability. *In vivo* rodent

models in turn have the advantage of a complex multi-organ system with many conserved genes across species, but they usually fail to reproduce pathological findings of neurodegenerative diseases, rely on human protein overexpression and are very time- and resource-consuming, especially for drug screening. Although both approaches have contributed to elucidating key pathological mechanisms of diseases, findings can often not be translated to human situations (McGonigle *et al.*, 2014; Genc *et al.*, 2019). A human model organism of the diseased cell type might therefore help to decipher key pathological events of neurological disorders, allowing for target identification, drug screening and therapy development that can further be tested in other more complex systems. The basis for this new test system was provided by the first generation of induced pluripotent stem cells from somatic cells in 2006 (Takahashi *et al.*, 2006).

3. Induced pluripotent stem cells

Induced pluripotent stem cells (iPSCs) are characterized by two unique features that all stem cells retain: the capacity of self-renewal and the capability of differentiation into specialized cell types. iPSCs as the name implies are pluripotent *i.e.* they possess the ability to differentiate into all cells of the three germ layers opposed to totipotent (ability to differentiate into cells of the whole organism, including extra-embryonic tissues), multipotent (ability to differentiate into cells of one lineage) or oligopotent (ability to differentiate into few cell types) stem cells.

The first established protocol to generate iPSCs from somatic cells, a process named reprogramming, was published by Takahashi and Yamanaka (2006) and was awarded the Nobel Prize only six years later. They generated iPSCs from mouse embryonic and human adult fibroblasts by retroviral delivery of the four transcription factors OCT3/4, KLF4, SOX2 and c-MYC (Takahashi *et al.*, 2006; Takahashi *et al.*, 2007). OCT3/4 and SOX2 are transcription factors of the core transcriptional regulatory circuitry of pluripotency-related genes (Boyer *et al.*, 2005), KLF4 functions as both tumor suppressor and oncogene and improves the efficiency of reprogramming (Dang *et al.*, 2000; Takahashi *et al.*, 2006) and c-MYC acts as a proto-oncogene

and enhances proliferation and transformation (Dang *et al.*, 2006).

These 'first generation' iPSCs resembled embryonic stem cells (ESCs) in morphology, proliferation and differentiation capacities. However, retroviral (as well as lentiviral) delivery of the transcription factors led to frequent integration into the host DNA, to silencing of some endogenous genes while other exogenous copies were not completely silenced or to carcinogenic action upon reactivation (c-MYC)(Takahashi *et al.*, 2006; Okita *et al.*, 2011). Furthermore, it was soon detected that these first iPSCs were only partially reprogrammed (Okita *et al.*, 2007). This caused a flood of improved protocols for reprogramming in an integration-free system, ranging from adenoviral and episomal plasmid delivery to piggyback transposition, Cre-recombinase excisable viruses, direct delivery of proteins and synthetically modified mRNAs (reviewed by Malik *et al.*, 2013). Furthermore, replacing c-MYC by its non-carcinogenic variant l-MYC or replacing both KLF4 and c-MYC by NANOG and LIN28 enhanced safety and efficiency (Yu *et al.*, 2007; Viswanathan *et al.*, 2008; Nakagawa *et al.*, 2010). NANOG is a transcription factor of the core transcriptional regulatory circuitry of pluripotency-related genes, while LIN28 is an mRNA binding protein that blocks microRNA-mediated differentiation of ESCs, promoting proliferation and accelerated iPSC formation (Yu *et al.*, 2007; Viswanathan *et al.*, 2008; Hanna *et al.*, 2009). Others have shown that efficiency can be increased by enhancers of epigenetic remodeling like sodium butyrate or valproic acid (Huangfu *et al.*, 2008; Mali *et al.*, 2010).

Upon successful generation, clonal expansion and selection of iPSCs, genomic integrity and pluripotency needs to be verified before continuing with further analysis. For this purpose, we excluded chromosomal aberrations that might have occurred during reprogramming, verified the presence of the reported mutation in the patient's original fibroblast and generated iPSC line and checked the non-integration of plasmids. Furthermore, to verify pluripotency, the expression of 1) alkaline phosphatase and 2) the transcription factors OCT3/4 and TRA1-81 was shown, 3) pluripotency-related transcript expression in a pattern similar to human embryonic stem cells (hESCs) and distinct to the original fibroblasts was verified and finally, 4) iPSCs were

shown to differentiate into cells of the three germ layers endoderm, mesoderm and ectoderm **(Schuster *et al.*, 2018,** Fig. 1). While the latter was assessed earlier by injecting iPSCs into immunodeficient mice and analyzing the developing teratomas (Yamanaka *et al.*, 2006), it is now sufficient to test the pluripotency of iPSCs via an embryoid body-based differentiation using defined media, a method initially described by Doetschman and colleagues for human embryonic stem cells (1985).

Up to now, iPSCs for rodents and humans were generated from a range of somatic cell types from blood, liver, stomach, pancreas, brain, intestine and adrenal glands, but the most frequently used cell types are fibroblasts, PBMCs and keratinocytes due to their easy accessibility (reviewed by Stadtfeld *et al.*, 2010). iPSCs allow many applications in the fields of drug development, disease modeling and tissue repair, due to their easy clonal expansion, the advantage of endogenous protein levels with the host's genetic background and the potential to generate all cell types of the human body. These characteristics also qualify iPSCs as an ideal tool for modeling neurological disorders, with various differentiation protocols available that allow the generation of a defined cell type of interest, like specific neurons or astrocytes (Fig. 1).

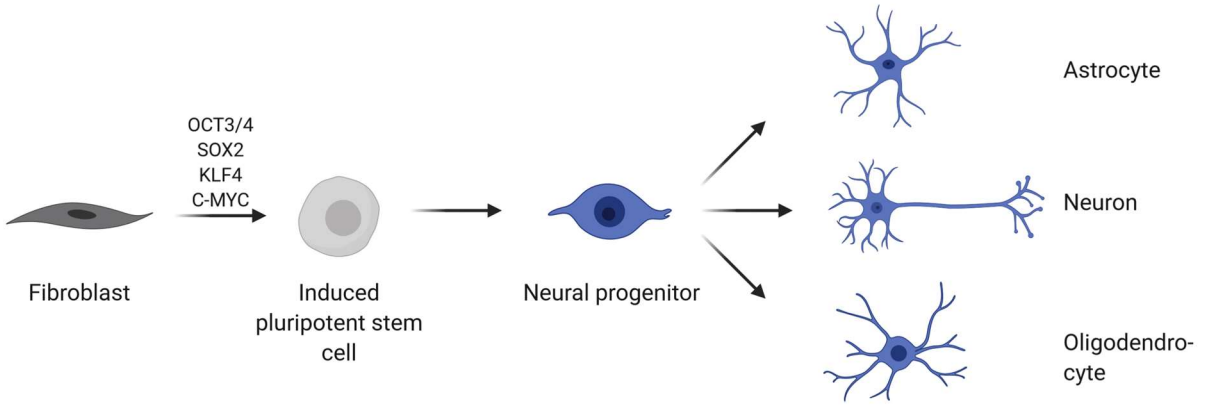

FIG. 1 | Generation of *in vitro* models for neurological disease modeling. Somatic cells such as fibroblasts from a patient or a healthy control can be reprogrammed to induced pluripotent stem cells (iPSCs) by the addition of the 4 Yamanaka factors OCT3/4, SOX2, KLF4 and C-MYC. iPSCs can be differentiated into neural progenitors, which in turn can be differentiated to cells of the astrocytic, neuronal or oligodendroglial lineage.

3.1 Neuronal differentiation

The mammalian neocortex consists of a six-layered structure with specialized cells with distinguishable morphological, neurochemical or electrophysiological properties in each layer. In general, all cortical cell types can be classified as either excitatory projection neurons or inhibitory interneurons. Intercortical connections are located in layer I to IV while neurons from layer V and VI signal to other brain areas.

Neuronal differentiation of stem cells (for both ESCs and iPSCs) recapitulates *in vivo* corticogenesis. First protocols for neuronal differentiation were based on the generation of free-floating embryoid bodies followed by adherent culture conditions with FGF2-guided differentiation into neural rosettes consisting of neuroepithelial cells (Zhang *et al.*, 2001; Koch *et al.*, 2009). Current methods usually utilize dual SMAD inhibition with the inhibitors noggin, dorsomorphin or LDN193189 together with SB431542 (Chambers *et al.*, 2009; Kim *et al.*, 2010). Noggin, dorsomorphin and LDN193189 all are potent BMP inhibitors, acting by blocking phosphorylation of SMAD1/5/8 and thereby preventing the transcription of pluripotency-associated genes (Chambers *et al.*, 2009; Kim *et al.*, 2010). SB431542 blocks phosphorylation of the TGFß1 receptors ALK4/5/7 and SMAD2/3, leading to TGFß/Activin/Nodal pathway inhibition which is crucial for pluripotency maintenance (James *et al.*, 2005; Smith *et al.*, 2008; Xu *et al.*, 2008). This dual inhibition increased the efficiency of neural induction to 80% $PAX6^+$ cells, an early neuronal marker, compared to ~10% only for administration of a single compound (Chambers *et al.*, 2009).

Telencephalic neural progenitors can further be differentiated via dorsal or ventral progenitors into excitatory projection neurons or inhibitory interneurons, respectively (Kim *et al.*, 2014a). The dorsal lineage is considered as the default pathway, but efficiency can be potentiated by retinoid signaling (Shi *et al.*, 2012). Upon prolonged differentiation for more mature neurons, cortical neurons can specifically be induced by MAPK and γ-secretase inhibition via DAPT and PD0325901, leading to complete loss of ventral neural progenitor-specific markers (Crawford *et*

al., 2007; Eiraku *et al.*, 2008). This induction can lead to the generation of both deep- and upper-layer cortical neurons at 7 or 10 weeks of differentiation, respectively, with the spatio-temporal separation reminiscent of *in vivo* corticogenesis (Eiraku *et al.*, 2008; Shi *et al.*, 2012). For other neuronal cell types, specific patterning factors are needed. Protocols are currently available for a wide range of neuronal cell types, including cholinergic neurons, cortical projection neurons, midbrain dopaminergic neurons, striatal neurons, spinal motor neurons, Purkinje cells and serotonergic neurons. More recently, differentiation protocols for astrocytes, oligodendrocytes and microglia were developed and optimized (reviewed by McComish *et al.*, 2018). For neurodegenerative disease modeling, the differentiation of iPSCs into candidate neural lineages is sometimes the key to recapitulating disease phenotypes.

Purkinje cells would be the cell type of choice to model cerebellar ataxias *in vitro*, but their large size, complex morphology, unique firing pattern and extensive maturation period renders them difficult to generate. The first iPSC-derived Purkinje cells required co-cultivation with human fetal cerebellar slices (Wang *et al.*, 2015). Needless to say, this impedes reproducibility in many laboratories around the world due to ethical constraints. An optimized and simplified protocol was published in 2018 that required extensive periods of cultivation and co-cultivation with mouse cerebellar progenitors (which did not work in the hands of Wang and colleagues (2015)), and still only yielded 10% Purkinje cells (Watson *et al.*, 2018). Furthermore, the very limited number of published protocols for Purkinje cell differentiation and the fact that protocols were not reproduced by other labs emphasizes the difficulty of generating Purkinje cells from iPSCs and highlights the need for reproducible and less complex protocols.

A great concern of all differentiation protocols still remains the low efficiency and the mentioned homogeneity of generated neurons. While dopaminergic neuronal protocols usually reach an efficiency of 10-30% of the desired cell type (Sanchez-Danes *et al.*, 2012) and lower motor neuron differentiation generates 50-55% of Islet1-positive cells but always includes astrocytes (Reinhardt *et al.*, 2013; Maury *et al.*, 2015), the protocol from Shi and colleagues (2012) to generate cortical

projection neurons of layer V and VI with slight modifications (Rehbach *et al.*, 2019) yielded 100% TUJ^+ and >75% cortical layer V marker $CTIP2^+$ cells in our hands. This homogeneity of cells was further highlighted by transcript expression analysis: we compared transcript data of cortical neurons of 2 control lines and 2 SCAR16 patients to transcript data of the BrainSpan atlas (http://www.brainspan.org) of the human developing brain, from fetal to 1 year of age postmortem tissue. The gene signature of all 4 generated cortical neurons was very similar, with the most significantly enriched co-expressed gene set being the neocortex and subcortex at post conception week (pcw) 12 to 21 and with the strongest correlation at pcw 16 **(Schuster *et al.*, in preparation,** Fig. 3**)**. This underlines the homogeneity of generated cortical neurons but also emphasizes an important aspect and a major drawback of iPSC-based disease modeling: generated cell types usually resemble prenatal fetal cells, which might render the modeling of neurodegenerative diseases, usually occuring late in life, more difficult.

However, while HSPs and SCAs are considered as neurodegenerative diseases, its causes are usually monogenic and therefore easier to analyze *in vitro*, compared to many sporadic forms of neurodegeneration. Furthermore, age of onset for many subtypes and many patients is already in early childhood. In addition to this, many forms of HSPs and SCAs are complex and not limited to one cell type, e.g. SCAR16 initially affects Purkinje cells with subsequent widespread neurodegeneration throughout the brain (Hayer *et al.*, 2017), indicating an effect of mutation that is less specific to one neuronal cell type. This led us to the selection of a protocol that is generating a homogenous class of neurons with an easy and less time-consuming differentiation protocol (as described above).

3.2 Disease modeling of neurodegenerative diseases using iPSC-derived neurons

The first iPSC lines from patients with neurodegeneration were described in 2008 (Dimos *et al.*, 2008), with more than 50 reports already being published in 2014 and numerous more thereafter,

including disease models of Alzheimer's disease (AD), Parkinson's disease (PD), amyotrophic lateral sclerosis (ALS), hereditary spastic paraplegias (HSPs) and spinocerebellar ataxias (SCAs) (reviewed by Hargus *et al.*, 2014). Many groups reported pathological changes in iPSC-derived neurons and even found treatment options. iPSC-derived neurons from AD patients showed an accumulation of Aß oligomers, leading to ER and oxidative stress which was reverted by docosahexaenoic acid treatment (Kondo *et al.*, 2013); iPSC-derived neurons from PD patients with *LRRK2* mutations showed mitochondrial deficits associated with increased cell vulnerability which could be rescued by coenyzyme Q(10), rapamycin or GW5074 administration (Cooper *et al.*, 2012). Another study analyzed neuromuscular junction-like structures from iPSCs of spinal muscular atrophy patients and they showed impaired clustering of acetylcholine receptors, which could be ameliorated by valproic acid and antisense oligonucleotide treatment (Yoshida *et al.*, 2015); and iPSC-derived neurons from ALS patients showed hypoexcitability, cytoplasmic FUS pathology and progressive axonal transport defects, all reverted by HDAC6 inhibition (Guo *et al.*, 2017). Diseases with monogenic causes like HSP or SCAs are ideal for disease modeling as there is a direct causal relationship between mutation and disease.

To analyze the fit of different cell types for disease modeling of motor neuron disorders (MNDs) like amyotrophic lateral sclerosis, hereditary spastic paraplegia, spinal muscular atrophy and other spasticity-related genes, we analyzed transcript expression of 168 disease-relevant genes in PBMCs, lymphoblasts, fibroblasts, iPSCs and iPSC-derived cortical neurons of 2 healthy controls (**Hauser *et al.*, in preparation**). We showed that as expected, transcript expression strongly varied between different cell types of the same donor but varied little between the same cell type of different donors. Of all analyzed genes, 30% were expressed highest in cortical neurons, 24% in fibroblasts, 16% in lymphoblasts, 13% in iPSCs and 8% in PBMCs, while 9% were not expressed in any of the analyzed cell types **(Hauser *et al.*, in preparation,** Fig. 3**)**. This indicates that blood analysis for many subtypes of the disease is not appropriate while cortical

neurons and fibroblasts stand out as better disease models. Interestingly, transcript levels of MND-related genes with highest expression in neurons were 3-fold higher than the average transcript levels of all 4 other cell lines (compared to approximately 2-fold for fibroblasts).

To be highlighted here are the two HSP-related genes *REEP1* and *SPAST* that show remarkably higher levels in cortical neurons compared to all other cell types, with a fold change of 200-20.000 for *REEP1* and 5-10 for *SPAST* (**Hauser *et al.*, in preparation,** Fig. 2, 4). Both genes are investigated in our lab; with generated iPSCs from SPG4 patients with mutations in *SPAST* (**Hauser *et al.*, 2016**), Rehbach and colleagues (2019) identified reduced neurite outgrowth, increased growth cones and axonal swellings in iPSC-derived neurons in a neuronal subtype-specific manner and with rescue by GW3965 treatment. Interestingly, axonal swellings are considered a pathological hallmark of HSP which further strengthens the usability of iPSC-derived neurons in neurological disease modeling.

Monogenic disorders are usually rare diseases with low incidence in the population. This limits tissue accessibility to study disease-relevant pathological changes *in vitro*. In addition to iPSCs, another technology highly enhanced the potential for proper disease modeling: genome editing by CRISPR/Cas9.

4. CRISPR/Cas9-mediated genome editing

Genome editing provides a tool for controlled inactivation or repair of a gene. This is often needed for proper disease modeling to either have a negative control of no remaining activity or to repair or insert mutations for an isogenic cell pair. Isogenic lines have the advantage of the identical genetic background with an exception of one particular gene which reduces the noise that is usually caused by varying genetic backgrounds. It thereby facilitates the detection of causative disturbances and the analysis of many large-scale methods like transcriptomics and proteomics.

In the past, the techniques of choice for DNA editing were based on zinc finger nucleases (ZFNs)

and transcription activator-like effector nucleases (TALENs), both relying on sequence-specific DNA-binding modules linked to non-specific DNA nucleases that cleave DNA (reviewed by Gaj *et al.*, 2013). The current method of choice for genome editing was first described in 2013 and is based on the system of Clustered Regularly Interspaced Short Palindromic Repeats (CRISPR) and CRISPR-associated protein (Cas)(Cong *et al.*, 2013; Mali *et al.*, 2013). CRISPR/Cas was discovered in eubacteria and archaea as a self-defense system that recognizes and destroys external DNA and RNA, thereby leading to acquired immunity against invading plasmids and viruses (Horvath *et al.*, 2010; Al-Attar *et al.*, 2011). The CRISPR/Cas system is divided into three types based on the classification system proposed by Makarova and colleagues (2011). The type II CRISPR/Cas9 system is best characterized and belongs to the adaptive immune system of *inter alia Staphylococcus pyogenes* (Sp). It consists of the SpCas9 (hereafter referred to as Cas9) nuclease and the non-coding RNAs CRISPR RNA (crRNA) and trans-activating RNA (tracrRNA). While the crRNA recognizes and binds to the target sequence, the tracrRNA interacts with the crRNA to guide the Cas9 protein to the target site, allowing for target-specific cleavage (Chylinski *et al.*, 2014)(Fig. 2). Binding is directed by protospacer-adjacent motifs (PAMs) which vary between CRISPR/Cas systems (Mojica *et al.*, 2009): Cas9 recognizes the bases 'NGG' where N refers to any nucleotide and cleaves 3 basepairs (bp) upstream of the PAM (Jinek *et al.*, 2012; Ran *et al.*, 2013b). This PAM sequence in the human genome is found every 8-12 bp, providing

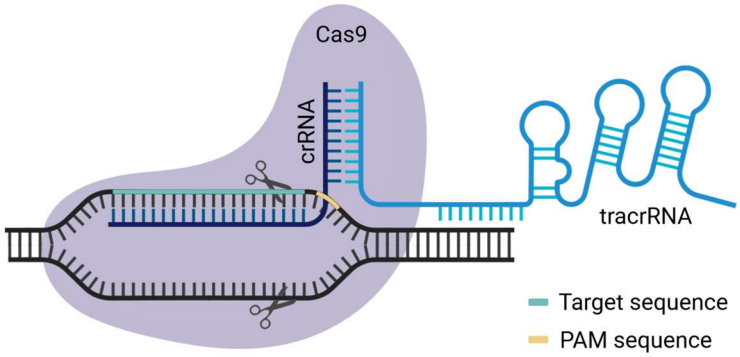

FIG. 2 | Components of CRISPR/Cas9 complex. CRISPR-RNA (crRNA) complementary to the target sequence together with a bound scaffolding trans-activating RNA (tracrRNA) directs Cas9 nuclease to the target site. The complex recognizes the protospacer-adjacent motif (PAM) sequence and cleaves DNA 3 basepairs upstream of the PAM, most frequently inducing a double-strand break. crRNA: CRISPR-RNA; tracrRNA: trans-activating RNA; PAM: protospacer-adjacent motif.

an accessible and global target for Cas9 (Ran *et al.*, 2013b). CRISPR/Cas9-mediated genome editing editing outplays previous genome editing techniques in terms of efficacy, simplicity and (Ran *et al.*, 2013b). CRISPR/Cas9-mediated genome editing outplays previous genome editing techniques in terms of efficacy, simplicity and multiplexing possibility. It involves designing crRNAs specific for the target site, transferring crRNAs, tracrRNAs and Cas9 to the cell and thereby inducing a site-specific double-strand break (DSB) that will be repaired by the host DNA repair system, leading to non-homologous end-joining (NHEJ) in most cases and homology-directed repair (HDR) on rare occasions. If NHEJ occurs, it frequently leads to arbitrary insertions or deletions (indels), usually shifting the open reading frame and thus resulting in a premature stop codon (Hefferin *et al.*, 2005). This repair mechanism is therefore of high interest for targeted gene disruption and generation of loss-of-function phenotypes. HDR events are rare but highly desired as the repair mechanism uses the homologous allele or an exogenous template like administered single-stranded oligodeoxynucleotides (ssODNs) to repair DSBs, allowing both single nucleotide changes and integration of whole exogenous sequences (van den Bosch *et al.*, 2002; Chen *et al.*, 2011; Ran *et al.*, 2013b).

Many protocols with slight modifications to enhance efficiency, stability and safety were published since the first discovery: efficiency and stability was improved by replacing the tracrRNA:crRNA duplex with a stable single guide RNA (sgRNA)(Jinek *et al.*, 2012); a nuclear localization sequence was integrated into Cas9 to enhance nuclear translocation (Cong *et al.*, 2013; Mali *et al.*, 2013); Cas9 nickases with mutations in specific domains were developed to only cleave one DNA strand (Ran *et al.*, 2013a; Murovec *et al.*, 2017); different delivery methods of sgRNA and Cas9 have been applied, ranging from plasmids, mRNA and protein to ribonucleoprotein (RNP) complexes; and the delivery of the complexes varied between electroporation, transfection or transduction (Liang *et al.*, 2015). Furthermore, a tracrRNA tagged with the fluorophore ATTO550 now allows for selection of cells with incorporated RNP complexes by fluorescence-activated cell sorting.

The major drawback of CRISPR/Cas9-mediated genome editing still remains the off-target effects, albeit occurring at a very low frequency only. Although cleavage at the target site is based on the complementarity of approximately 20 bp of the crRNA and the target sequence, a partial complementarity with mismatch pairings may lead to DNA cleavage at off-target sites. Several bioinformatical tools that are used for designing crRNAs predict possible off-target effects and calculate the likelihood of this cleavage based on the number, the position and the distribution of mismatches (Hsu *et al.*, 2013). SpCas9, for example, tolerates up to six mismatches at target sites (out of 18-24 nucleotides)(Jinek *et al.*, 2012).

Off-target cleavage is reduced by the delivery of RNP complexes (Kim *et al.*, 2014b; Liang *et al.*, 2015), by an inducible and therefore temporarily restricted expression of Cas9 (Cao *et al.*, 2016), a titrated dosage of Cas9 and sgRNA (Hsu *et al.*, 2013; Liang *et al.*, 2015) and most notably by Cas9 nickases (Ran *et al.*, 2013a; Cho *et al.*, 2014; Iyer *et al.*, 2015; Murovec *et al.*, 2017). Although the reduction in off-target frequency is sufficient for many *in vitro* disease models, it still renders *in vivo* applications for permanent gene correction in patients difficult.

For disease modeling, as mentioned above, an efficient method for gene is often desired. Chen and colleagues (2014) optimized the generation of knockouts by applying two sgRNAs for one gene for dual cleavage of the DNA and deletion of the DNA fragment in between the two cleavage sites. This has one major advantage: the successful cleavage can easily be detected and screened for with PCR product amplification and agarose gel electrophoresis.

For proper disease modeling of SCAR16, we generated a homozygous knockout of *STUB1* by designing two crRNAs for exon 2 and 3 followed by the formation of two crRNA-ATTO550-tracrRNA complexes and the formation of a ribonucleoprotein complex by adding Cas9 protein (see workflow in Fig. 3). We then harvested iPSCs and nucleofected them followed by fluorescence-activated cell sorting of ATTO550-positive cells, single cell seeding and manual picking of colonies. DNA of those clones was isolated, amplified by PCR, tested on gel electrophoresis and verified by Sanger sequencing for homozygous and heterozygous clones.

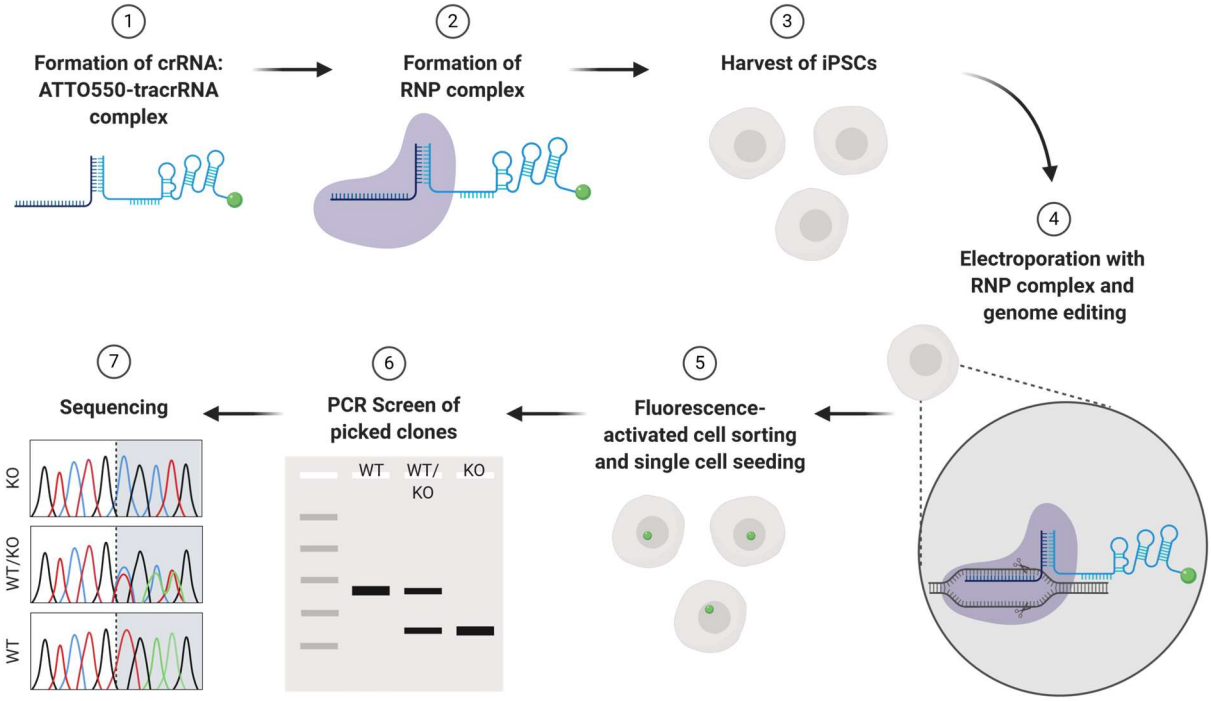

FIG. 3 | Schematic workflow for CRISPR/Cas9-dual cleavage gene knockout. (1) Two distinct single guide (sg) RNAs are generated by the formation of a complex of target-specific CRISPR-RNA (crRNA) and an ATTO550-labelled trans-activating RNA (tracrRNA). (2) Cas9 binds to the sgRNA, forming a ribonucleoprotein (RNP) complex. (3) The cells to be edited, iPSCs, are harvested and (4) electroporated with the RNP complex. RNP complexes bind to target sequences and cleave DNA 3 bp upstream of the protospacer-adjacent motif (PAM). (5) After incubation, cells are sorted by fluorescence-activated cell sorting and cells positive for ATTO550 are seeded as single cells. (6) After approximately 7 days, colonies are picked manually, DNA is isolated and amplified by PCR and clones are tested with agarose gel electrophoresis for dual cleavage. (7) Selected clones are sequenced by Sanger sequencing to confirm the homozygous or heterozygous knockout. RNP: ribonucleoprotein; iPSC: induced pluripotent stem cells; WT: wildtype; KO: knockout.

Top 5 off-target effects per crRNA as predicted by CRISPOR (Haeussler *et al.*, 2016) were excluded by Sanger sequencing, and generated iPSCs were characterized based on genomic integrity and pluripotency **(Schuster *et al.*, 2019,** Fig. 1). Combining the iPSC technology with CRISPR/Cas9-mediated genome editing to create an isogenic knockout and the differentiation into the proper cell type that is affected by the disease allows for ideal disease modeling of monogenic neurological disorders such as SCAR16.

5. Carboxy-terminus of the heat shock cognate 70 interacting protein

The gene 'STIP1 homology and U-box containing protein 1' (*STUB1*) codes for the protein 'C-terminus of the heat shock cognate 70 interacting protein' (CHIP). Mutations in *STUB1* cause early-onset autosomal recessive cerebellar ataxia type 16 (SCAR16, OMIM 615768), a movement

disorder characterized by atrophy of the cerebellum, brain stem and spinal cord. Symptoms range from loss of muscle coordination, unsteady gait, impaired fine motor skills and a slurry speech to epilepsy, hypogonadism and cognitive impairment (Shi *et al.*, 2013; Heimdal *et al.*, 2014; Shi *et al.*, 2014; Synofzik *et al.*, 2014; Bettencourt *et al.*, 2015; Hayer *et al.*, 2017), indicating a broad neurodegeneration. 19 pathogenic variants as summarized by the Human Gene Mutation Database (www.hgmd.cf.ac.uk) were described as of yet.

CHIP plays a crucial role in protein quality control and maintenance of cellular homeostasis. Acting as an asymmetric homodimer (Zhang *et al.*, 2005), it can bind to the C-termini of chaperones like HSC70/HSP70 and HSP90 modulating their activity via its tetratricopeptide repeat (TPR) domain (Ballinger *et al.*, 1999). Via its U-box domain, it tags chaperone-bound and other substrates with ubiquitin through its E3 ligase activity (Jiang *et al.*, 2001; Murata *et al.*, 2003). This dual role of CHIP of both molecular co-chaperone and E3 ubiquitin ligase is exceptional. CHIP enables poly-ubiquitination with both Lysin-48- and Lysin-63-linked chains, leading to the degradation via the ubiquitin-proteasome system and the autophagy-lysosome system, respectively (Zhang *et al.*, 2005; Yao, 2010; Guo *et al.*, 2015). More recently, CHIP was identified as a regulator of many other important cellular processes like cAMP/AMPK signaling (Schisler *et al.*, 2013; Rinaldi *et al.*, 2019), chaperone-mediated autophagy (Ferreira *et al.*, 2015), necroptosis (Seo *et al.*, 2016; Tang *et al.*, 2018), oxidative metabolism (Ravi *et al.*, 2018) and the regulation of TFEB activity and thereby regulation of macroautophagy (Guo *et al.*, 2015; Sha *et al.*, 2017).

Further highlighting the importance of CHIP, it was shown to be cytoprotective in many neurodegenerative diseases by degrading *i.a.* α-synuclein (Shin *et al.*, 2005; Tetzlaff *et al.*, 2008), LRRK2 (Ding *et al.*, 2009), APP and BACE1 (Kumar *et al.*, 2007; Singh *et al.*, 2015) and huntingtin (Jana *et al.*, 2005; Miller *et al.*, 2005). This leads to the assumption that CHIP may be a key player of neurodegeneration and a promising target for the treatment of many neurodegenerative diseases. Strengthening the aforementioned role of CHIP in neurodegeneration, CHIP

overexpression caused attenuated tau aggregation *in vivo* (Sahara *et al.*, 2005), decreased Aß levels and stabilized APP levels *in vivo* (Kumar *et al.*, 2007) and reduced α-synuclein-associated inclusion bodies *in vitro* (Shin *et al.*, 2005).

CHIP is strongly expressed in heart, skeletal muscle and brain; all are tissues with high metabolic activity (Ballinger *et al.*, 1999). In rodent brains, CHIP expression is strongest in neurons of the cerebellum, pons, medulla oblongata, hippocampus and cerebral cortex (Sahara *et al.*, 2005; Anderson *et al.*, 2010). CHIP knockout in flies, worms and mice leads to reduced lifespan and an increased ageing phenotype (Min *et al.*, 2008; Tawo *et al.*, 2017). $CHIP^{-/-}$ mice are viable but display severe cerebellar atrophy specifically in the Purkinje cell layer, with a distinct motor and cognitive impairment phenotype and aging-induced cardiac hypertrophy (Min *et al.*, 2008; Shi *et al.*, 2014). They presented with decreased stress tolerance, increased oxidative damage and soluble aberrantly folded proteins that were rarely seen in their wildtype littermates (Dai *et al.*, 2003; Min *et al.*, 2008; Shi *et al.*, 2014). Most strikingly 20% of $CHIP^{-/-}$ offspring die postnatally and 100% of mice die upon thermal challenge (Dai *et al.*, 2003), suggesting a key role of CHIP in stress response, and more specifically the heat shock response (HSR).

6. Heat shock response

The heat shock response is induced by environmental stressors such as heat, heavy metals and reactive oxygen species and pathophysiological stressors such as protein aggregation, inflammation and tissue injury. It is a cellular process that increases the number of heat shock proteins (HSPs) rapidly upon stress induction, to prevent and reverse protein misfolding and to reestablish cellular homeostasis (reviewed by Richter *et al.*, 2010). This increase of heat shock proteins is regulated by its key transcription factor heat shock factor 1 (HSF1). Under basal conditions, HSF1 is present in the cytosol in its' inactive monomeric state, bound to HSC70/HSP70 and HSP90 (Abravaya *et al.*, 1991)(Fig. 4, left panel). Only few misfolded proteins are present that can usually be refolded by chaperones. Upon stress, misfolded proteins

accumulate, leading to recruitment of chaperones and dissociation of those HSPs from HSF1 (Santoro, 2000)(Fig. 4, right panel). HSF1 quickly trimerizes and various post-translational modifications like phosphorylation, acetylation and SUMOylation occur, modulating its' activity. Trimerized HSF1 with bound CHIP translocates to the nucleus (Baler *et al.*, 1993; Sarge *et al.*, 1993; Dai *et al.*, 2003; Kim *et al.*, 2005). It then binds to heat shock elements and induces the transcription of HSPs within less than 30 minutes, leading to the synthesis and an enrichment of HSPs within hours (Baler *et al.*, 1993; Sarge *et al.*, 1993). Stress inducibility is highest for chaperones of the HSP70 (encoded by *inter alia HSPA1A*, *HSPA1B*, *HSPA1L*, *HSPA6*) and the HSP40 family (*DNAJB1*, *DNAJB2*, *DNAJB6*), while the expression of many chaperones is not altered upon stress (reviewed by Hageman *et al.*, 2009). HSPs can either facilitate refolding

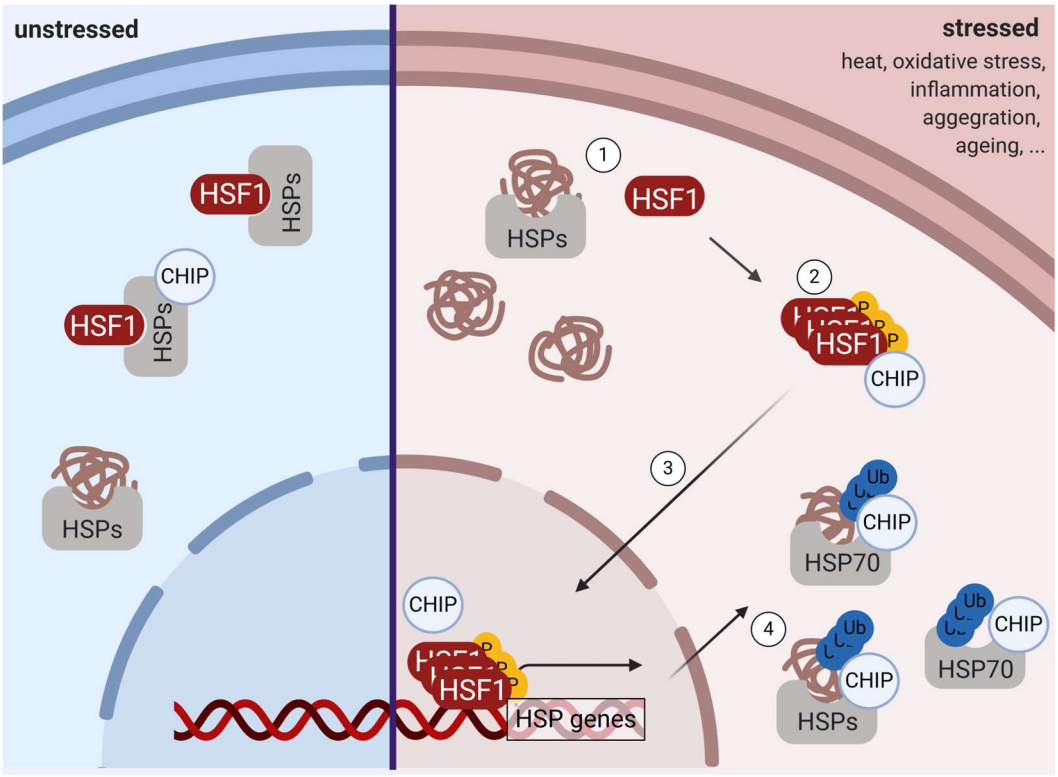

FIG. 4 | Heat shock response in unstressed and stressed cells. (Left panel) In unstressed cells, monomeric HSF1 is shielded by heat shock proteins (HSPs) like HSC70 or HSP90 and the few misfolded proteins that are present get refolded by chaperones. (Right panel) Upon stressors like heat, oxidative stress, inflammation, protein aggregation or ageing, the amount of misfolded proteins increases. (1) This leads to recruitment of heat shock proteins and thereby release of HSF1 which (2) quickly trimerizes, undergoes post-translational modifications (e.g. phosphorylation) and (3) translocates to the nucleus together with bound CHIP. Trimeric HSF1 binds to heat shock elements and leads to (4) transcription of heat shock proteins, mainly of the HSP70 and HSP40 family. These proteins bind to misfolded and aggregated proteins and either lead to refolding or tagging with ubiquitin, where CHIP is involved. HSPs that did not bind misfolded proteins can be tagged with ubiquitin by CHIP and get degraded. CHIP: C-terminus of the heat shock cognate 70 interacting protein; HSF1: heat shock factor 1; HSPs: heat shock proteins; P: phosphorylation; Ub: ubiquitin.

of misfolded proteins or allow tagging of them with ubiquitin which leads to proteasomal or lysosomal degradation and consequently to cytoprotection (reviewed by Richter *et al.*, 2010). Other small HSPs (sHSPs) like HSPB1, HSPB5 and HSPB8 assist chaperones by binding to unfolded proteins to prevent further aggregation (Acunzo *et al.*, 2012). Once the HSP levels exceed the need and the cellular homeostasis is re-established, 'naked' HSPs inhibit HSF1 again by binding to it, providing a negative feedback loop for HSR induction and their own transcription (Abravaya *et al.*, 1991; Baler *et al.*, 1992; Vjestica *et al.*, 2013). Furthermore, CHIP can tag excess HSPs with ubiquitin, leading to their degradation (Qian *et al.*, 2006). The detailed role of CHIP in the HSR will be discussed in the next chapter. Proteotoxic stress is considered among the most common causes of neurodegenerative diseases. In many cases such as AD, PD, HD and ALS, proteotoxic stress has directly been linked to compromised HSR *in vitro* and/or *in vivo* (reviewed by San Gil *et al.*, 2017). Neurons are considered to be more vulnerable to stress and homeostatic disturbances in protein quality control as a consequence of their postmitotic state that prevents dilution of misfolded and aggregated proteins by cell division. This highlights the significance of chaperones in neuroprotection, and the need of careful selection of appropriate disease cell types.

6.1 Modeling the HSR in SCAR16 patient-derived fibroblasts and cortical neurons

CHIP not only mediates essential protein triage decisions to maintain cellular homeostasis, it is also involved in HSR activation and recovery: CHIP and HSF1 directly interact upon stress stimuli, leading to subsequent increased HSP70 expression in COS7 and HEK293T cells and CHIP overexpression increased HSF1 activation (Dai *et al.*, 2003; Kim *et al.*, 2005; Qian *et al.*, 2006). The interaction is dependent on a functional TPR domain, as mutant K30A CHIP – HSF1 interaction was abolished (Dai *et al.*, 2003). In addition to that, CHIP also plays a role in HSR recovery by ubiquitin tagging of excess HSP70, leading to its degradation. This is dependent on

both a functional TPR and U-box domain. The affinity of CHIP is higher for HSP70 and other HSPs with bound misfolded proteins than for 'naked' HSPs, ensuring a depletion of misfolded proteins before HSPs will be tagged with ubiquitin and degraded. Furthermore, CHIP's affinity for HSP70 is higher than for HSC70 (Qian *et al.*, 2006).

As mentioned previously, 100% of CHIP$^{-/-}$ mice die upon thermal challenge at 42°C for 15 min and HSP70 expression upon heat shock in CHIP$^{-/-}$ mice is strongly reduced in most tissues, with almost absent levels in brain, heart and spleen (Dai *et al.*, 2003).

It needs to be highlighted that all experiments *in vitro* up to now were performed in cells of mesodermal origin, which are of questionable relevance for disease modeling as CHIP mutations in humans lead to a neurodegenerative phenotype. We therefore analyzed the effect of *STUB1* mutations on HSR in patient-derived cells *in vitro*, in both fibroblasts and neurons as the disease-relevant cell type.

By analyzing patient- and control-derived fibroblasts from skin biopsies, we were able to replicate previous findings from cell lines that indicate an impaired HSR induction on transcript and impaired HSR recovery on protein level, with remaining higher HSP70 expression in patient-derived cells **(Schuster *et al.*, in preparation,** Fig. 2**)**. This suggests either an impaired ubiquitination of HSP70 by CHIP and less degradation or higher misfolded protein levels and therefore a higher need for more HSP70, or a combination of both.

In contrast to the observations in our patient-derived fibroblasts, we could not detect an impaired HSR induction or recovery in cortical neurons of *STUB1* patients. Although we did not see a difference in HSF1 levels in the nucleus upon heat shock, we saw an even higher *HSPA1A/B* and *DNAJB1* transcript level in patients' neurons compared to controls. On protein level, though, almost no change in HSP70 levels upon heat shock or recovery can be seen, without any difference between control and patient cells **(Schuster *et al.*, in preparation,** Fig. 5**)**. The difference in the observation in neurons and fibroblasts may have several reasons: 1) an impaired HSR in the brain might be relevant and disease-causing but not in neurons (astrocytes show a

stronger HSR *in vivo* and might be the more relevant cell type; or specific cell types like Purkinje cells might show higher HSR induction), 2) alterations of the HSR that were seen in patient-derived fibroblasts but not in cortical neurons are not disease-relevant, as the diseased cell type does not show any changes, or 3) the low HSR is an *in vitro* artifact as the basal HSP70 level is already very high and this might not represent the cellular complexity of the *in vivo* situation. High basal HSP70 levels might by caused by neuronal monocultures, by cell culture conditions (like media composition or 2D monolayer structure) or by the embryonic age of iPSC-derived neurons, as *e.g. HSPA1A* expression is highest in fetal tissue (Hageman *et al.*, 2009). Persistently high levels of HSP70 are detrimental to cells (Feder *et al.*, 1992; Volloch *et al.*, 1999) so additional induction of HSP70 upon stress might be prevented in iPSC-derived cortical neurons.

Interestingly, comparing the cell viability of fibroblasts and CNs upon prolonged heat stress, we observed a higher stress vulnerability and toxicity in fibroblasts compared to neurons: while only 30% of fibroblasts were viable after 4h at 42.5°C, still >95% of neurons were viable, yet in both cases independent of functional CHIP **(Schuster *et al.*, in preparation,** Fig. 1, 4). A lower HSR induction in neurons might be linked to the higher resistance to this stress stimulus.

6.2 Comparing the HSR in different cell types and tissues

Although the genetic code is identical throughout all cells of the body, the transcript and protein expression varies greatly. While the HSR is evolutionarily well conserved across species, the tissue and cell variability of the expression of heat shock proteins varies greatly in humans: Hageman and Kampinga (2009) analyzed human expression data from 45 different tissues and 7 developmental stages (ranging from embryoid blast to adult) from the NCBI UniGene database. They observed strong tissue specificity of most HSPH (HSP100 family), HSPA (HSP70 family) and DNAJ (HSP40 family) isoforms, but the expression of *HSPA1A* is the most variable across tissues and developmental stages. Focusing on analyses of the brain, heat shock in rodents *in vivo* led to strongest HSP70 induction in the dentate gyrus, hypothalamus and the cerebellum

(Blake *et al.*, 1990; Li *et al.*, 1992). Other HSPs like DNAJB2A (HSP70 family) and HSJ1a/b (HSP40 family) are highly enriched in neuronal tissue in general (Cheetham *et al.*, 1992; Chapple *et al.*, 2003). *In vitro* analyses that compared heat shocked glial cells to heat shocked neurons revealed a higher induction of HSP70 in glial cells (Nishimura *et al.*, 1991; Marcuccilli *et al.*, 1996; Vogel *et al.*, 1997; Batulan *et al.*, 2003). Causes for the lower HSP70 induction in neurons are still a matter of debate. Some claim that differentially expressed co-chaperone levels might be the cause, with the basal expression level of the CHIP- and thereby HSR-inhibiting co-chaperone HSPBP1 being higher in neurons compared to glial cells (Zhao *et al.*, 2017) while the basal expression level of *HSPB1*/HSP27 is inverted. However, levels of HSP27 were shown to increase in neurons upon heat shock, while they do not change in astrocytes (Satoh *et al.*, 1995). Differences can also be caused by post-translational modifications of the HSP70 promoter, as acetylation upon heat shock is lower in cortical neurons compared to PC12 cells (Gomez *et al.*, 2015), making it less accessible for HSF1 binding.

We detected a specificity of *HSPB1* and *HSPB8* induction on transcript level upon heat shock for neurons compared to fibroblasts, although basal levels of both were higher in fibroblasts compared to neurons, indicating an important role of both small HSPs in stress coping in neurons. Vice versa we could detect a stronger *HSPA1A/B* induction upon heat shock in fibroblasts compared to neurons (**Schuster *et al.*, in preparation,** Fig. 2,5).

7. *STUB1*-mutant effects independent of the HSR

CHIP plays a key role in protein quality control via its two functional domains, the TPR domain and the U-box domain. Mutations in *STUB1* that were linked to SCAR16 were previously shown to lead to a destabilized structure of CHIP (Pakdaman *et al.*, 2017; Kanack *et al.*, 2018; Shi *et al.*, 2018). Other mutations were reported to impair CHIP's ability to ubiquitinate its substrates (Heimdal *et al.*, 2014; Ronnebaum *et al.*, 2014; Pakdaman *et al.*, 2017; Kanack *et al.*, 2018; Shi *et al.*, 2018; Madrigal *et al.*, 2019).

Gene ontology (GO) enrichment analysis of proteomic data of cortical neurons of 3 healthy controls and 3 *STUB1* patients revealed the absence of some protein folding and ubiquitin system-related proteins in patient-derived cortical neurons. Contrarily, GO terms of oxidative stress coping were enriched in patients only (**Schuster *et al.*, in preparation,** Fig. 6). The relevance of specific substrate ubiquitination is yet unknown, as the human genome codes for more than 600 E3 ligases that have overlapping substrates. Morishima and colleagues (2008) reported a redundancy of the E3 ligases Parkin and CHIP for many substrates like nitric oxide synthase (NOS), the glucocorticoid receptor (GR) and expanded glutamine androgen receptor. This highlights the importance of identifying selective and unique substrates of CHIP which might cause proteotoxicity upon accumulation and subsequent cell death.

8. Conclusion & Outlook

Within the scope of this thesis, we generated induced pluripotent stem cells from patients with SCAR16 and a *STUB1*-CRISPR/Cas9-mediated homozygous knockout and differentiated all iPSC lines into cortical neurons. We tried to elucidate the effect of CHIP mutations on the HSR in cortical neurons but did not observe a substantial difference between patient and control lines and a very weak induction of HSP70 on protein level in all cell lines. However, the impairment of the HSR by dysfunctional CHIP as described previously was observed in patient-derived fibroblasts compared to healthy controls. As discussed earlier, the difference between dysregulated HSR by CHIP mutations in fibroblasts and cortical neurons might have several reasons: 1) disturbances in the HSR are not disease-relevant, 2) dysfunctional HSR in cortical neurons might not be causative for the disease but another cell type of the brain e.g. astrocytes that were described to have a higher HSR induction compared to neurons might trigger the dysfunction of neurons, or 3) the weak HSR induction and the high basal HSP70 level might be an *in vitro* artifact of e.g. the monoculture and might not represent the cellular complexity of the *in vivo* situation.

The data of this doctoral thesis highlights the importance of careful selection of disease models. iPSCs allow for disease modeling in cells with patient-specific genetic backgrounds and endogenous protein levels; however, we did not observe a dysregulation in iPSC-derived cortical neurons that we could detect in patient-derived fibroblasts.

Considering the possible causes of this difference, changing the cell type might be of interest. As astrocytes *in vivo* show a stronger HSR, the same experimental setup for heat shock response analysis should be tested in iPSC-derived astrocytes. Furthermore, recent advances in 3D organoids that are generated *in vitro* but mimic the *in vivo* architecture of the organ with multiple cell types hold promise for modeling neurodegenerative diseases, but they bear the disadvantages of long cultivation, cell death in the organoids' cores caused by low nutrient and gas exchange as well as high variability between experiments and lines (reviewed by Grenier *et al.*, 2019). So far, only one protocol for cerebellar organoids from hESCs was published (Muguruma *et al.*, 2015), but generation was not replicated for iPSCs.

It would also be of high interest to analyze cell type-specific responses in $CHIP^{-/-}$ mice which might elucidate the role of neurons and astrocytes in stress coping and a potential dysregulation caused by dysfunctional CHIP.

Overcoming the existing challenges of finding the right *in vitro* disease model might help to elucidate key pathological events of SCAR16 and help to improve therapeutic approaches for patients. Given the importance of CHIP in central protein triage decisions, understanding the pathophysiology of SCAR16 and modifying CHIP levels can help to mitigate other neurodegenerative diseases as well.

9. References

Abravaya K, Phillips B, & Morimoto RI. (1991). Attenuation of the heat shock response in HeLa cells is mediated by the release of bound heat shock transcription factor and is modulated by changes in growth and in heat shock temperatures. *Genes Dev, 5*(11), 2117-2127.

Acunzo J, Katsogiannou M, & Rocchi P. (2012). Small heat shock proteins HSP27 (HspB1), alphaB-crystallin (HspB5) and HSP22 (HspB8) as regulators of cell death. *Int J Biochem Cell Biol, 44*(10), 1622-1631.

Al-Attar S, Westra ER, van der Oost J, & Brouns SJ. (2011). Clustered regularly interspaced short palindromic repeats (CRISPRs): the hallmark of an ingenious antiviral defense mechanism in prokaryotes. *Biol Chem, 392*(4), 277-289.

Anderson LG, Meeker RB, Poulton WE, & Huang DY. (2010). Brain distribution of carboxy terminus of Hsc70-interacting protein (CHIP) and its nuclear translocation in cultured cortical neurons following heat stress or oxygen-glucose deprivation. *Cell Stress Chaperones, 15*(5), 487-495.

Baler R, Dahl G, & Voellmy R. (1993). Activation of human heat shock genes is accompanied by oligomerization, modification, and rapid translocation of heat shock transcription factor HSF1. *Mol Cell Biol, 13*(4), 2486-2496.

Baler R, Welch WJ, & Voellmy R. (1992). Heat shock gene regulation by nascent polypeptides and denatured proteins: hsp70 as a potential autoregulatory factor. *J Cell Biol, 117*(6), 1151-1159.

Ballinger CA, Connell P, Wu Y, Hu Z, Thompson LJ, Yin LY, & Patterson C. (1999). Identification of CHIP, a novel tetratricopeptide repeat-containing protein that interacts with heat shock proteins and negatively regulates chaperone functions. *Mol Cell Biol, 19*(6), 4535-4545.

Batulan Z, Shinder GA, Minotti S, He BP, Doroudchi MM, Nalbantoglu J, ... Durham HD. (2003). High threshold for induction of the stress response in motor neurons is associated with failure to activate HSF1. *J Neurosci, 23*(13), 5789-5798.

Bettencourt C, de Yebenes JG, Lopez-Sendon JL, Shomroni O, Zhang X, Qian SB, ... Rizzu P. (2015). Clinical and Neuropathological Features of Spastic Ataxia in a Spanish Family with Novel Compound Heterozygous Mutations in STUB1. *Cerebellum, 14*(3), 378-381.

Bird TD. (2019). Hereditary ataxia overview. In *GeneReviews®[Internet]*: University of Washington, Seattle.

Blackstone C, O'Kane CJ, & Reid E. (2011). Hereditary spastic paraplegias: membrane traffic and the motor pathway. *Nat Rev Neurosci, 12*(1), 31-42.

Blake MJ, Nowak TS, Jr., & Holbrook NJ. (1990). In vivo hyperthermia induces expression of HSP70 mRNA in brain regions controlling the neuroendocrine response to stress. *Brain Res Mol Brain Res, 8*(1), 89-92.

Boyer LA, Lee TI, Cole MF, Johnstone SE, Levine SS, Zucker JP, ... Young RA. (2005). Core transcriptional regulatory circuitry in human embryonic stem cells. *Cell, 122*(6), 947-956.

Cao J, Wu L, Zhang SM, Lu M, Cheung WK, Cai W, ... Yan Q. (2016). An easy and efficient inducible CRISPR/Cas9 platform with improved specificity for multiple gene targeting. *Nucleic Acids Res, 44*(19), e149.

Chambers SM, Fasano CA, Papapetrou EP, Tomishima M, Sadelain M, & Studer L. (2009). Highly efficient neural conversion of human ES and iPS cells by dual inhibition of SMAD signaling. *Nat Biotechnol, 27*(3), 275-280.

Chapple JP, & Cheetham ME. (2003). The chaperone environment at the cytoplasmic face of the endoplasmic reticulum can modulate rhodopsin processing and inclusion formation. *J Biol Chem, 278*(21), 19087-19094.

Cheetham ME, Brion JP, & Anderton BH. (1992). Human homologues of the bacterial heat-shock protein DnaJ are preferentially expressed in neurons. *Biochem J, 284 (Pt 2)*, 469-476.

Chen F, Pruett-Miller SM, Huang Y, Gjoka M, Duda K, Taunton J, ... Davis GD. (2011). High-frequency genome editing using ssDNA oligonucleotides with zinc-finger nucleases. *Nat Methods, 8*(9), 753-755.

Chen X, Xu F, Zhu C, Ji J, Zhou X, Feng X, & Guang S. (2014). Dual sgRNA-directed gene knockout using CRISPR/Cas9 technology in Caenorhabditis elegans. *Sci Rep, 4*, 7581.

Cho SW, Kim S, Kim Y, Kweon J, Kim HS, Bae S, & Kim JS. (2014). Analysis of off-target effects of CRISPR/Cas-derived RNA-guided endonucleases and nickases. *Genome Res, 24*(1), 132-141.

Chylinski K, Makarova KS, Charpentier E, & Koonin EV. (2014). Classification and evolution of type II CRISPR-Cas systems. *Nucleic Acids Res, 42*(10), 6091-6105.

Cong L, Ran FA, Cox D, Lin S, Barretto R, Habib N, ... Zhang F. (2013). Multiplex genome engineering using CRISPR/Cas systems. *Science, 339*(6121), 819-823.

Cooper O, Seo H, Andrabi S, Guardia-Laguarta C, Graziotto J, Sundberg M, ... Isacson O. (2012). Pharmacological rescue of mitochondrial deficits in iPSC-derived neural cells from patients with familial Parkinson's disease. *Sci Transl Med, 4*(141), 141ra190.

Crawford TQ, & Roelink H. (2007). The notch response inhibitor DAPT enhances neuronal differentiation in embryonic stem cell-derived embryoid bodies independently of sonic hedgehog signaling. *Dev Dyn, 236*(3), 886-892.

Dai Q, Zhang C, Wu Y, McDonough H, Whaley RA, Godfrey V, ... Patterson C. (2003). CHIP activates HSF1 and confers protection against apoptosis and cellular stress. *EMBO J, 22*(20), 5446-5458.

Dang CV, O'Donnell KA, Zeller KI, Nguyen T, Osthus RC, & Li F. (2006). The c-Myc target gene network. *Semin Cancer Biol, 16*(4), 253-264.

Dang DT, Pevsner J, & Yang VW. (2000). The biology of the mammalian Kruppel-like family of transcription factors. *Int J Biochem Cell Biol, 32*(11-12), 1103-1121.

Dimos JT, Rodolfa KT, Niakan KK, Weisenthal LM, Mitsumoto H, Chung W, ... Eggan K. (2008). Induced pluripotent stem cells generated from patients with ALS can be differentiated into motor neurons. *Science, 321*(5893), 1218-1221.

Ding X, & Goldberg MS. (2009). Regulation of LRRK2 stability by the E3 ubiquitin ligase CHIP. *PLoS One, 4*(6), e5949.

Doetschman TC, Eistetter H, Katz M, Schmidt W, & Kemler R. (1985). The in vitro development of blastocyst-derived embryonic stem cell lines: formation of visceral yolk sac, blood islands and myocardium. *J Embryol Exp Morphol, 87*, 27-45.

Eiraku M, Watanabe K, Matsuo-Takasaki M, Kawada M, Yonemura S, Matsumura M, ... Sasai Y. (2008). Self-organized formation of polarized cortical tissues from ESCs and its active manipulation by extrinsic signals. *Cell Stem Cell, 3*(5), 519-532.

Feder JH, Rossi JM, Solomon J, Solomon N, & Lindquist S. (1992). The consequences of expressing hsp70 in Drosophila cells at normal temperatures. *Genes Dev, 6*(8), 1402-1413.

Ferreira JV, Soares AR, Ramalho JS, Pereira P, & Girao H. (2015). K63 linked ubiquitin chain formation is a signal for HIF1A degradation by Chaperone-Mediated Autophagy. *Sci Rep, 5*, 10210.

Gaj T, Gersbach CA, & Barbas CF, 3rd. (2013). ZFN, TALEN, and CRISPR/Cas-based methods for genome engineering. *Trends Biotechnol, 31*(7), 397-405.

Genc B, Gozutok O, & Ozdinler PH. (2019). Complexity of Generating Mouse Models to Study the Upper Motor Neurons: Let Us Shift Focus from Mice to Neurons. *Int J Mol Sci, 20*(16).

Gomez AV, Cordova G, Munita R, Parada GE, Barrios AP, Cancino GI, ... Andres ME. (2015). Characterizing HSF1 Binding and Post-Translational Modifications of hsp70 Promoter in Cultured Cortical Neurons: Implications in the Heat-Shock Response. *PLoS One, 10*(6), e0129329.

Grenier K, Kao J, & Diamandis P. (2019). Three-dimensional modeling of human neurodegeneration: brain organoids coming of age. *Mol Psychiatry*.

Guo D, Ying Z, Wang H, Chen D, Gao F, Ren H, & Wang G. (2015). Regulation of autophagic flux by CHIP. *Neurosci Bull, 31*(4), 469-479.

Guo W, Naujock M, Fumagalli L, Vandoorne T, Baatsen P, Boon R, ... Van Den Bosch L. (2017). HDAC6 inhibition reverses axonal transport defects in motor neurons derived from FUS-ALS patients. *Nat Commun, 8*(1), 861.

Haeussler M, Schonig K, Eckert H, Eschstruth A, Mianne J, Renaud JB, ... Concordet JP. (2016). Evaluation of off-target and on-target scoring algorithms and integration into the guide RNA selection tool CRISPOR. *Genome Biol, 17*(1), 148.

Hageman J, & Kampinga HH. (2009). Computational analysis of the human HSPH/HSPA/DNAJ family and cloning of a human HSPH/HSPA/DNAJ expression library. *Cell Stress Chaperones, 14*(1), 1-21.

Hanna J, Saha K, Pando B, van Zon J, Lengner CJ, Creyghton MP, ... Jaenisch R. (2009). Direct cell reprogramming is a stochastic process amenable to acceleration. *Nature, 462*(7273), 595-601.

Hargus G, Ehrlich M, Hallmann AL, & Kuhlmann T. (2014). Human stem cell models of neurodegeneration: a novel approach to study mechanisms of disease development. *Acta Neuropathol, 127*(2), 151-173.

Hauser S, Erzler M, Theurer Y, Schuster S, Schule R, & Schols L. (2016). Establishment of SPAST mutant induced pluripotent stem cells (iPSCs) from a hereditary spastic paraplegia (HSP) patient. *Stem Cell Res, 17*(3), 485-488.

Hauser S, Schuster S, Heuten E, Höflinger P, Admard J, Schelling Y, ... Schöls L. Comparative transcriptional profiling of motor neuron disorders in various human cell culture models., In preparation. .

Hayer SN, Deconinck T, Bender B, Smets K, Zuchner S, Reich S, ... Synofzik M. (2017). STUB1/CHIP mutations cause Gordon Holmes syndrome as part of a widespread multisystemic neurodegeneration: evidence from four novel mutations. *Orphanet J Rare Dis, 12*(1), 31.

Hedera P. (2018). Hereditary spastic paraplegia overview. In *GeneReviews®[Internet]*: University of Washington, Seattle.

Hefferin ML, & Tomkinson AE. (2005). Mechanism of DNA double-strand break repair by non-homologous end joining. *DNA Repair (Amst), 4*(6), 639-648.

Heimdal K, Sanchez-Guixe M, Aukrust I, Bollerslev J, Bruland O, Jablonski GE, ... Johansson S. (2014). STUB1 mutations in autosomal recessive ataxias - evidence for mutation-specific clinical heterogeneity. *Orphanet J Rare Dis, 9*, 146.

Horvath P, & Barrangou R. (2010). CRISPR/Cas, the immune system of bacteria and archaea. *Science, 327*(5962), 167-170.

Hsu PD, Scott DA, Weinstein JA, Ran FA, Konermann S, Agarwala V, ... Zhang F. (2013). DNA targeting specificity of RNA-guided Cas9 nucleases. *Nat Biotechnol, 31*(9), 827-832.

Huangfu D, Maehr R, Guo W, Eijkelenboom A, Snitow M, Chen AE, & Melton DA. (2008). Induction of pluripotent stem cells by defined factors is greatly improved by small-molecule compounds. *Nat Biotechnol, 26*(7), 795-797.

Iyer V, Shen B, Zhang W, Hodgkins A, Keane T, Huang X, & Skarnes WC. (2015). Off-target mutations are rare in Cas9-modified mice. *Nat Methods, 12*(6), 479.

James D, Levine AJ, Besser D, & Hemmati-Brivanlou A. (2005). TGFbeta/activin/nodal signaling is necessary for the maintenance of pluripotency in human embryonic stem cells. *Development, 132*(6), 1273-1282.
Jana NR, Dikshit P, Goswami A, Kotliarova S, Murata S, Tanaka K, & Nukina N. (2005). Co-chaperone CHIP associates with expanded polyglutamine protein and promotes their degradation by proteasomes. *J Biol Chem, 280*(12), 11635-11640.
Jiang J, Ballinger CA, Wu Y, Dai Q, Cyr DM, Hohfeld J, & Patterson C. (2001). CHIP is a U-box-dependent E3 ubiquitin ligase: identification of Hsc70 as a target for ubiquitylation. *J Biol Chem, 276*(46), 42938-42944.
Jinek M, Chylinski K, Fonfara I, Hauer M, Doudna JA, & Charpentier E. (2012). A programmable dual-RNA-guided DNA endonuclease in adaptive bacterial immunity. *Science, 337*(6096), 816-821.
Kanack AJ, Newsom OJ, & Scaglione KM. (2018). Most mutations that cause spinocerebellar ataxia autosomal recessive type 16 (SCAR16) destabilize the protein quality-control E3 ligase CHIP. *J Biol Chem, 293*(8), 2735-2743.
Kim DS, Lee JS, Leem JW, Huh YJ, Kim JY, Kim HS, ... Kim DW. (2010). Robust enhancement of neural differentiation from human ES and iPS cells regardless of their innate difference in differentiation propensity. *Stem Cell Rev Rep, 6*(2), 270-281.
Kim DS, Ross PJ, Zaslavsky K, & Ellis J. (2014a). Optimizing neuronal differentiation from induced pluripotent stem cells to model ASD. *Front Cell Neurosci, 8*, 109.
Kim S, Kim D, Cho SW, Kim J, & Kim JS. (2014b). Highly efficient RNA-guided genome editing in human cells via delivery of purified Cas9 ribonucleoproteins. *Genome Res, 24*(6), 1012-1019.
Kim SA, Yoon JH, Kim DK, Kim SG, & Ahn SG. (2005). CHIP interacts with heat shock factor 1 during heat stress. *FEBS Lett, 579*(29), 6559-6563.
Klockgether T, Mariotti C, & Paulson HL. (2019). Spinocerebellar ataxia. *Nat Rev Dis Primers, 5*(1), 24.
Koch P, Opitz T, Steinbeck JA, Ladewig J, & Brustle O. (2009). A rosette-type, self-renewing human ES cell-derived neural stem cell with potential for in vitro instruction and synaptic integration. *Proc Natl Acad Sci U S A, 106*(9), 3225-3230.
Kondo T, Asai M, Tsukita K, Kutoku Y, Ohsawa Y, Sunada Y, ... Inoue H. (2013). Modeling Alzheimer's disease with iPSCs reveals stress phenotypes associated with intracellular Abeta and differential drug responsiveness. *Cell Stem Cell, 12*(4), 487-496.
Kumar P, Ambasta RK, Veereshwarayya V, Rosen KM, Kosik KS, Band H, ... Querfurth HW. (2007). CHIP and HSPs interact with beta-APP in a proteasome-dependent manner and influence Abeta metabolism. *Hum Mol Genet, 16*(7), 848-864.
Kuo SH. (2019). Ataxia. *Continuum (Minneap Minn), 25*(4), 1036-1054.
Li Y, Chopp M, Yoshida Y, & Levine SR. (1992). Distribution of 72-kDa heat-shock protein in rat brain after hyperthermia. *Acta Neuropathol, 84*(1), 94-99.
Liang X, Potter J, Kumar S, Zou Y, Quintanilla R, Sridharan M, ... Chesnut JD. (2015). Rapid and highly efficient mammalian cell engineering via Cas9 protein transfection. *J Biotechnol, 208*, 44-53.
Lo Giudice T, Lombardi F, Santorelli FM, Kawarai T, & Orlacchio A. (2014). Hereditary spastic paraplegia: clinical-genetic characteristics and evolving molecular mechanisms. *Exp Neurol, 261*, 518-539.
Madrigal SC, McNeil Z, Sanchez-Hodge R, Shi CH, Patterson C, Scaglione KM, & Schisler JC. (2019). Changes in protein function underlie the disease spectrum in patients with CHIP mutations. *J Biol Chem, 294*(50), 19236-19245.
Makarova KS, Haft DH, Barrangou R, Brouns SJ, Charpentier E, Horvath P, ... Koonin EV. (2011). Evolution and classification of the CRISPR-Cas systems. *Nat Rev Microbiol, 9*(6), 467-477.
Mali P, Chou BK, Yen J, Ye Z, Zou J, Dowey S, ... Cheng L. (2010). Butyrate greatly enhances derivation of human induced pluripotent stem cells by promoting epigenetic remodeling and the expression of pluripotency-associated genes. *Stem Cells, 28*(4), 713-720.
Mali P, Yang L, Esvelt KM, Aach J, Guell M, DiCarlo JE, ... Church GM. (2013). RNA-guided human genome engineering via Cas9. *Science, 339*(6121), 823-826.
Malik N, & Rao MS. (2013). A review of the methods for human iPSC derivation. *Methods Mol Biol, 997*, 23-33.
Manto M, Gandini J, Feil K, & Strupp M. (2019). Cerebellar ataxias: an update. *Curr Opin Neurol*.
Marcuccilli CJ, Mathur SK, Morimoto RI, & Miller RJ. (1996). Regulatory differences in the stress response of hippocampal neurons and glial cells after heat shock. *J Neurosci, 16*(2), 478-485.
Maury Y, Come J, Piskorowski RA, Salah-Mohellibi N, Chevaleyre V, Peschanski M, ... Nedelec S. (2015). Combinatorial analysis of developmental cues efficiently converts human pluripotent stem cells into multiple neuronal subtypes. *Nat Biotechnol, 33*(1), 89-96.
McComish SF, & Caldwell MA. (2018). Generation of defined neural populations from pluripotent stem cells. *Philos Trans R Soc Lond B Biol Sci, 373*(1750).
McGonigle P, & Ruggeri B. (2014). Animal models of human disease: challenges in enabling translation. *Biochem Pharmacol, 87*(1), 162-171.
Miller VM, Nelson RF, Gouvion CM, Williams A, Rodriguez-Lebron E, Harper SQ, ... Paulson HL. (2005). CHIP suppresses polyglutamine aggregation and toxicity in vitro and in vivo. *J Neurosci, 25*(40), 9152-9161.
Min JN, Whaley RA, Sharpless NE, Lockyer P, Portbury AL, & Patterson C. (2008). CHIP deficiency decreases longevity, with accelerated aging phenotypes accompanied by altered protein quality control. *Mol Cell Biol, 28*(12), 4018-4025.

Mojica FJ, Diez-Villasenor C, Garcia-Martinez J, & Almendros C. (2009). Short motif sequences determine the targets of the prokaryotic CRISPR defence system. *Microbiology, 155*(Pt 3), 733-740.
Morishima Y, Wang AM, Yu Z, Pratt WB, Osawa Y, & Lieberman AP. (2008). CHIP deletion reveals functional redundancy of E3 ligases in promoting degradation of both signaling proteins and expanded glutamine proteins. *Hum Mol Genet, 17*(24), 3942-3952.
Muguruma K, Nishiyama A, Kawakami H, Hashimoto K, & Sasai Y. (2015). Self-organization of polarized cerebellar tissue in 3D culture of human pluripotent stem cells. *Cell Rep, 10*(4), 537-550.
Murata S, Chiba T, & Tanaka K. (2003). CHIP: a quality-control E3 ligase collaborating with molecular chaperones. *Int J Biochem Cell Biol, 35*(5), 572-578.
Murovec J, Pirc Z, & Yang B. (2017). New variants of CRISPR RNA-guided genome editing enzymes. *Plant Biotechnol J, 15*(8), 917-926.
Nakagawa M, Takizawa N, Narita M, Ichisaka T, & Yamanaka S. (2010). Promotion of direct reprogramming by transformation-deficient Myc. *Proc Natl Acad Sci U S A, 107*(32), 14152-14157.
Nishimura RN, Dwyer BE, Clegg K, Cole R, & de Vellis J. (1991). Comparison of the heat shock response in cultured cortical neurons and astrocytes. *Brain Res Mol Brain Res, 9*(1-2), 39-45.
Okita K, Ichisaka T, & Yamanaka S. (2007). Generation of germline-competent induced pluripotent stem cells. *Nature, 448*(7151), 313-317.
Okita K, Matsumura Y, Sato Y, Okada A, Morizane A, Okamoto S, ... Yamanaka S. (2011). A more efficient method to generate integration-free human iPS cells. *Nat Methods, 8*(5), 409-412.
Pakdaman Y, Sanchez-Guixe M, Kleppe R, Erdal S, Bustad HJ, Bjorkhaug L, ... Aukrust I. (2017). In vitro characterization of six STUB1 variants in spinocerebellar ataxia 16 reveals altered structural properties for the encoded CHIP proteins. *Biosci Rep, 37*(2).
Qian SB, McDonough H, Boellmann F, Cyr DM, & Patterson C. (2006). CHIP-mediated stress recovery by sequential ubiquitination of substrates and Hsp70. *Nature, 440*(7083), 551-555.
Ran FA, Hsu PD, Lin CY, Gootenberg JS, Konermann S, Trevino AE, ... Zhang F. (2013a). Double nicking by RNA-guided CRISPR Cas9 for enhanced genome editing specificity. *Cell, 154*(6), 1380-1389.
Ran FA, Hsu PD, Wright J, Agarwala V, Scott DA, & Zhang F. (2013b). Genome engineering using the CRISPR-Cas9 system. *Nat Protoc, 8*(11), 2281-2308.
Ravi S, Parry TL, Willis MS, Lockyer P, Patterson C, Bain JR, ... Schisler JC. (2018). Adverse Effects of Fenofibrate in Mice Deficient in the Protein Quality Control Regulator, CHIP. *J Cardiovasc Dev Dis, 5*(3).
Rehbach K, Kesavan J, Hauser S, Ritzenhofen S, Jungverdorben J, Schule R, ... Brustle O. (2019). Multiparametric rapid screening of neuronal process pathology for drug target identification in HSP patient-specific neurons. *Sci Rep, 9*(1), 9615.
Reinhardt P, Glatza M, Hemmer K, Tsytsyura Y, Thiel CS, Hoing S, ... Sterneckert J. (2013). Derivation and expansion using only small molecules of human neural progenitors for neurodegenerative disease modeling. *PLoS One, 8*(3), e59252.
Richter K, Haslbeck M, & Buchner J. (2010). The heat shock response: life on the verge of death. *Mol Cell, 40*(2), 253-266.
Rinaldi L, Delle Donne R, Catalanotti B, Torres-Quesada O, Enzler F, Moraca F, ... Feliciello A. (2019). Feedback inhibition of cAMP effector signaling by a chaperone-assisted ubiquitin system. *Nat Commun, 10*(1), 2572.
Ronnebaum SM, Patterson C, & Schisler JC. (2014). Emerging evidence of coding mutations in the ubiquitin-proteasome system associated with cerebellar ataxias. *Hum Genome Var, 1*, 14018.
Ruano L, Melo C, Silva MC, & Coutinho P. (2014). The global epidemiology of hereditary ataxia and spastic paraplegia: a systematic review of prevalence studies. *Neuroepidemiology, 42*(3), 174-183.
Sahara N, Murayama M, Mizoroki T, Urushitani M, Imai Y, Takahashi R, ... Takashima A. (2005). In vivo evidence of CHIP up-regulation attenuating tau aggregation. *J Neurochem, 94*(5), 1254-1263.
San Gil R, Ooi L, Yerbury JJ, & Ecroyd H. (2017). The heat shock response in neurons and astroglia and its role in neurodegenerative diseases. *Mol Neurodegener, 12*(1), 65.
Sanchez-Danes A, Richaud-Patin Y, Carballo-Carbajal I, Jimenez-Delgado S, Caig C, Mora S, ... Raya A. (2012). Disease-specific phenotypes in dopamine neurons from human iPS-based models of genetic and sporadic Parkinson's disease. *EMBO Mol Med, 4*(5), 380-395.
Santoro MG. (2000). Heat shock factors and the control of the stress response. *Biochem Pharmacol, 59*(1), 55-63.
Sarge KD, Murphy SP, & Morimoto RI. (1993). Activation of heat shock gene transcription by heat shock factor 1 involves oligomerization, acquisition of DNA-binding activity, and nuclear localization and can occur in the absence of stress. *Mol Cell Biol, 13*(3), 1392-1407.
Satoh JI, & Kim SU. (1995). Differential expression of heat shock protein HSP27 in human neurons and glial cells in culture. *J Neurosci Res, 41*(6), 805-818.
Schisler JC, Rubel CE, Zhang C, Lockyer P, Cyr DM, & Patterson C. (2013). CHIP protects against cardiac pressure overload through regulation of AMPK. *J Clin Invest, 123*(8), 3588-3599.
Schule R, & Schols L. (2011). Genetics of hereditary spastic paraplegias. *Semin Neurol, 31*(5), 484-493.
Schule R, Wiethoff S, Martus P, Karle KN, Otto S, Klebe S, ... Schols L. (2016). Hereditary spastic paraplegia: Clinicogenetic lessons from 608 patients. *Ann Neurol, 79*(4), 646-658.

Schuster S, Heuten E, Velic A, Macek B, Admard J, Ossowski S, ... Schöls L. The effect of CHIP mutations on the heat shock response is cell type-dependent., In preparation.
Schuster S, Saravanakumar S, Schols L, & Hauser S. (2019). Generation of a homozygous CRISPR/Cas9-mediated knockout human iPSC line for the STUB1 locus. *Stem Cell Res, 34*, 101378.
Schuster S, Schelling Y, Synofzik M, Hoflinger P, Schols L, & Hauser S. (2018). Establishment of STUB1/CHIP mutant induced pluripotent stem cells (iPSCs) from a patient with Gordon Holmes syndrome/SCAR16. *Stem Cell Res, 29*, 166-169.
Seo J, Lee EW, Sung H, Seong D, Dondelinger Y, Shin J, ... Song J. (2016). CHIP controls necroptosis through ubiquitylation- and lysosome-dependent degradation of RIPK3. *Nat Cell Biol, 18*(3), 291-302.
Sha Y, Rao L, Settembre C, Ballabio A, & Eissa NT. (2017). STUB1 regulates TFEB-induced autophagy-lysosome pathway. *EMBO J, 36*(17), 2544-2552.
Shi CH, Rubel C, Soss SE, Sanchez-Hodge R, Zhang S, Madrigal SC, ... Schisler JC. (2018). Disrupted structure and aberrant function of CHIP mediates the loss of motor and cognitive function in preclinical models of SCAR16. *PLoS Genet, 14*(9), e1007664.
Shi CH, Schisler JC, Rubel CE, Tan S, Song B, McDonough H, ... Xu YM. (2014). Ataxia and hypogonadism caused by the loss of ubiquitin ligase activity of the U box protein CHIP. *Hum Mol Genet, 23*(4), 1013-1024.
Shi Y, Kirwan P, & Livesey FJ. (2012). Directed differentiation of human pluripotent stem cells to cerebral cortex neurons and neural networks. *Nat Protoc, 7*(10), 1836-1846.
Shi Y, Wang J, Li JD, Ren H, Guan W, He M, ... Tang B. (2013). Identification of CHIP as a novel causative gene for autosomal recessive cerebellar ataxia. *PLoS One, 8*(12), e81884.
Shin Y, Klucken J, Patterson C, Hyman BT, & McLean PJ. (2005). The co-chaperone carboxyl terminus of Hsp70-interacting protein (CHIP) mediates alpha-synuclein degradation decisions between proteasomal and lysosomal pathways. *J Biol Chem, 280*(25), 23727-23734.
Singh AK, & Pati U. (2015). CHIP stabilizes amyloid precursor protein via proteasomal degradation and p53-mediated trans-repression of beta-secretase. *Aging Cell, 14*(4), 595-604.
Smith JR, Vallier L, Lupo G, Alexander M, Harris WA, & Pedersen RA. (2008). Inhibition of Activin/Nodal signaling promotes specification of human embryonic stem cells into neuroectoderm. *Dev Biol, 313*(1), 107-117.
Stadtfeld M, & Hochedlinger K. (2010). Induced pluripotency: history, mechanisms, and applications. *Genes Dev, 24*(20), 2239-2263.
Synofzik M, Schule R, Schulze M, Gburek-Augustat J, Schweizer R, Schirmacher A, ... Bauer P. (2014). Phenotype and frequency of STUB1 mutations: next-generation screenings in Caucasian ataxia and spastic paraplegia cohorts. *Orphanet J Rare Dis, 9*, 57.
Takahashi K, Tanabe K, Ohnuki M, Narita M, Ichisaka T, Tomoda K, & Yamanaka S. (2007). Induction of pluripotent stem cells from adult human fibroblasts by defined factors. *Cell, 131*(5), 861-872.
Takahashi K, & Yamanaka S. (2006). Induction of pluripotent stem cells from mouse embryonic and adult fibroblast cultures by defined factors. *Cell, 126*(4), 663-676.
Tang MB, Li YS, Li SH, Cheng Y, Zhang S, Luo HY, ... Xu YM. (2018). Anisomycin prevents OGD-induced necroptosis by regulating the E3 ligase CHIP. *Sci Rep, 8*(1), 6379.
Tawo R, Pokrzywa W, Kevei E, Akyuz ME, Balaji V, Adrian S, ... Hoppe T. (2017). The Ubiquitin Ligase CHIP Integrates Proteostasis and Aging by Regulation of Insulin Receptor Turnover. *Cell, 169*(3), 470-482 e413.
Tetzlaff JE, Putcha P, Outeiro TF, Ivanov A, Berezovska O, Hyman BT, & McLean PJ. (2008). CHIP targets toxic alpha-Synuclein oligomers for degradation. *J Biol Chem, 283*(26), 17962-17968.
van den Bosch M, Lohman PH, & Pastink A. (2002). DNA double-strand break repair by homologous recombination. *Biol Chem, 383*(6), 873-892.
Viswanathan SR, Daley GQ, & Gregory RI. (2008). Selective blockade of microRNA processing by Lin28. *Science, 320*(5872), 97-100.
Vjestica A, Zhang D, Liu J, & Oliferenko S. (2013). Hsp70-Hsp40 chaperone complex functions in controlling polarized growth by repressing Hsf1-driven heat stress-associated transcription. *PLoS Genet, 9*(10), e1003886.
Vogel P, Dux E, & Wiessner C. (1997). Effect of heat shock on neuronal cultures: importance of protein synthesis and HSP72 induction for induced tolerance and survival. *Metab Brain Dis, 12*(3), 203-217.
Volloch VZ, & Sherman MY. (1999). Oncogenic potential of Hsp72. *Oncogene, 18*(24), 3648-3651.
Wang S, Wang B, Pan N, Fu L, Wang C, Song G, ... Zhang YA. (2015). Differentiation of human induced pluripotent stem cells to mature functional Purkinje neurons. *Sci Rep, 5*, 9232.
Watson LM, Wong MMK, Vowles J, Cowley SA, & Becker EBE. (2018). A Simplified Method for Generating Purkinje Cells from Human-Induced Pluripotent Stem Cells. *Cerebellum, 17*(4), 419-427.
Xu RH, Sampsell-Barron TL, Gu F, Root S, Peck RM, Pan G, ... Thomson JA. (2008). NANOG is a direct target of TGFbeta/activin-mediated SMAD signaling in human ESCs. *Cell Stem Cell, 3*(2), 196-206.
Yamanaka S, & Takahashi K. (2006). [Induction of pluripotent stem cells from mouse fibroblast cultures]. *Tanpakushitsu Kakusan Koso, 51*(15), 2346-2351.
Yao TP. (2010). The role of ubiquitin in autophagy-dependent protein aggregate processing. *Genes Cancer, 1*(7), 779-786.

Yoshida M, Kitaoka S, Egawa N, Yamane M, Ikeda R, Tsukita K, … Saito MK. (2015). Modeling the early phenotype at the neuromuscular junction of spinal muscular atrophy using patient-derived iPSCs. *Stem Cell Reports, 4*(4), 561-568.

Yu J, Vodyanik MA, Smuga-Otto K, Antosiewicz-Bourget J, Frane JL, Tian S, … Thomson JA. (2007). Induced pluripotent stem cell lines derived from human somatic cells. *Science, 318*(5858), 1917-1920.

Zhang M, Windheim M, Roe SM, Peggie M, Cohen P, Prodromou C, & Pearl LH. (2005). Chaperoned ubiquitylation--crystal structures of the CHIP U box E3 ubiquitin ligase and a CHIP-Ubc13-Uev1a complex. *Mol Cell, 20*(4), 525-538.

Zhang SC, Wernig M, Duncan ID, Brustle O, & Thomson JA. (2001). In vitro differentiation of transplantable neural precursors from human embryonic stem cells. *Nat Biotechnol, 19*(12), 1129-1133.

Zhao T, Hong Y, Yin P, Li S, & Li XJ. (2017). Differential HspBP1 expression accounts for the greater vulnerability of neurons than astrocytes to misfolded proteins. *Proc Natl Acad Sci U S A, 114*(37), E7803-E7811.

Figure 1-4 of this synopsis were created with BioRender.com.

LIST OF PUBLICATIONS AND MANUSCRIPTS

The following publications originated within the scope of this PhD thesis:
(marked with *: included in this dissertation; marked with #: equal contribution)

1. * **Schuster S**, Schelling Y, Synofzik M, Höflinger P, Schöls L, Hauser S (2018). Establishment of STUB1/CHIP mutant induced pluripotent stem cells (iPSCs) from a patient with Gordon Holmes syndrome/SCAR16. *Stem Cell Res,* 29:166-169.

2. * **Schuster S**, Saravanakumar S, Schöls L, Hauser S (2019). Generation of a homozygous CRISPR/Cas9-mediated knockout human iPSC line for the *STUB1* locus. *Stem Cell Res,* 34:101378.

3. * **Schuster S**, Heuten E, Velic A, Admard J, Synofzik M, Ossowski S, Macek B, Hauser S#, Schöls L#. CHIP mutations affect the heat shock response differently in human fibroblasts and iPSC-derived neurons. In preparation.

4. * Hauser S, Erzler M, Theurer Y, **Schuster S**, Schüle R, Schöls L (2016). Establishment of *SPAST* mutant induced pluripotent stem cells (iPSCs) from a hereditary spastic paraplegia (HSP) patient. *Stem Cell Res,* 17(3):485-488.

5. * Hauser S, **Schuster S**, Heuten E, Höflinger P, Admard J, Schelling Y, Ossowski S, Schöls L. Comparative transcriptional profiling of motor neuron disorder-associated genes in various human cell culture models. In preparation.

6. Hauser S, **Schuster S**, Theurer Y, Synofzik M, Schöls L (2016). Generation of optic atrophy 1 patient-derived induced pluripotent stem cells (iPS-OPA1-BEHR) for disease modeling of complex optic atrophy syndromes. *Stem Cell Res*,17(2):426-429.

7. Hauser S#, Poenisch M#, Schelling Y, Höflinger P, **Schuster S**, Teegler A, Betten R, Gustafsson JA, Hübener-Schmid J, Schlake T, Chevessier-Tünnesen F, Horscroft N, Björkhem I, Schöls L (2019). mRNA as Novel Treatment Strategy for Hereditary Spastic Paraplegia Type 5. *Mol Ther Meth Clin D,* 15:359-370.

8. Hosseinzadeh Z, Hauser S, Singh Y, Pelzl L, **Schuster S**, Sharma Y, Höflinger P, Zacharopoulou N, Stournaras C, Rathbun D, Zrenner E, Schöls L#, Lang F# (2020). Decreased Na^+/K^+ ATPase Activity and Depolarized Cell Membrane in Neurons Differentiated from Chorea-Acanthocytosis Patients. *Sci. Rep.* In revision.

9. Zimmermann M#, **Schuster S**#, Boesch S, Korenke C, Mohr J, Reichbauer J, Kernstock C, Kotzot D, Spahlinger V, Schüle R, Schöls L (2020). FIG4 mutations leading to Parkinsonism and a phenotypical continuum between CMT4J and Yunis Varón syndrome. *Park Rel Dis.* In revision.

10. Haller P#, **Schuster S**#, Sporbeck K, Hauser S, Braulke T, Saftig P, Schöls L, Proikas-Cezanne T. Impaired selective autophagy in Charcot Marie Tooth neuropathy type 4J. In preparation.

11. Hengel H, Maroofian R, Dyack S, MacKay S, Schatz U, Fleger M, Balousha G, Ghanem Z, Casadei N, Velic A, Macek B, Hauser S, **Schuster S**, Hannan S, Bauer P, Haack T, Schöls L. Bi-allelic variants in BCAS3 cause developmental encephalopathy with syndromic features and progressive pyramidal tract affection. In preparation.

12. Ulmer U, Nagel M, **Schuster S**, Höflinger P, Bentrup A, Reichbauer J, Hauser S, Schöls L, Synofzik M, Othman A, Schüle R. Mutations in *GBA2* cause dysregulated glucose-ceramide metabolism in iPSC-derived neurons. In preparation.

STATEMENT OF CONTRIBUTIONS

1. **Schuster S**, Schelling Y, Synofzik M, Höflinger P, Schöls L, Hauser S (2018). Establishment of STUB1/CHIP mutant induced pluripotent stem cells (iPSCs) from a patient with Gordon Holmes syndrome/SCAR16. *Stem Cell Res,* 29:166-169.

   Within the scope of this paper, we reprogrammed fibroblasts of a SCAR16 patient to iPSCs and characterized generated iPSCs based on genomic integrity and pluripotency.

   This project was designed by Schuster S, Hauser S, Schöls L.
   Experiments were performed by Schuster S.
   Technical assistance was provided by Schelling Y, Höflinger P.
   Data analysis was performed by Schuster S.
   The skin biopsy was provided by Synofzik M.
   Funding was provided by Schöls L.
   The manuscript draft was written by Schuster S.
   The manuscript was revised by Schelling Y, Synofzik M, Höflinger P, Schöls L, Hauser S.

2. **Schuster S**, Saravanakumar S, Schöls L, Hauser S (2019). Generation of a homozygous CRISPR/Cas9-mediated knockout human iPSC line for the *STUB1* locus. *Stem Cell Res,* 34:101378.

   As presented in this paper, we generated CRISPR-Cas9-mediated knockouts of the STUB1 locus in a control iPSC line and characterized the generated line validating its genomic integrity and pluripotency.

   This project was designed by Schuster S, Hauser S.
   Experiments were performed by Schuster S.
   Technical assistance was provided by Saravanakumar S.
   Data analysis was performed by Schuster S.
   Funding was provided by Schöls L.
   The manuscript draft was written by Schuster S.
   The manuscript was revised by Saravanakumar S, Schöls L, Hauser S.

3. **Schuster S**, Heuten E, Velic A, Admard J, Synofzik M, Ossowski S, Macek B, Hauser S, Schöls L. CHIP mutations affect the heat shock response differently in human fibroblasts and iPSC-derived neurons. In preparation.

   We analyzed fibroblasts of 3 healthy controls and 3 SCAR16 patients for differences in the heat shock response upon heat shock and recovery with various techniques. We further extended theses analyses to cortical neurons of 3 healthy controls, 3 SCAR16 patients and a CRISPR/Cas9-mediated *STUB1*(-/-) cell line. For a broader picture, we also performed proteomic analyses with LC-MS/MS on 3 control and 3 patient cortical neurons.

   This project was designed by Schuster S, Hauser S, Schöls L.
   Experiments were performed by Schuster S, Heuten E (fractionation protocol establishment, technical help in cell culture), Velic A (Proteomic analysis).
   Data analysis was performed by Schuster S; Admard J, Ossowski S (both: RNA sequencing analysis); Velic A, Macek B (both: proteomic analysis).
   Fibroblasts were provided by Synofzik M.
   Funding was provided by Schöls L.
   The manuscript draft was written by Schuster S.
   The manuscript was revised by Heuten E, Velic A, Admard J, Synofzik M, Ossowski S, Macek B, Hauser S, Schöls L.

4. Hauser S, Erzler M, Theurer Y, **Schuster S**, Schüle R, Schöls L (2016). Establishment of *SPAST* mutant induced pluripotent stem cells (iPSCs) from a hereditary spastic paraplegia (HSP) patient. *Stem Cell Res,* 17(3):485-488.

   Within the scope of this paper, we have reprogrammed fibroblasts of an SPG4 patient to iPSCs and have characterized generated iPSCs based on genomic integrity and pluripotency.

   This project was designed by Hauser S.
   Experiments were performed by Erzler M, Theurer Y, Schuster S.
   Technical assistance was provided by Theurer Y.
   Data analysis was performed by Hauser S, Erzler M, Schuster S.
   The skin biopsy was provided by Schüle R.
   Funding was provided by Schöls L.
   The manuscript draft was written by Hauser S.
   The manuscript was revised by Erzler M, Theurer Y, Schuster S, Schüle R, Schöls L.

5. Hauser S, **Schuster S**, Heuten E, Höflinger P, Admard J, Schelling Y, Ossowski S, Schöls L. Comparative transcriptional profiling of motor neuron disorder-associated genes in various human cell culture models. In preparation.

   For the project presented in this paper, we isolated RNA of 2 healthy individuals of lymphocytes, lymphoblasts, fibroblasts, iPSCs and iPSC-derived cortical neurons. We performed RNA Sequencing and analyzed transcript expression of spasticity-related genes in the 5 different cell types.

   This project was designed by Hauser S, Schöls L.
   Experiments were performed by Schuster S, Heuten E, Höflinger P, Schelling Y. Data analysis was performed by Hauser S, Schuster S; Admard J, Ossowski S (both: RNA sequencing analysis).
   Funding was provided by Schöls L.
   The manuscript draft was written by Hauser S.
   The manuscript was revised by Schuster S, Heuten E, Höflinger P, Admard J, Schelling Y, Ossowski S, Schöls L.

APPENDED PUBLICATIONS

Establishment of STUB1/CHIP mutant induced pluripotent stem cells (iPSCs) from a patient with Gordon Holmes syndrome / SCAR16.

Schuster S, Schelling Y, Synofzik M, Höflinger P, Schöls L, Hauser S (2018). Establishment of STUB1/CHIP mutant induced pluripotent stem cells (iPSCs) from a patient with Gordon Holmes syndrome/SCAR16. *Stem Cell Res,* 29:166-169.

Stem Cell Research 29 (2018) 166–169

Contents lists available at ScienceDirect

Stem Cell Research

journal homepage: www.elsevier.com/locate/scr

Lab Resource: Single Cell Line

Establishment of *STUB1*/CHIP mutant induced pluripotent stem cells (iPSCs) from a patient with Gordon Holmes syndrome/SCAR16

Stefanie Schuster [a,b,c], Yvonne Schelling [b], Matthis Synofzik [a,b], Philip Höflinger [a,b,c], Ludger Schöls [a,b], Stefan Hauser [b,*]

[a] Hertie Institute for Clinical Brain Research, University of Tübingen, Tübingen, Germany
[b] German Center for Neurodegenerative Diseases (DZNE), Tübingen, Germany
[c] Graduate School of Cellular and Molecular Neuroscience, University of Tübingen, Tübingen, Germany

ARTICLE INFO

Article history:
Received 29 January 2018
Received in revised form 27 March 2018
Accepted 4 April 2018
Available online 9 April 2018

ABSTRACT

STUB1/CHIP is a central component of cellular protein homeostasis and interacts with key proteins involved in the pathogenesis of many neurodegenerative diseases. Here, we reprogrammed human skin fibroblasts from a 12-year-old male patient with recessive spinocerebellar ataxia type 16 (OMIM #615768), carrying compound heterozygous mutations (c.355C>T, c.880A>T) in *STUB1*. Genomic integrity of the iPSC line HIHCNi001-A without transgene integration and genomic aberration but with maintained disease-relevant mutations was proven by SNP array analysis and Sanger sequencing while pluripotency was verified by the expression of important pluripotency markers and the capacity to differentiate into cells of all three germ layers.

Resource table.

Unique stem cell line identifier	HIHCNi001-A
Alternative name(s) of stem cell line	iPSC-STUB1
Institution	Hertie Institute for Clinical Brain Research and German Center for Neurodegenerative Diseases (DZNE), University of Tübingen, Germany
Contact information of distributor	Stefan Hauser, Stefan.hauser@dzne.de
Type of cell line	Induced pluripotent stem cell (iPSC)
Origin	Human
Additional origin info	12 years, male
Cell Source	Fibroblasts
Clonality	clonal
Method of reprogramming	Non-integrating episomal plasmids
Genetic Modification	NO
Type of Modification	N/A
Associated disease	Spinocerebellar ataxia, autosomal recessive 16 (SCAR16), OMIM #615768
Gene/locus	*STUB1*, c.[355C>T]; c.[880A>T]
Method of modification	N/A
Name of transgene or resistance	N/A
Inducible/constitutive system	N/A
Date archived/stock date	December 2016
Cell line repository/bank	N/A
Ethical approval	Institutional Review Board of the Medical Faculty, University of Tübingen Approval Number: 598/2011BO1

Resource utility

CHIP is a central component of cellular protein homeostasis and interacts with several key proteins associated with neurodegenerative diseases, with mutations in *STUB1* leading to SCAR16 (Hayer et al., 2017; Synofzik et al., 2014). iPSC-derived neurons will help to further decipher the exact role of this neurodegenerative key protein, including central steps in the pathogenesis of SCAR16.

Resource details

HIHCNi001-A was generated by reprogramming fibroblasts cultured from a skin biopsy of a 12 year old boy suffering from autosomal recessive spinocerebellar ataxia type 16 (SCAR16). SCAR16 patients develop a severe early-onset multi-systemic neurodegenerative disorder resulting in a broad phenotypic spectrum, including cerebellar ataxia, spasticity, epilepsy and hypogonadism. While it is of high interest to determine the pathophysiological role of CHIP, the protein encoded by *STUB1*, it is also a promising possible key player of neurodegeneration as it interacts with *inter alia* α-Synuclein, LRRK2, Huntingtin, Ataxin-3 and Tau. Our patient carried two heterozygous mutations c.355C >T and c.880A >T in the *STUB1* gene leading to a premature stop p. Arg119* and an amino acid exchange p.Ile294Phe on the protein level. Compound heterozygosity of the mutations was shown by segregation analysis (Hayer et al., 2017). Fibroblasts were reprogrammed by the delivery of episomal plasmids encoding human OCT4, SOX2, KLF4, L-MYC (OSKM) and LIN28 (Okita et al., 2011). iPSCs exhibited a morphology

* Corresponding author.
E-mail address: stefan.hauser@dzne.de. (S. Hauser).

https://doi.org/10.1016/j.scr.2018.04.001

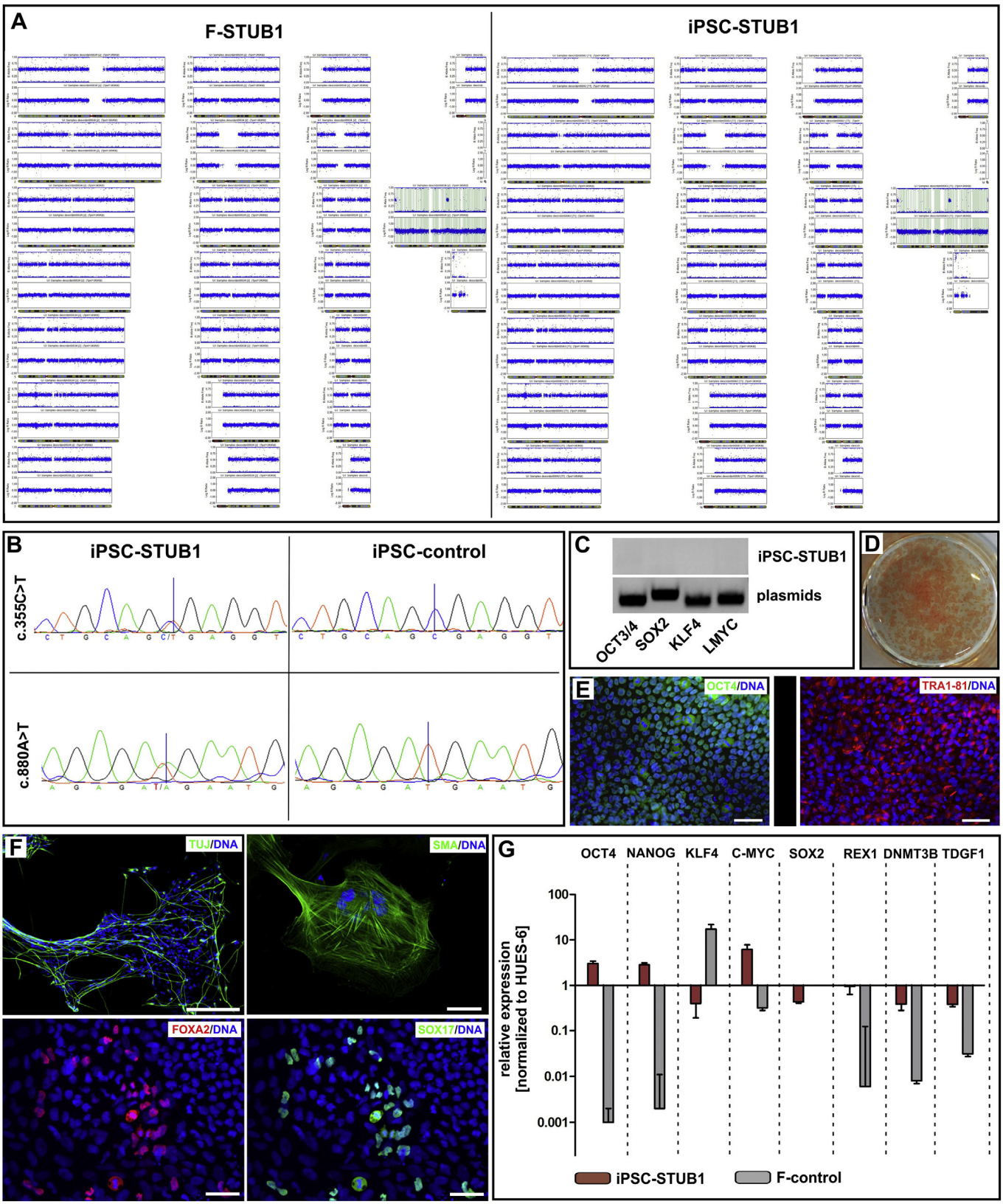

Fig. 1. Characterization and validation of HIHCNi001-A.

similar to those of human embryonic stem cells and were assessed after manual picking and expansion for several passages. Cells expressed pluripotency-associated surface markers such as alkaline phosphatase (Fig. 1D) and did not express exogenous reprogramming factors after passage 5 (Fig. 1C). Endogenous expression of pluripotency genes OCT4 and TRA1-81 on protein level was verified by immunocytochemistry (Fig. 1E). OCT4, NANOG, KLF4, c-MYC, SOX2, REX1, DNMT3B and TDGF1 were further verified on transcript level *via* qRT-PCR to have a

Table 1
Characterization and validation.

Classification	Test	Result	Data
Morphology	Photography	Normal	Not shown, available with author
Phenotype	Qualitative analysis	Immunocytochemistry of pluripotency markers: OCT4, TRA1-81	Fig. 1 panel E
	Quantitative analysis	qRT-PCR for OCT4, NANOG, KLF4, c-MYC, SOX2, REX1, DNMT3B and TDGF1	Fig. 1 panel G
Genotype/identity	Whole genome SNP genotyping with Infinium OmniExpressExome-8 BeadChip (Illumina) Spacing (kb): Mean: 3,03, Median: 1,36	No larger chromosomal aberrations or copy number variations; Genotype 46, XY	Fig. 1 panel A
Mutation analysis	Sequencing	Compound heterozygous, c.355C>T and c.880A>T	Fig. 1 panel B
	Southern Blot OR WGS	N/A	
Microbiology and virology	Mycoplasma	Mycoplasma testing by RT-PCR, negative	Supplementary file 1
Differentiation potential	Embryoid body formation	Smooth muscle actin (SMA), β-tubulin (TUJ) and FOXA2, SOX17	Fig. 1 panel F
Donor screening	HIV 1 + 2 Hepatitis B, Hepatitis C	N/A	
Genotype additional info	Blood group genotyping	N/A	
	HLA tissue typing	N/A	

similar expression compared to the human embryonic stem cell line HUES 6 and a discriminative expression pattern compared to fibroblasts (Fig. 1G). Pluripotency was further demonstrated by embryoid-body-based differentiation to endodermal, mesodermal and ectodermal cell lineage (Fig. 1F). Genomic integrity was confirmed by SNP genotyping (Fig. 1A) and Sanger sequencing of the mutation site (Fig. 1B) of both original fibroblasts and generated iPSCs. The cell line was confirmed to be mycoplasma-free (Suppl. Fig. 1).

Materials and methods

Culturing and reprogramming fibroblasts

Human dermal fibroblasts were cultured in fibroblast culture medium [DMEM high glucose (Life Technologies) + 10% FBS (Life Technologies)] for 10 days at 37 °C, 5% CO_2. Reprogramming was achieved by nucleofection with the episomal plasmids pCXLE-hUL, pCXLE-hSK and pCXLE-hOCT4 as described by Okita et al. Briefly, 10^5 cells were nucleofected with 1 μg of each plasmid. After electroporation, fibroblasts were cultivated in fibroblast medium before adding FGF2 (2 ng/ml (Peprotech)) on day 2. The following day, medium was changed to Essential 8 (E8) medium with 100 μM NaB (Sigma-Aldrich). After 3–4 weeks with medium change every other day, colonies were picked and expanded on matrigel-coated plates in E8 medium. After ≥5 passages, iPSCs were genomically and functionally analysed, passaged or frozen in E8 medium with 40% KO-SR (Life Technologies), 10% DMSO (Sigma-Aldrich) and 1 μM Y-27632 (Abcam Biochemicals) (Table 1).

Genomic integrity analysis

To verify genomic integrity, DNA of iPSCs and fibroblasts was isolated with DNeasy Blood & Tissue Kit (Qiagen) according to the manufacturer's instructions. Whole-genome SNP genotyping was conducted

Table 2
Reagents details.

Antibodies used for immunocytochemistry

	Antibody	Dilution	Company Cat # and RRID
Pluripotency markers	Goat anti-OCT4	1:100	Santa Cruz, AB_653551
	Mouse anti-TRA1-81	1:500	Millipore, AB_177638
In vitro differentiation	Mouse anti-SMA	1:100	Dako, AB_2223500
	goat anti-SOX17	1:250	R&D Systems, AB_355060
	rabbit anti-FOX-A2	1:300	Millipore, AB_390153
	mouse anti-TUJ	1:1000	Sigma Aldrich, AB_477590
Secondary antibodies	Alexa Fluor 488 Donkey anti-Goat IgG	1:300	Life Technologies
	Alexa Fluor 488 Goat anti-Rabbit IgG	1:300	Life Technologies
	Alexa Fluor 488 Goat anti-Mouse IgG	1:300	Life Technologies
	Alexa Fluor 568 Goat anti-Mouse IgG	1:300	Life Technologies
	Alexa Fluor 568 Goat anti-Rabbit igG	1:300	Life Technologies

Primers

	Target	Forward primer	Reverse primer (5′–3′)
Episomal plasmids	KLF4	CCACCTCGCCTTACACATGAAG	TAGCGTAAAAGGAGCAACATAG
	L-MYC	GGCTGAGAAGAGGATGGCTAC T	TTTGTTTGACAGGAGCGACAA
	OCT3/4	CATTCAAACTGAGGTAAGGG	TAGCGTAAAAGGAGCAACATAG
	SOX2	TTCACATGTCCCAGCACTACCAG	TTTGTTTGACAGGAGCGACAAT
Pluripotency markers (qPCR)	c-MYC	ATTCTCTGCTCTCCTCGACG	CTGTGAGGAGGTTTGCTGTG
	DNMT3B	ACGACACAGAGGACACACAT	AAGCCCTTGATCTTTCCCCA
	KLF4	CCATCTTTCTCCACGTTCGC	CGTTGAACTCCTCGGTCTCT
	NANOG	CAAAGGCAAACAACCCACTT	TGCGTCACACCATTGCTATT
	OCT4	GGAAGGTATTCAGCCAAACG	CTCCAGGTTGCCTCTCACTC
	SOX2	TGATGGAGACGGAGCTGAAG	GCTTGCTGATCTCCGAGTTG
	TDGF1	GGTCTGTGCCCCATGACA	AGTTCTGGAGTCCTGGAAGC
Housekeeping gene (qPCR)	GAPDH	AGGTCGGAGTCAACGGATTT	ATCTCGCTCCTGGAAGATGG
Targeted sequencing	Mutation_1	GCTACCTGAAGATGCAGCAG	TGAGCCTGGAGAGGTAAGAG
	Mutation_2	GTGCAGTGCCCCTTTTCAG	GTCCAACAGCAGAACTTGGG

using Infinium OmniExpressExome-8-BeadChip (Illumina) and GenomeStudio V2.0.3 (Illumina) for evaluation. Copy number analysis was performed using CNVPartition plugin (Illumina). Early mosaicism states were evaluated by manual review on B allele frequency plots on chromosomal level. DNA was also sequenced for both mutations in *STUB1* using mutation-specific primers (Table 2) according to standard procedures, using 3130xl Genetic Analyzer (Applied Biosystems) and Staden 2.0.0b10 (Staden Sourceforge) for visualisation. To verify non-integration of plasmids, RT-PCR was performed with plasmid-specific primers (Table 2).

Pluripotency assessment

iPSCs were fixed with 4% paraformaldehyde (PFA) and either assessed for alkaline phosphatase expression or permeabilized with 0.1% Triton X-100, blocked with 5% FBS and stained overnight at 4 °C with primary antibodies for immunocytochemical analysis (Table 2). Samples were visualized after staining with Alexa Fluor 488- or 568-conjugated secondary antibodies (Table 2) for 1 h at room temperature. Nuclei were counterstained with Hoechst 33,342 (1:10.000, Invitrogen). Samples were embedded in ProLong Gold Antifade Reagent (Life Technologies) and observed with AxioImager Z1 (Zeiss). On transcript level, qRT-PCR with primers specific for pluripotency genes (Table 2) was performed: RNA was extracted with High Pure RNA Isolation Kit (Roche) according to manufacturer's instructions and reverse-transcribed to cDNA, using Transcriptor High Fidelity cDNA Synthesis Kit (Roche). qRT-PCR was performed as triplicates with LightCycler 480 SYBR Green I Master (Roche). Normalization of C_T values for GAPDH and the reference hESC line HUES6 was achieved by using the $2^{-\Delta\Delta Ct}$ method. Pluripotency was further confirmed by embryoid-body based differentiation by cultivating iPSCs in EB medium (80% DMEM/F12 (Life Technologies), 20% KO-SR, 1× NEAA (Sigma-Aldrich), 1× Penicillin-Streptomycin (Merck Millipore), 2 mM L-Glutamine (Gibco), 0.1 mM β-Mercaptoethanol (Merck)) on AggreWell 800 Plates (StemCell Technologies) with medium change on day 2. Embroid bodies were collected on day 4 and plated onto 0.1% gelatine- or matrigel-coated plates, for *endo*- and mesodermal or ectodermal differentiation, respectively. Cells were cultivated for 2–3 weeks with medium change every other day and immunocytochemically stained for SMA, TUJ, FOXA2 and SOX17 (Table 2).

Supplementary data to this article can be found online at https://doi.org/10.1016/j.scr.2018.04.001.

Acknowledgements

cDNA of the cell line HUES6 was kindly provided by the MPI for Molecular Medicine, Münster, Germany. M.S. was supported by a grant from the Else Kröner Fresenius Stiftung.

References

Hayer, S.N., Deconinck, T., Bender, B., Smets, K., Zuchner, S., Reich, S., et al., 2017. STUB1/CHIP mutations cause Gordon Holmes syndrome as part of a widespread multisystemic neurodegeneration: evidence from four novel mutations. Orphanet J. Rare Dis. 12 (1), 31.

Okita, K., Matsumura, Y., Sato, Y., Okada, A., Morizane, A., Okamoto, S., et al., 2011. A more efficient method to generate integration-free human iPS cells. Nat. Methods 8 (5), 409–412.

Synofzik, M., Schüle, R., Schulze, M., Gburek-Augustat, J., Schweizer, R., Schirmacher, A., et al., 2014. Phenotype and frequency of STUB1 mutations: next-generation screenings in Caucasian ataxia and spastic paraplegia cohorts. Orphanet J. Rare Dis. 9, 57.

Generation of a homozygous CRISPR/Cas9-mediated knockout human iPSC line for the *STUB1* locus.

Schuster S, Saravanakumar S, Schöls L, Hauser S (2019). Generation of a homozygous CRISPR/Cas9-mediated knockout human iPSC line for the *STUB1* locus. *Stem Cell Res,* 34:101378.

Stem Cell Research 34 (2019) 101378

Contents lists available at ScienceDirect

Stem Cell Research

journal homepage: www.elsevier.com/locate/scr

Lab resource: Stem Cell Line

Generation of a homozygous CRISPR/Cas9-mediated knockout human iPSC line for the *STUB1* locus

Stefanie Schuster[a,b,c], Srinethe Saravanakumar[a], Ludger Schöls[a,b], Stefan Hauser[b,*]

[a] Hertie Institute for Clinical Brain Research, University of Tübingen, Tübingen, Germany
[b] German Center for Neurodegenerative Diseases (DZNE), Tübingen, Germany
[c] Graduate School of Cellular and Molecular Neuroscience, University of Tübingen, Tübingen, Germany

A B S T R A C T

STUB1/CHIP is a central component of cellular protein homeostasis and interacts with key proteins involved in the pathogenesis of many neurodegenerative diseases. Missense and truncating mutations in *STUB1* lead to SCAR16. For ideal *in vitro* disease modelling with isogenic controls, we generated a CHIP knockout cell line from a healthy control with no CHIP functionality, but remaining genomic integrity and verified pluripotency.

Resource table

Unique stem cell line identifier	HIHCNi004-A-1
Alternative name(s) of stem cell line	iPSC-STUB1_KO
Institution	Hertie Institute for Clinical Brain Research, University of Tübingen, and German Center for Neurodegenerative Diseases (DZNE), Germany
Contact information of distributor	Stefanie Schuster Stefanie.schuster@klinikum.uni-tuebingen.de Ludger Schöls ludger.schoels@uni-tuebingen.de
Type of cell line	iPSC
Origin	Human
Additional origin info	Female, 37 years
Cell Source	Fibroblasts
Clonality	Clonal
Method of reprogramming	Non-integrating episomal plasmids
Genetic Modification	YES
Type of Modification	CRISPR/Cas9-mediated gene knockout
Associated disease	Spinocerebellar ataxia, autosomal recessive 16 (SCAR16), OMIM #615768
Gene/locus	*STUB1*; c.283-438del, p.Val94Alafs*5 (homozygous)
Method of modification	CRISPR/Cas9
Name of transgene or resistance	N/A
Inducible/constitutive system	N/A
Date archived/stock date	September 2018
Cell line repository/bank	N/A
Ethical approval	Institutional Review Board of the Medical Faculty, University of Tübingen Approval Number: 598/2011BO1

Resource utility

CHIP is a central component of cellular protein homeostasis and interacts with several key proteins associated with neurodegenerative diseases, with mutations in *STUB1* leading to SCAR16. For ideal *in vitro* disease modelling with isogenic controls, we generated a CHIP knockout cell line with no CHIP functionality.

Resource details

A skin biopsy was obtained from a healthy 37-year old woman (Control, CO) and cultured fibroblasts were reprogrammed by the delivery of episomal plasmids encoding human OCT4, SOX2, KLF4, L-MYC and LIN28. iPSCs exhibited a morphology similar to those of human embryonic stem cells (hESCs) and were assessed after manual picking and expansion for several passages. iPSC-CO (HIHCNi004-A) were then nucleofected with two crRNA-Atto550 tracrRNA RNP complexes targeting exon 2 and 3 of *STUB1*, followed by fluorescence-activated cell sorting (FACS) of Atto550^{+}-cells, single cell seeding and manual picking. Homozygous knock-out state was confirmed to be c.283-438del, p.Val94Alafs*5 (Fig. 1B), leading to nonsense-mediated decay and a loss of CHIP protein as shown by protein expression analysis (Suppl. Fig. 1) (Table 1).

iPSC-STUB1_KO (HIHCNi004-A-1) was verified to be pluripotent by the expression of pluripotency-associated surface markers such as

* Corresponding author.
E-mail address: stefan.hauser@dzne.de (S. Hauser).

https://doi.org/10.1016/j.scr.2018.101378
Received 16 November 2018; Received in revised form 17 December 2018; Accepted 20 December 2018
Available online 21 December 2018

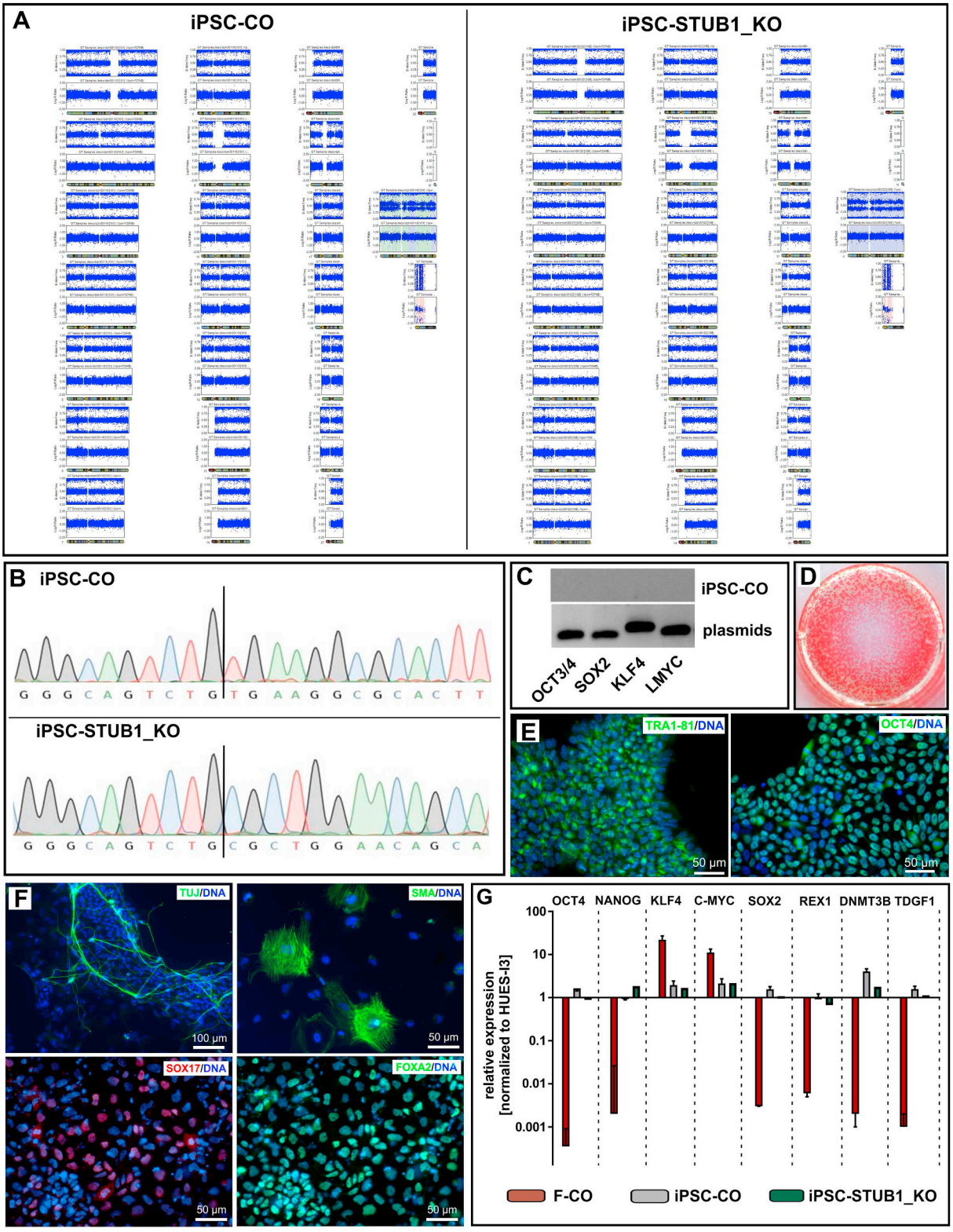

Fig. 1. Characterization and validation of HIHCNi004-A-1.

alkaline phosphatase (Fig. 1D), the absence of exogenous reprogramming factors after passage 5 (Fig. 1C) and the expression of endogenous pluripotency genes OCT4 and TRA1–81 on protein level as shown by immunocytochemistry (Fig. 1E). OCT4, NANOG, KLF4, c-MYC, SOX2, REX1, DNMT3B and TDGF1 were further transcriptionally expressed in a similar pattern compared to the hESC line HUES-I3 and the original iPSC line iPSC-CO (Fig. 1G). Pluripotency was furthermore demonstrated by embryoid body-based differentiation to endodermal, mesodermal and ectodermal cell lineage (Fig. 1F). Genomic integrity was confirmed by whole genome SNP genotyping (Fig. 1A). Top 5 off-target

Table 1
Characterization and validation.

Classification	Test	Result	Data
Morphology	Photography	Normal	Supplementary file 2
Phenotype	Qualitative analysis	Immunocytochemistry of pluripotency markers OCT4 and TRA1–81; Expression of alkaline phosphatase	Fig. 1 panel E Fig. 1 panel D
	Quantitative analysis	qRT-PCR for OCT4, NANOG, KLF4, c-MYC, SOX2, REX1, DNMT3B and TDGF1	Fig. 1 panel G
Genotype	Whole genome SNP genotyping with Infinium OmniExpressExome-8 BeadChip (Illumina) Spacing (kb): Mean: 3,03; Median: 1,36	No larger chromosomal aberrations or copy number variations upon CRISPR/Cas9 mediated genome editing	Fig. 1 panel A
Identity	STR analysis	7 sites; F-CO, iPSC-CO and iPSC-STUB1_KO all matched	Submitted in archive with journal
Mutation analysis	Sequencing	c.283-438del p.Val94Alafs*5	Fig. 1 panel B
	Southern Blot OR WGS	N/A	
Microbiology and virology	Mycoplasma	Mycoplasma testing by RT-PCR, negative	Supplementary file 3
Differentiation potential	Embryoid body formation	Smooth muscle actin (SMA), β-tubulin (TUJ) and FOXA2, SOX17	Fig. 1 panel F
Donor screening	HIV 1 + 2 Hepatitis B, Hepatitis C	N/A	N/A
Genotype additional info	Blood group genotyping	N/A	N/A
	HLA tissue typing	N/A	N/A

Table 2
Reagents details.

Antibodies used for immunocytochemistry and Western Blotting

	Antibody	Dilution	Company Cat # and RRID
Pluripotency Markers	Rabbit anti-OCT4	1:100	Proteintech, AB_2167545 Millipore, AB_177638
	Mouse anti-TRA1–81	1:500	
In vitro Differentiation	Mouse anti-SMA	1:100	Dako, AB_2223500 R&D Systems, AB_355060
	goat anti-SOX17	1:250	
	rabbit anti-FOX-A2	1:300	Millipore, AB_390153 Sigma Aldrich, AB_477590
	mouse anti-TUJ	1:1000	
Western Blotting	Rabbit anti-CHIP	1:10.000	Abcam, AB_2751008 Meridian Life Science, AB_151542
	Mouse anti-GAPDH	1:10.000	
Secondary antibodies	Alexa Fluor 488 Goat anti-Mouse IgG	1:1000	Life Technologies
	Alexa Fluor 488 Goat anti-Rabbit IgG	1:1000	Life Technologies
	Alexa Fluor 488 Donkey anti-Rabbit IgG	1:1000	Life Technologies
	Alexa Fluor 568 Donkey anti-Goat IgG	1:1000	Life Technologies
	Peroxidase-conjugated AffiniPure goat anti mouse	1:10.000	Jackson ImmunoResearch
	Peroxidase-conjugated AffiniPure goat anti-rabbit	1:10.000	Jackson ImmunoResearch

Primers

	Target	Forward primer Reverse primer (5′-3′)
Episomal Plasmids	KLF4	CCACCTCGCCTTACACATGAAG TAGCGTAAAAGGAGCAACATAG
	L-MYC	GGCTGAGAAGAGGATGGCTAC TTTGTTTGACAGGAGCGACAAT
	OCT3/4	CATTCAAACTGAGGTAAGGG TAGCGTAAAAGGAGCAACATAG
	SOX2	TTCACATGTCCCAGCACTACCAG TTTGTTTGACAGGAGCGACAAT
Pluripotency Markers (qPCR)	c-MYC	GACTCTGAGGAGGAACAAGA TGATCCAGACTCTGACCTTT
	DNMT3B	GAGTATCAGGATGGGAAGGA ATAGCCTGTCGCTTGGA
	KLF4	CCATCTTTCTCCACGTTCGC CGTTGAACTCCTCGGTCTCT
	NANOG	CAAAGGCAAACAACCCACTT TGCGTCACACCATTGCTATT
	OCT4	GGAAGGTATTCAGCCAAACG CTCCAGGTTGCCTCTCACTC
	SOX2	TGATGGAGACGGAGCTGAAG GCTTGCTGATCTCCGAGTTG
	TDGF1	GGTCTGTGCCCCATGACA AGTTCTGGAGTCCTGGAAGC
Housekeeping Gene (qPCR)	GAPDH	AGGTCGGAGTCAACGGATTT ATCTCGCTCCTGGAAGATGG
Targeted sequencing of CHIP KO	CHIP	TGATTCTAGCCAGAGCGCAG TCGGGAGTCGGTGATTCAGA

CRISPR Guide RNAs

	Target	Sequence PAM Sequence
crRNAs	CHIP exon 2	GCTGGACGGGCAGTCTGTGA AGG
	CHIP exon 3	GAATCGCGAAGAAGAAGCGC TGG

effects of Cas9 for both crRNAs were excluded by Sanger sequencing (data not shown). The cell line was confirmed to be mycoplasma-free (Suppl. Fig.3). STR analysis of 7 loci confirmed cell identity of fibroblasts, iPSC-CO and iPSC-STUB1_KO.

In summary, we have generated a human disease-specific homozygous CHIP knockout iPSC line. This will serve, together with patient-derived generated iPSCs (Schuster et al., 2018), as an ideal tool for *in vitro* disease modelling and pathological study of SCAR16.

Materials and methods

Fibroblast reprogramming

For reprogramming, 10^5 human dermal fibroblasts were nucleofected with 1 µg of each episomal plasmid pCXLE-hUL, pCXLE-hSK and pCXLE-hOCT4, as described by Okita et al., 2011 After electroporation, fibroblasts were cultivated in fibroblast medium [DMEM high glucose +10% FBS (Life Technologies)] before adding FGF2 (2 ng/ml (Peprotech)) on day 2. The following day, medium was changed to Essential 8 (E8) medium with 100 µM NaB (Sigma-Aldrich). After 3–4 weeks with medium change every other day, colonies were picked and expanded on matrigel-coated plates in E8 medium. iPSCs were frozen in E8 medium with 40% KO-SR (Life Technologies), 10% DMSO (Sigma-Aldrich) and 1 µM Y-27632 (Abcam Biochemicals).

CRISPR/Cas9-mediated gene knockout

For *STUB1*/CHIP knockout, 6×10^5 iPSC-CO cells of passage 14 were nucleofected with two crRNA-Atto550 tracrRNA RNP complexes (Table 2) (Integrated DNA Technologies) in Amaxa Nucleofection Solution (Lonza) with supplement, followed by FACS of Atto550$^+$-iPSCs, single-cell seeding and picking after 5–8 days. Homozygous knockout state was confirmed by PCR analysis of DNA and Sanger sequencing using knockout-specific primers (Table 2) according to standard procedures, using 3130xl Genetic Analyzer (Applied Biosystems) and CRISP-ID (Dehairs et al., 2016) for visualisation. Top 5 off-target effects were excluded for both crRNAs by Sanger sequencing (data not shown).

Genomic integrity analysis

To verify genomic integrity, DNA of iPSC-CO and iPSC-STUB1_KO was isolated with DNeasy Blood & Tissue Kit (Qiagen) according to manufacturer's instructions. Whole-genome SNP genotyping was conducted using Infinium OmniExpressExome-8-BeadChip (Illumina) and GenomeStudio V2.0.3 for evaluation. Copy number analysis was performed using CNVPartition plugin (Illumina). Early mosaicism states were evaluated by manual review on B-allele frequency plots on chromosomal level. STR analysis of 7 loci confirmed cell identity. To verify non-integration of plasmids, RT-PCR was performed with plasmid-specific primers (Table 2).

Pluripotency assessment

iPSCs were fixed with 4% PFA and assessed for alkaline phosphatase expression. For immunocytochemical analysis, fixed iPSCs were permeabilized and blocked, followed by overnight staining with primary antibodies at 4 °C and staining with Alexa Fluor 488- or 568-conjugated secondary antibodies (Table 2) for 1 h at room temperature. Nuclei were counterstained with Hoechst 33342 (1:10.000, Invitrogen). Immunofluorescence was visualized with AxioImager Z1 (Zeiss).

On transcript level, qRT-PCR with pluripotency genes-specific primers (Table 2) was performed: RNA was extracted with High Pure RNA Isolation Kit (Roche) according to manufacturer's instructions and reverse-transcribed to cDNA, using Transcriptor High Fidelity cDNA Synthesis Kit (Roche). qRT-PCR was performed as triplicates with SYBR Select Master Mix (Applied Biosystems). C_T values were normalized to GAPDH and the reference hESC line I3 with the $2^{-\Delta\Delta Ct}$ method. Pluripotency was further confirmed by embryoid body-based differentiation by cultivating iPSCs in EB medium (80% DMEM/F12 (Life Technologies), 20% KO-SR, 1× NEAA (Sigma-Aldrich), 1× Penicillin-Streptomycin (Merck Millipore), 2 mM L-Glutamine (Gibco), 0.1 mM β-Mercaptoethanol (Merck)) on AggreWell800 Plates (StemCell Technologies) with medium change on day 2. Embryoid bodies were collected (day 4) and plated onto 0.1% gelatine- or matrigel-coated plates, for *endo*- and mesodermal or ectodermal differentiation, respectively. Cells were cultivated for 2–3 weeks and immunocytochemically stained for SMA, TUJ, FOXA2 and SOX17 (Table 2).

Acknowledgements

cDNA of the human embryonic cell line I3 was kindly provided by the Institute of Reconstructive Neurobiology, Bonn, Germany.

Appendix A. Supplementary data

Supplementary data to this article can be found online at https://doi.org/10.1016/j.scr.2018.101378.

References

Dehairs, J., Talebi, A., Cherifi, Y., Swimmen, J.V., 2016. CRISP-ID: decoding CRISPR mediated indels by Sanger sequencing. Sci. Rep. 6, 28973.

Okita, K., Matsumura, Y., Sato, Y., Okada, A., Morizane, A., Okamoto, S., et al., 2011. A more efficient method to generate integration-free human iPS cells. Nat. Methods 8 (5), 409–412.

Schuster, S., Schelling, Y., Synofzik, M., Höflinger, P., Schöls, L., Hauser, S., 2018. Establishment of STUB1/CHIP mutant induced pluripotent stem cells (iPSCs) from a patient with Gordon Holmes syndrome/SCAR16. Stem Cell Res. 29, 166–169.

CHIP mutations affect the heat shock response differently in human fibroblasts and iPSC-derived neurons.

Schuster S, Heuten E, Velic A, Admard J, Ossowski S, Synofzik M, Macek B, Hauser S, Schöls L (2020). CHIP mutations affect the heat shock response differently in human fibroblasts and iPSC-derived neurons. In preparation.

The effect of CHIP mutations on the heat shock response differs between SCAR16 patient fibroblasts and iPSC-derived neurons.

Schuster S[1,2,3], Heuten E[1], Velic A[4], Admard J[5], Ossowski S[5], Synofzik M[1], Macek B[4], Hauser S[2,*], Schöls L[1,2,*].

1. Department of Neurology and Hertie Institute for Clinical Brain Research, University of Tübingen, Tübingen, Germany.
2. German Center for Neurodegenerative Diseases (DZNE), Tübingen, Germany.
3. Graduate School of Cellular and Molecular Neuroscience, University of Tübingen, Tübingen, Germany.
4. Proteome Center Tübingen, University of Tübingen, Tübingen, Germany.
5. Institute for Medical Genetics and Applied Genomics, University of Tübingen, Tübingen, Germany.

* these authors contributed equally to this work.

Correspondence: Stefan.hauser@dzne.de, ludger.schoels@uni-tuebingen.de

ABSTRACT

CHIP encoded by the gene *STUB1* is a co-chaperone and E3 ligase that acts as a key regulator of cellular protein homeostasis. Mutations in *STUB1* cause autosomal recessive spinocerebellar ataxia type 16 (SCAR16) with widespread neurodegeneration manifesting as spastic-ataxic gait disorder, dementia and epilepsy. CHIP$^{-/-}$ mice present display severe cerebellar atrophy, show high perinatal lethality and impaired heat stress tolerance. To decipher the pathomechanism underlying SCAR16 we investigated the heat shock response (HSR) in primary fibroblasts of SCAR16 patients. We found impaired HSR induction and recovery compared to healthy controls. HSPA1A/B transcript levels (coding for HSP70) were reduced upon heat shock but HSP70 protein levels were higher upon recovery in patient compared to control fibroblasts. As SCAR16 primarily affects the central nervous system we next investigated HSR in cortical neurons derived from iPSC lines of three patients with *STUB1* mutations. We found SCAR16 cortical neurons to be surprisingly resistant to heat stress. Neurons of both SCAR16 patients and healthy controls expressed high basal levels of HSP70 compared to fibroblasts. While heat stress resulted in strong increases of transcript levels of many HSPs, this did not translate into higher HSP70 protein levels upon heat shock independent of *STUB1* mutations. In addition, the HSR was similar in neurons from a homozygous *STUB1* knockout generated by CRISPR/Cas9-mediated genome editing from an isogenic healthy control line. Proteomic analysis of cortical neurons showed dysfunctional protein (re)folding and a higher basal oxidative stress level in patients. Our results question the role of impaired HSR in SCAR16 neuropathology and highlight the need for careful selection of proper cell types for modelling human diseases.

INTRODUCTION

Mutations in *STUB1 (STIP1 homology and U-box containing protein 1)* cause early-onset autosomal recessive cerebellar ataxia type 16 (OMIM 615768), a movement disorder that is characterized by atrophy of the cerebellum, brain stem and spinal cord, leading to loss of muscle coordination, unsteady gait, impaired fine motor skills and a slurry speech (Shi *et al.*, 2013; Bettencourt *et al.*, 2015). Recently, patients with *STUB1* ataxia were shown to present a broader neurodegeneration with complex clinical phenotypes of cognitive impairment, epilepsy and hypogonadism in addition to spastic-ataxic movement disorder (Shi *et al.*, 2013; Heimdal *et al.*,

2014; Shi *et al.*, 2014; Synofzik *et al.*, 2014; Hayer *et al.*, 2017). *STUB1* codes for the 'C-terminus of HSC70-interacting protein' (CHIP) which plays an important role in protein quality control. Its two major functions are linked to two distinct structural domains: Via its tetratricopeptide repeat (TPR) domain, CHIP acts as a co-chaperone of HSC70/HSP70 and HSP90 and inhibits ATPase and refolding activity (Ballinger *et al.*, 1999). Via its U box domain, it acts as an E3 ligase tagging chaperone-bound but also other substrates with ubiquitin (Jiang *et al.*, 2001; Murata *et al.*, 2003). Degradation of those proteins or organelles occurs via the ubiquitin-proteasome system (UPS) or the autophagy-lysosome system (Zhang *et al.*, 2005; Yao, 2010; Guo *et al.*, 2015). Both mechanisms play a major role in protein quality control and sustain proper cellular homeostasis.

More recently, CHIP was identified as regulator of many other processes like TFEB activity and thereby macroautophagy regulation (Guo *et al.*, 2015; Sha *et al.*, 2017), necroptosis (Seo *et al.*, 2016; Tang *et al.*, 2018), cAMP and AMPK signaling (Schisler *et al.*, 2013; Rinaldi *et al.*, 2019), oxidative metabolism (Ravi *et al.*, 2018), chaperone-mediated autophagy (Ferreira *et al.*, 2015) and neuronal preconditioning (Lizama *et al.*, 2018). In addition to this, CHIP was shown to be cytoprotective in many forms of neurodegeneration by degrading *inter alia* α-synuclein (Shin *et al.*, 2005; Tetzlaff *et al.*, 2008), LRRK2 (Ding *et al.*, 2009), APP and BACE1 (Kumar *et al.*, 2007; Singh *et al.*, 2015) as well as huntingtin (Jana *et al.*, 2005; Miller *et al.*, 2005). This leads to the assumption that CHIP may be a key player of neurodegeneration and a promising target for the treatment of many neurodegenerative diseases. Furthermore, CHIP was previously linked to cardiac and muscular disorders and several different types of cancers (reviewed by Joshi *et al.*, 2016).

CHIP expression is highest in tissues with high metabolic activity, i.e. heart, skeletal muscle and brain (Ballinger *et al.*, 1999). In mouse brains, CHIP is expressed primarily in neurons of the cerebellum, pons, medulla oblongata, hippocampus and cerebral cortex (Sahara *et al.*, 2005; Anderson *et al.*, 2010). $CHIP^{-/-}$ mice display severe cerebellar atrophy specifically in the Purkinje cell layer, with a distinct motor impairment phenotype. Furthermore, CHIP knockout mice were shown to have decreased stress tolerance and increased age-related phenotypes leading to decreased lifespan and a gonadal dysfunction (Dai *et al.*, 2003; Min *et al.*, 2008; Shi *et al.*, 2014). Upon thermal challenge, 100% of $CHIP^{-/-}$ mice die during heat shock or shortly after (Dai *et al.*, 2003), suggesting a key role of CHIP in stress response, and more specifically the heat shock response (HSR).

Environmental stressors such as heat, heavy metals and reactive oxygen species, but also pathophysiological stressors such as protein aggregation, inflammation and tissue injury can induce HSR, which is characterized by the rapid increase of heat shock protein expression (reviewed by Richter *et al.*, 2010). This induction of heat shock proteins is regulated by the key transcription factor heat shock factor 1 (HSF1). Under basal conditions, HSF1 is present in the cytoplasm in its inactive monomeric form, shielded by HSC70/HSP70 and HSP90 (Abravaya *et al.*, 1991). Upon stress, the chaperones blocking HSF1 are recruited to the site of accumulating misfolded proteins, thereby releasing HSF1 (Santoro, 2000). HSF1 quickly trimerizes, undergoes post-translational modifications that modulate its activity and translocates to the nucleus (Sarge *et al.*, 1993). Here it binds to heat shock responsive elements, leading to transcription of heat shock proteins such as *HSPA1A/B* (encoding HSP70) and *DNAJB1* (encoding HSP40) that act to refold or clear misfolded proteins and confer cytoprotection (reviewed by Richter *et al.*, 2010). Other small HSPs (sHSPs) like HSPB1, HSPB5 and HSPB8 assist by binding to unfolded proteins

to prevent aggregation (Acunzo *et al.*, 2012). Once cellular homeostasis is reestablished, free HSPs inhibit HSF1 and attenuate the HSR (Abravaya *et al.*, 1991; Baler *et al.*, 1992; Vjestica *et al.*, 2013), allowing a tight regulation of protein quality control during stress conditions.
CHIP was shown to directly interact with HSF1 upon stress induction, co-translocating from the cytoplasm to the nucleus and thereby increasing HSP70 expression in non-neuronal cell types like fibroblasts, HEK cells and retinal epithelium cells, with no or a reduced response in $CHIP^{-/-}$ or $CHIP^{mut}$ cells (Dai *et al.*, 2003; Kim *et al.*, 2005; Qian *et al.*, 2006). Furthermore, CHIP expression is required for HSP70 turnover upon recovery (Qian *et al.*, 2006). Dai and colleagues also showed that HSP70 expression upon heat shock in $CHIP^{-/-}$ mice was strongly reduced compared to wildtype in most tissues, with almost complete absence of HSP70 in brain, heart and spleen (Dai *et al.*, 2003).
To understand the pathomechanism induced by mutant *STUB1*, we assessed HSR in fibroblasts of 3 SCAR16 patients and 3 healthy controls and found an impaired HSR in patients. To reflect the central nervous system as the major focus of disease in SCAR16, we next investigated HSR in cortical neurons (CN) generated from iPSCs. While heat stress resulted in increased transcript levels of HSPs, this surprisingly did not translate into higher protein levels of HSP70. Proteomic analysis of patient and control CN showed disturbances in protein folding, the ubiquitin system and oxidative stress response. Both approaches question the role of impaired HSR in SCAR16 neuropathology and highlight the need for careful selection of proper cell types for disease modelling.

MATERIALS & METHODS

Patients

Three patients with genetically confirmed compound heterozygous or homozygous mutations in *STUB1* were included in this study. Patient STUB1_1 had a homozygous c.367C>G; p.L123V mutation whereas patients STUB1_2 and STUB1_3 carried compound heterozygous mutations c.355C>T; p.R119*; c.880A>T, p.I294T and c.433A>C, p.K145Q; c.728C>T, p.P243L, respectively (Hayer *et al.*, 2017). All patients were severely affected by SCAR16 with ataxia (3/3), spasticity (3/3), epilepsy (2/3), dementia (2/3) and hypogonadism (1/3). The controls were age- and gender-matched for fibroblast analyses and gender-matched for induced pluripotent stem cell (iPSC)-derived neuronal analyses. Detailed information on study participants and cell lines is provided in Supplementary Table S1. The study has been approved by the Ethics Committee of the University of Tübingen (vote 598/2011BO1). Informed written consent was obtained from all participants or their legal guardian.

Fibroblast cultivation

Human dermal fibroblasts were obtained from skin biopsies and maintained at 37°C, 5% CO_2 and 100% relative humidity in fibroblast medium consisting of Dulbecco's Modified Eagle Medium (DMEM) (Merck Millipore) supplemented with 10% fetal bovine serum (FBS) (Thermo Fisher Scientific) in cell culture flasks. Upon reaching high confluency, cells were split by washing with PBS followed by 5 min trypsination and passaging into new flasks or seeding at a defined density depending on the assay (20.000 cells / cm^2 for immunocytochemical analysis; 30.000 cells / cm^2 for protein analysis).

Reprogramming of fibroblasts to iPSCs

Induced pluripotent stem cells were generated from fibroblasts according to a previously published protocol (Okita *et al.*, 2011) with minor modifications. In brief, 10^5 human dermal fibroblasts were nucleofected with 1 µg of each episomal plasmid (pCXLE-hUL, pCXLE-hSK and pCXLE-hOCT4 (Addgene)) with Nucleofector 2D (Lonza). Fibroblasts were cultivated in fibroblast medium before adding 2 ng/ml FGF2 (Peprotech) on day 2. The following day, medium was changed to Essential 8 (E8) medium [DMEM/F12 (Life Technologies), 64 mg/l L-Ascorbic acid 2-phosphate magnesium (Sigma Aldrich), 1% ITS-Supplement 100x (Life Technologies), 10 ng/ml FGF2, 2 ng/ml TGFß1 (Peprotech), 100 ng/ml Heparin (Sigma Aldrich)] with 100 µM NaB (Sigma-Aldrich). After 3–4 weeks with medium change every other day, colonies were manually picked and expanded onto Matrigel-coated plates (Corning) in a feeder-free system in E8 medium. iPSCs were frozen in E8 medium with 40% KO-SR (Life Technologies), 10% DMSO (Sigma Aldrich) and 10 µM Y-27632 (Selleckchem). Genomic integrity was confirmed by excluding plasmid integration and performing whole genome SNP genotyping (Infinium OmniExpressExome-8-BeadChip (Illumina) or CytoScan HD technology (Affymetrix)), Copy number analysis (CNVPartition plugin (Illumina)), and resequencing of the mutation sites. Pluripotency was confirmed by ALP expression, immunocytochemical analysis of pluripotency markers, transcript analysis of pluripotency genes and embryoid-body based differentiation of iPSCs into cells of all 3 germ layers. For detailed descriptions, see (2018).

Targeted *STUB1* Knockout with CRISPR/Cas9

To generate the *STUB1* knockout line STUB1(-/-), we targeted exon 2 and 3 of *STUB1* in a dual-cleavage approach to enhance efficiency of knockout generation. Crispr-RNAs (crRNAs) (Integrated DNA Technologies) were designed with the CRISPOR web-tool (Haeussler *et al.*, 2016). iPSCs of control line CO5 were nucleofected with two crRNA-ATTO550-tracrRNA (Integrated DNA Technologies) ribonucleoprotein (RNP) complexes with Cas9 protein (Integrated DNA Technologies) followed by fluorescence-activated cell sorting (FACS) of $ATTO550^+$ cells with Sony Cell Sorter SH800Z, single cell seeding and manual picking and expansion of clones. Homozygous or heterozygous knockout was validated by PCR analysis and Sanger Sequencing. Top 5 exonic off-target effects as predicted by CRISPOR for each cleavage site were excluded by Sanger sequencing in the isogenic control as well as the generated clones. For detailed experimental setup and characterization of STUB1(-/-), see (Schuster *et al.*, 2019).

Neuronal differentiation

To model SCAR16 *in vitro*, we generated neurons of cortical layer V and VI according to a published protocol (Shi *et al.*, 2012; Rehbach *et al.*, 2019) with modifications. In brief, iPSCs were dissociated with 0.02% EDTA (Carl Roth) in PBS (Sigma Aldrich) and seeded at a density of $3 \times 10^5/cm^2$ in E8 medium supplemented with 10 µM Y-27632. The following day, medium was replaced by neural induction medium (1:1 N2/B27, 500 nM LDN-193189 (Th. Geyer), 10 µM SB431542 (Sigma Aldrich)) with medium change every day. The neural induction medium was supplemented with 20 ng/ml FGF2 on day 8. The next day, cultures were split by detachment with Accutase (Sigma Aldrich) for 10 min and seeded in N2/B27 medium with 20 ng/ml FGF2 and 10 µM RI onto Matrigel-coated 6 well plates. N2/B27 medium with 20 ng/ml FGF2 was added on the next day. From day 11 onward, cells were cultured in N2/B27 medium with medium

change every other day. Neural precursors were dissociated and frozen on day 19. For maturation, frozen precursors were thawed and seeded in N2/B27 medium with 10 µM Y-27632, with medium change every other day. On day 26, cells were detached with Accutase and reseeded at the desired assay density (for immunocytochemical staining: 1 x 10^5/cm^2; for protein and RNA isolation: 4-6 x 10^5/cm^2) on Poly-L-Ornithine (Sigma Aldrich) and Matrigel-coated wells. On day 27 and 29, medium was changed to N2/B27 supplemented with 10 µM PD0325901 (Tocris) and 10 µM DAPT (Sigma Aldrich). From day 31 and up to the analysis on day 36, the cells were cultured in N2/B27 medium with medium changes every other day.
For heat shock experiments, cells were exposed to 42.5°C with prewarmed medium for 1h, with direct harvesting of cells for RNA isolation and protein fractionation and an additional 4, 8 or 24h recovery at 37°C for protein analysis.

Immunocytochemistry and image analysis

Cells were washed with PBS followed by fixation with 4% paraformaldehyde (PFA, Merck Millipore) and subsequent washing. Fixed cells were permeabilized and blocked with 5% BSA (Sigma Aldrich) in PBS with 0.1% Triton-X100 (Carl Roth). Afterwards, cells were stained with: anti-ß-III-tubulin (TUJ, mouse, 1:1000, T8660, Sigma Aldrich), anti-CTIP2 (rat, 1:200, ab18465, Abcam), anti-HSF1 (rabbit, 1:500, 4356T, Cell Signaling Technology) and/or anti-HSP70 (mouse, 1:500, ADI-SPA-810, Enzo Life Sciences); all followed by Alexa-Fluor conjugated secondary antibodies (Invitrogen). Hoechst 33258 staining (1:10.000, H1398, Invitrogen) was used to counterstain for nuclei. Coverslips were mounted with Dako Mounting Solution (Agilent Dako) onto microscope slides. 4-5 random fields per coverslip per cell line were used for quantification. Images were acquired using Observer Z1 fluorescence microscope (Carl Zeiss), exposure time was kept constant. Quantifications were conducted with the cell counter plugin in FiJi (Schindelin *et al.*, 2012) and threshold mask settings in ImageJ (https://imagej.nih.gov/ij/).

Transcript analysis by qRT-PCR

For RNA isolation, cells were scraped off in RLT buffer (Qiagen) and lysed in the well. RNA was isolated with RNeasy Mini kit (Qiagen) according to the manufacturer's instructions. A total of 500 ng RNA was reverse-transcribed into cDNA with RevertAid First Strand cDNA Synthesis Kit (Thermo Fisher Scientific) according to manufacturer's instructions. For real-time polymerase chain reaction, 3 µl of 1.25 ng/µl cDNA was mixed with 2 µl of 2 µM primer pairs and 5 µl of SYBR Green Select Master Mix (Applied Biosystems). Primers are listed in Supplementary Table S2. The qRT-PCR program was as follows: 50°C for 2 min, 95°C for 2 min, followed by 40 cycles of 95°C for 1s, 60°C for 30s and 72°C for 5s, and subsequently 95°C for 15s, 60°C for 1 min and 95°C for 15s. Specificity of PCR products was confirmed by melting curve analysis. Real-time PCR amplifications were performed on the Viia7 Real-Time PCR System (Applied Biosystems) and primers were run in triplicate. The house-keeping genes GAPDH and TBP were amplified to standardize the amount of sample cDNA. Analysis was performed with QuantStudio Software V1.3 (Thermo Fisher Scientific).

Cell viability analysis

Fibroblasts were seeded at a density of 12.5 x 10^4/cm^2 on 96 well plates in triplicate, CNs were seeded at a density of 3 x 10^5/cm^2 on D33 on 96 well plates coated with Poly-L-ornithine and

Matrigel in quadruplicate. To assess cell viability upon heat shock, CyQuant Direct Cell Proliferation Assay (Thermo Fisher Scientific) was used according to manufacturer's instructions. In brief, CQD nucleic acid stain and CQD background suppressor dye were diluted in PBS and added to the cells, followed by 1h incubation at 37°C. 1% Triton-X100 was used as negative control for cell viability. The plate reader SpectraMax M (Molecular Devices) was set to 42.5°C or 44°C and plates were measured for 6h with excitation/emission at 485/525 nm.

Protein isolation

Pellets of primary fibroblasts or CNs were lysed in RIPA buffer (Sigma Aldrich) containing 1x cOmplete protease inhibitor cocktail (PI) (Roche) for 45 min on a rotator at 4°C. Cell debris was pelleted at 15.800 x g at 4°C for 30 min. Protein concentration was determined using the Pierce BCA Protein Assay Kit (Thermo Fisher Scientific) according to manufacturer's instructions.

Subcellular fractionation

To separate nuclei from cytoplasm in CNs, a protocol by Abcam with slight modifications was applied. In brief, cells were scraped off on ice in fractionation buffer [20 mM HEPES (pH 7.4) (Carl Roth), 10 mM KCl (Carl Roth), 2 mM $MgCl_2$ (Merck Millipore), 1 mM EDTA (Carl Roth), 1 mM EGTA (AppliChem), 1 mM DTT (AppliChem), 1 x PI] and incubated for 15 min on ice. Samples were then passed through a 27 gauge needle (Sigma Aldrich) 10 times followed by 20 min incubation on ice. Samples were centrifuged at 750 x g for 5 min at 4°C and supernatant containing cytoplasm was transferred to a fresh tube. ¼ of the total amount of 5x RIPA buffer [750 mM NaCl (VWR), 5% Igepal CA-630 (Sigma Aldrich), 2.5% Sodium deoxycholate (Carl Roth), 0.5% SDS (Sigma Aldrich), 250 mM Tris (pH 8.0) (AppliChem)] with 1 x PI was added. The nuclear pellet was washed with fractionation buffer followed by 10 more passes through a 27 gauge needle and 10 min centrifugation at 750 x g, 4°C. The supernatant was discarded, the pellet was resuspended in 1x RIPA buffer + PI and sonicated to shear genomic DNA. Protein isolation was followed according to the procedure described above.

Western blotting and densitometric analysis

10-30 µg of protein was eluted in 5 x Pink buffer (Thermo Fisher Scientific) at 95°C. Samples were separated on 10% polyacrylamide gels in 1 x NuPAGE MOPS SDS running buffer (Novex) and transferred onto a Hypond-P polyvinylidene difluoride (PVDF) membrane (Merck Millipore). Membranes were blocked in 5% milk in TBS-T, incubated overnight with primary antibodies: ß-actin (mouse, 1:20.000, A5441, Thermo Fisher Scientific), CHIP (rabbit, 1:10.000, ab134064, Abcam), H3 (HRP-tagged, 1:100.000, ab21054, Abcam), HSF1 (1:1000), HSP70 (1:50.000), HSP90 (mouse, 1:100.000, ADI-SPA-831-050, Enzo Life Sciences) in Western Blocking Reagent (Roche) at 4°C, followed by three washes with TBS-T and incubation with HRP-conjugated secondary antibodies (Jackson ImmunoResearch) for 1h at room temperature. Proteins were visualized using the Immobilon Western chemiluminescent HRP substrate (Merck Millipore). Bands were quantified with ImageJ and normalized to respective loading controls.

RNA Sequencing analysis

Isolated RNA at a concentration of 20 ng/µl was further purified with Illumina's TruSeq mRNA v2Kit (polyA). Biological triplicates were sequenced on a HiSeq2500 using paired-end chemistry,

2x125 cycles. The sequence depth was approx. 100 million reads per sample. Runs were performed at DeCODE genetics, Reykjavik, Iceland.
To assess the differentiation state of generated CNs, cross-platform comparisons with spatio-temporal data from developing human brain of the BrainSpan Atlas (https://www.brainspan.org) were performed by pairwise comparison of generated CNs with each BrainSpan Atlas sample. By ranking gene expression for each pairwise comparison, rank difference values for all genes were used to calculate Spearman Rank correlation coefficients. Wilcoxon's rank-sum test was assessed if a category of interest (neocortex, subcortex, ganglionic eminence (GE), cerebellum) had significantly higher Spearman correlation coefficients than the background of all paired correlations. –Log 10 p-values of significant differences of CNs and spatio-temporal brain data were shown in heat maps.

Mass spectrometry

Equal amounts of samples were purified using SDS PAGE (Invitrogen). Coomassie-stained gel pieces were excised and in-gel digested using Trypsin as described previously (Borchert *et al.*, 2010). Extracted peptides were desalted using C18 StageTips and subjected to LC/MS-MS analysis, performed on an Easy nano-LC (Thermo Fisher Scientific) coupled to an LTQ Orbitrap Elite (Thermo Fisher Scientific) as decribed elsewhere (Franz-Wachtel *et al.*, 2012). Equal amounts of the peptide mixtures were injected onto the column in HPLC solvent A (0.1% formic acid) at a flow rate of 500 nl/min and subsequently eluted with an 127 minute segmented gradient of 5–33-50-90% of HPLC solvent B (80% acetonitrile in 0.1% formic acid) at a flow rate of 200 nl/min. On Orbitrap Elite the 15 most intense precursor ions were sequentially fragmented in each scan cycle. In all measurements, sequenced precursor masses were excluded from further selection for 60 s. The target values were 5000 charges for MS/MS fragmentation and 106 charges for the MS scan. CNs of 3 controls (CO4, CO5, CO6) and 3 *STUB1* patients (STUB1_1, STUB1_2 and STUB1_3) were analyzed.

Mass spectrometry data processing

The data was processed using MaxQuant software suite v.1.5.2.8 (Cox *et al.*, 2008). Database search was performed in MaxQuant, using the Andromeda search engine (Cox *et al.*, 2011). MS/MS spectra were searched against a target-decoy Uniprot database consisting of 95972 protein entries from Homo sapiens and 245 commonly observed contaminants. Full specificity was required for trypsin, up to two missed cleavages were allowed. Carbamidomethylation of cysteine was set as fixed modification, oxidation of methionine and acetylation of the N-terminus were set as variable modifications. Initial mass tolerance was set to 4.5 parts per million (ppm) for precursor ions and 0.5 dalton (Da) for fragment ions. Peptide, protein and modification site identifications were reported at a false discovery rate (FDR) of 0.01, estimated by the target/decoy approach (Elias *et al.*, 2007). The label-free algorithm was enabled, as was the 'match between runs' option (Luber *et al.*, 2010). Label-free quantification (LFQ) protein intensities from the MaxQuant data output were used for relative protein quantification. Downstream bioinformatical analysis (two-sample t-tests and Volcano plots) was performed using the Perseus software package, version 1.5.0.15. Data was filtered for contaminants, reverse and only identified by site entries.

Statistical analysis

All statistical analyses were performed using GraphPad Prism software (version 8). One-way ANOVA or a two-tailed t-test was applied. P-values were corrected for multiple comparisons and $P < 0.05$ was considered statistically significant. Unless indicated otherwise, all data is shown as mean ± standard error of the mean (SEM).

RESULTS

CHIP mutations do not alter viability of fibroblasts during prolonged heat stress

As CHIP has been linked to cell viability upon heat shock, we assessed the effect of prolonged heat stress on viability of fibroblasts in 3 patients with *STUB1* mutations (STUB1_1, STUB1_2, STUB1_3) in comparison to 3 healthy controls (CO1, CO2, CO3)(for further details, see Suppl. Table S1). For analysis, we exposed cells to either 42.5°C or 44°C for 6h and quantified the signal with the CyQuant Direct Cell Proliferation assay. Cell viability decreased rapidly between 3 and 4 hours of prolonged heat stress at 42.5°C (Mean ± SEM (in %); 3h HS: 86.67 ± 9.16; 4h HS: 29.01 ± 1.15)(Fig. 1A). At 44°C, cell death mostly occurred after 2-3 hours of maintained heat shock (2h HS: 87.53 ± 3.16; 3h HS: 41.5 ± 6.95; 4h HS: 24.88 ± 0.54)(Fig. 1B). No consistent difference was detected between patients and controls. We therefore could not determine an effect of *STUB1* mutations on fibroblast viability upon prolonged heat stress.

STUB1 mutations cause impaired heat shock response induction and recovery in fibroblasts

Previous reports have shown that CHIP plays a role in both induction and recovery of the HSR in HEK and HeLa cells as well as fibroblasts. To test whether CHIP mutations lead to dysfunctional HSR, we analyzed HSF1 translocation upon heat shock, HSR induction by transcript analysis and protein expression analysis and HSR recovery by protein analysis in 3 STUB1 patient- and 3 healthy age- and gender-matched control-derived fibroblasts.
For the analysis of HSF1 translocation from cytoplasm to nucleus, we fixed cells after 1h heat shock at 42.5°C and immunocytochemically stained for HSF1, HSP70 and Hoechst (Fig. 2A). In all 6 cell lines (3 patients, 3 controls), HSF1 and HSP70 protein was barely detectable in unstressed conditions. Upon heat shock, HSF1 levels in the nuclei strongly increased and HSP70 accumulated in nuclear bodies. Adding 4h of recovery at 37°C, HSF1 levels in the nuclei returned to baseline, but cytosolic expression of HSP70 increased strongly. Representative images of 2 cell lines are shown in Figure 2A. Upon quantification of nuclear HSF1 levels at 1h of heat shock, we saw a trend towards lower HSF1 levels in patients compared to controls (Mean ± SEM (in %), Controls: 92.3 ± 5.0; Patients: 80.0 ± 4.5; $P = 0.09$)(Fig. 2B).
Analyzing transcripts of heat shock-related genes, we saw a strong increase of *HSPA1A/B (*coding for HSP70) and *DNAJB1* (coding for HSP40) upon 1h of heat shock (Fig. 2C, D). This induction, however, was significantly lower in patients compared to controls (Mean ± SEM*; HSPA1A/B*: controls: 31.89 ± 1.39 fold, patients: 11.44 ± 5.25 fold ($P = 0.004$); *DNAJB1*: controls: 6.17 ± 0.25 fold, patients 2.42 fold ± 0.71 ($P = 0.001$)). Levels in controls and patients decreased with additional 4h of recovery. *HSPB1* (coding for HSP27) and *HSPB8* (coding for HSP22) transcription slightly increased upon recovery (*HSPB1*: controls: 1.86 ± 0.1 fold, patients: 1.56 ± 0.25 fold; *HSPB8*: controls: 2.61 ± 0.09 fold, patients 1.86 ± 0.27 fold ($P = 0.10$)) (Fig. 2C, D). *HSP90aa1* (HSP90), *HSPA8* (HSC70) and *HSPA5* (BiP/GRP78) were neither strongly altered upon heat shock or

recovery nor different between patients and controls (Suppl. Fig. S1).
On protein level, we saw low levels of HSP70 under basal conditions in all cell lines and a strong induction of HSP70 at 1h hs + 4h recovery (Mean ± SEM; unstressed controls: 1 ± 0.23; 1h hs + 4h recovery Controls: 6.03 ± 0.36; unstressed patients: 1.67 ± 0.33; 1h hs + 4h recovery patients: 7.34 ± 1.1). Induction was 6.0 fold in controls and 4.39 fold in patients (P = 0.1). However, HSP70 turnover and thus HSR recovery differs in controls and patients with prolonged recovery times with significantly higher HSP70 levels after 24h recovery in patients (Controls: 2.88 ± 0.76; Patients: 7.07 ± 1.55; P = 0.0004).
In summary, we were able to show that HSF1 translocates to the nucleus upon heat shock in fibroblasts with a slight but not significant reduction caused by *STUB1* mutations. This led to a significantly lower induction of *HSPA1A/B* and *DNAJB1* in patients. HSP70 protein levels were strongly induced at 1h hs + 4h recovery compared to unstressed levels in both patients and controls, but levels in patients remained high at 8h and 24h after heat shock, indicating an impaired HSR recovery and HSP70 turnover.

iPSC-derived cortical neurons show typical morphology and express neuronal markers

As SCAR16 primarily affects the central nervous system, we next investigated the HSR in cortical neurons. For this, we generated induced pluripotent stem cells from three SCAR16 patients (STUB1_1, STUB1_2, STUB1_3) and three gender-matched healthy controls (CO4, CO5, CO6)(for further details, see Suppl. Table S1). Genomic integrity and pluripotency was confirmed for all cell lines (data not shown; for details, see (Schuster *et al.*, 2018)). Additionally, we generated a *STUB1* knockout line STUB1(-/-) by CRISPR/Cas9-mediated genome editing from the isogenic control line CO5 (Schuster *et al.*, 2019). iPSCs were differentiated into cortical neurons according to a previously published protocol with slight modifications (Shi *et al.*, 2012; Rehbach *et al.*, 2019)(Fig. 3A). After 36 days of differentiation, the cultures were highly homogeneous, with all cells being positive for ß-III-tubulin (TUJ) and with >75% of cells being positive for CTIP2 (Mean ± SEM, 86.7 ± 1.3%), a cortical layer V marker (Fig. 3B). There was no significant difference in the percentage of CTIP2-positive nuclei between *STUB1* patients, knockout and controls.
To assess the spatial and temporal identity of the generated CNs and to exclude differences in differentiation potential and state, we compared transcript analysis data of biological triplicates of CO4, CO5, STUB1_2 and STUB1_3 with transcript data of the human developing brain (Human BrainSpan atlas, http://www.brainspan.org, data from fetal and early childhood postmortem tissue up to 1 year of age). The gene signature of both patients' and controls' iPSC-derived cortical neurons most significantly matched the co-expressed gene sets in neocortex and subcortex at post conception week (pcw) 12 to 21 with the strongest correlation at pcw 16 (Fig. 3C). The 4 analyzed cell lines display only slight differences in the expression patterns independent of *STUB1* mutations and show the same temporo-spatial pattern.
In generated CNs, we quantified *STUB1* transcript levels and CHIP protein expression levels. On transcript level, patients STUB1_1 and STUB1_3 showed no difference to controls (Fig. 3D) while on protein level, CHIP expression was reduced in both patient CNs to 25% of control levels (Fig. 3E). STUB1_2 neurons showed a reduced *STUB1* transcript level to 25% (Fig. 1D) resulting in an even lower protein level of 15% compared to wild-type (Fig. 3E). STUB1(-/-) showed a transcript level of 3% compared to controls (Fig. 3D), and no detectable protein (Fig. 3E), confirming the homozygous knockout of *STUB1*.

CHIP mutations do not alter cell viability during prolonged heat stress in cortical neurons

To examine the effect of heat shock on viability of CNs, we exposed CNs of 3 controls, 3 *STUB1* patients and STUB1(-/-) to prolonged heat stress of either 42.5°C or 44°C for 6 h. Interestingly, signal intensity of the CyQuant Direct Cell Proliferation Assay slightly increased in all cell lines at 42.5°C and only reached levels below baseline after more than 4h of heat stress. Upon 6h of heat stress a mean value of 85.5 ± 11.1% of viable cells was reached (Fig. 4A). At 44°C, lethality of CNs was higher, reaching a mean value of 55.0 ± 10.3% of viable cells after 6h of heat stress (Fig. 4B). No consistent difference in cell viability was observable between controls, patients and the STUB1(-/-) line.

Mutations in *STUB1* do not impair the heat shock response in cortical neurons

We next investigated the HSR in CNs after 1h of heat shock at 42.5°C. To assess nuclear translocation of HSF1 we performed subcellular fractionation of nucleus and cytoplasm. Proper separation of nuclei from the cytoplasmic fraction was verified by presence and absence of histone 3 (H3), respectively (Suppl. Fig. S2A). In unstressed conditions, HSF1 was highly expressed in the cytosol and weakly expressed in the nucleus. Upon heat shock, HSF1 got hyperphosphorylated as seen by a mass shift and translocated to the nucleus (Fig.5A), since almost no HSF1 remained in the cytosol after heat shock. HSF1 translocation and expression levels were not altered by mutant *STUB1* (Fig. 5A). CHIP levels were shown to diminish after heat shock in the cytosol in controls but did not increase drastically in the nucleus.
On transcript level, heat strongly induced the transcription of *HSPA1A/B* (encoding HSP70) and *DNAJB1* (encoding HSP40) (Fig. 5B, C). This induction was significantly higher in patients and STUB1(-/-) compared to controls (Mean ± SEM; *HSPA1A/B* in controls: 12.06 ± 1.18 fold, in patients: 21.38 ± 3.25 fold (P = 0.017) and in STUB1(-/-): 24 fold (P = 0.03); *DNAJB1* in controls 11.06 ± 0.46 fold, in patients: 17.28 ± 2.9 fold (P = 0.038) and in STUB1(-/-) 18 fold (P = 0.1)). After 4h of recovery levels decreased in all lines again (*HSPA1A/B* in controls: 7.31 ± 0.54 fold, in patients: 10.26 ± 1.81 fold, in STUB1(-/-) 6.3 fold; *DNAJB1* in controls: 2.40 ± 0.22 fold, in patients: 2.58 ± 0.61 fold, in STUB1(-/-): 1.7 fold). *HSPB1* (encoding HSP27) and *HSPB8* (encoding HSP22) transcription slightly increased upon heat shock by 2-4 fold but highly increased after 4h recovery at 37°C (*HSPB1* in controls: 28.16 ± 7.86 fold, in patients: 11.25 ± 2.05 fold (P = 0.037) , in STUB1(-/-): 15.3 fold (P = 0.3); *HSPB8*: in controls: 98.5 ± 57.65 fold, in patients: 4.5 ± 0.7 fold (P = 0.11), in STUB1(-/-): 5.7 fold (P = 0.3)). The increase of *HSPB1* was significantly higher in controls compared to patients. However, variability for *HSPB1* and *HSPB8* was very high in between lines, probably caused by low basal expression levels. *HSP90aa1* (HSP90), *HSPA8* (HSC70) and *HSPA5* (BiP/GRP78) were neither strongly altered upon heat shock or recovery nor different between patients and controls (Suppl. Fig. S2B, C).
Unexpectedly, on protein level, HSP70 expression under basal conditions was already very high in CNs, with slight variations between lines and independent of *STUB1* mutations (Suppl. Fig. S2D). We barely saw an increase of HSP70 after heat shock and various times of recovery (increase upon 1h hs + 4h recovery normalized to baseline (Mean ± SEM) of controls: 1.27 ± 0.3 fold; patients: 1.12 ± 0.15 fold; STUB1(-/-): 1.25 fold). However, comparing absolute HSP70 levels, we saw a slightly lower levels in patients compared to controls (unstressed HSP70 level of controls: 1 ± 0.16, patients: 0.47 ± 0.07, P = 0.27; STUB1(-/-): 0.58; 1h hs + 4h recovery HSP70 level

of controls: 1.22 ± 0.29, patients: 0.52 ± 0.07, $P = 0.25$; STUB1(-/-): 0.73) (Fig. 5D).
In summary, we were able to show that HSF1 translocates to the nucleus upon heat shock in CNs and leads to the induction of *HSPA1A/B* and *DNAJB1* transcripts which surprisingly did not translate to increased HSP70 protein levels. Induction of *HSPA1A/B* and *DNAJB1* was significantly higher in patients and STUB1(-/-) compared to controls. Furthermore, we barely saw an induction of HSP70 on protein level in both controls and patients.

Proteome analysis of cortical neurons reveals impaired protein folding and ubiquitination in patients

Proteomic analysis based on mass spectrometry with LC/MS-MS and label-free quantification was applied to identify quantitative differences in proteome-wide protein levels between CNs of controls and patients (N=3 for both biological groups). We identified 53 proteins with significantly altered levels (Fig. 6A); 28 proteins were increased (Fig. 6B, upper panel) and 25 proteins were reduced in controls compared to patients (Fig. 6B, lower panel). Additionally, 185 proteins were exclusively expressed in at least 2 control cell lines but in no patient cell line (Suppl. Table S3) and 228 proteins were exclusively expressed in at least 2 patient cell lines but in no control cell line (Suppl. Table S4). Based on Webgestalt analysis (Liao *et al.*, 2019) of proteins that were exclusively expressed in at least 2 controls, gene ontology (GO) terms of protein folding and refolding and the ubiquitin system were highly enriched (Fig. 6C, left panel). Oppositely, GO terms of oxidative stress coping were enriched in patients only (Fig. 6C, right panel). Considering specific interaction partners of CHIP, we found differences between controls and patients for some proteins including PSEN1/2, IGF1R, TRAF2 and TRAF6 (Suppl. Fig. S3).

DISCUSSION

Proteotoxic stress and a compromised HSR is associated with many neurodegenerative diseases such as Alzheimer's disease, Parkinson's disease, Huntington's disease or amyotrophic lateral sclerosis (reviewed by San Gil *et al.*, 2017). This suggests an innate susceptibility of neurons to stress, homeostatic changes and disturbances in protein quality control and highlights the significance of chaperones in neuroprotection.
In the present study, we investigated the pathological effect of *STUB1* mutations causing SCAR16 on the HSR. Analyzing patient-derived fibroblasts, we confirmed an impaired HSR induction on transcript level and an impaired HSR recovery on protein level. Furthermore, we developed a human iPSC-based SCAR16 disease model to properly model the disease in cortical neurons as the affected cell type. Despite differences on heat-inducible transcript levels in *STUB1*-mutant cortical neurons, we could not detect an impaired heat shock induction or recovery in CNs of *STUB1* patients on protein level.
In a rodent model of SCAR16, $CHIP^{-/-}$ mice exhibit decreased stress tolerance, pronounced heat sensitivity, increased oxidative stress and lethality upon heat shock (Dai *et al.*, 2003; Min *et al.*, 2008). *In vitro*, CHIP knockdown in mesodermal cell lines caused reduced cell viability upon prolonged heat stress and impaired induction and recovery of the HSR (Dai *et al.*, 2003; Kim *et al.*, 2005; Qian *et al.*, 2006; Zhang *et al.*, 2015).
In human SCAR16 cell models we found a striking difference in heat stress tolerance between cell types. Whereas less than 30% of fibroblasts survived 4h of heat shock at 42.5°C, more than 95% of neurons were still viable. This might indicate a higher stress vulnerability of fibroblasts

and a stronger response to this toxic stimulus. While Dai and colleagues (2003) reported 50% lethality of murine CHIP(-/-) fibroblasts at 60min of 42°C, our patient-derived fibroblasts did not show relevant lethality after 60min of heat shock at 42.5°C. This difference might be due to small levels of CHIP remaining in patient fibroblasts with some residual activity which potentially rescues the drastic toxic effect seen in complete CHIP knockout fibroblasts. Our data implies that *STUB1* mutations and thereby dysfunctional CHIP do not affect the cell viability negatively upon heat shock in fibroblasts and CNs.

We next evaluated the induction of HSR and its recovery in patient- and control-derived fibroblasts. By immunocytochemical analysis of heat shocked cells, we could show that HSF1 translocated to the nucleus in patients and controls, with a trend towards lower levels in controls. Furthermore, analyzing different transcript levels in fibroblasts, we observed a lower increase in *HSPA1A/B* and *DNAJB1* transcript levels upon heat shock in patients compared to controls. This might be caused by slightly lower nuclear HSF1 levels or by differential posttranslational modifications (PTMs) of HSF1, as PTMs were reported to strongly alter the activity of HSF1 (reviewed by Gomez-Pastor *et al.*, 2018). On protein level, surprisingly, we do not see a reduced HSP70 level in patients compared to controls after 4h recovery from heat shock as it would be expected from the lower transcript levels but a 6-7 fold increase in both biological groups. Yet, we see an impaired HSR recovery, as indicated by remaining high levels of HSP70 after prolonged recovery (8 and 24h), in line with the results by Qian and colleagues (2006). This leads to the conclusion that either HSP70 ubiquitin tagging is reduced because CHIP is mutated or that the amount of misfolded proteins in patients is simply higher, requiring a prolonged higher expression of HSPs in those cells, or a combination of both. In conclusion, we confirm an impaired induction and recovery of HSR caused by dysfunctional CHIP, though for the first time in patient-derived cells.

As SCAR16 primarily causes degeneration of the central nervous system, we next sought to analyze the HSR in patient neurons. We therefore generated patient-specific iPSCs from fibroblasts and differentiated those, together with gender-matched controls, into cortical neurons as a disease-relevant cell type. This provides a disease model with endogenous protein levels and the patient's own genetic background.

We could show that the translocation of HSF1 from the cytoplasm to the nucleus upon heat shock occurs invariable of CHIP functionality, suggesting no direct impact of CHIP mutations on trimerization of HSF1 or its translocation in CNs. CHIP levels declined upon heat shock in the cytoplasm, but did not correspondingly increase in the nucleus. Potentially, nuclear CHIP levels did already return to baseline in our experimental setup with 1h heat shock, as Anderson and colleagues showed a strong accumulation in the nucleus only 5-10 minutes after heat shock and a decrease back to baseline within 30-60 mins (Anderson *et al.*, 2010).

Analyzing transcript levels of heat shock proteins, we observed a higher increase in *HSPA1A/B* and *DNAJB1* transcript levels upon heat shock in patient neurons compared to controls, independent of nuclear HSF1 levels. This might be caused by differential PTMs of HSF1 as described above. Higher *HSPA1A/B* and *DNAJB1* transcription might also be caused by 'pre-conditioning' to stress and thermotolerance in patients: Levels of misfolded proteins are presumably higher in CHIP mutant cells, causing mild proteotoxic stress and an induction of HSR prior to the heat stimulus which potentiates the HSR upon subsequent stress exposure (Burdon, 1987). Stress pre-conditioning might only play a role in cortical neurons and not in fibroblasts as non-dividing cells are more vulnerable to proteotoxic stress in general.

Transcript levels of the small HSPs (sHSPs) *HSPB1* (coding for HSP27) and *HSPB8* (coding for HSP22) were strongly increased at recovery steps of heat shock, indicating two stages of transcript induction with an early induction of *HSPA1A/B* and *DNAJB1* and, unexpectedly, a delayed induction of *HSPB1* and *HSPB8*. HSP27 and HSP22 bind to unfolded proteins, prevent their aggregation and protect cells from toxicity caused by aggregates. Both sHSPs also enable stress resistance and inhibit apoptosis (Acunzo *et al.*, 2012). This might be the explanation for higher levels in controls compared to patients and a delayed induction. Interestingly, mutations in both *HSPB1* and *HSPB8* induce neurodegeneration, highlighting the importance of both sHSPs in the stress response in neurons in particular.

On protein level, unexpectedly, we neither detected a prominent induction of HSP70 protein nor a difference in HSP70 level upon recovery. HSP70 levels at 4h recovery after heat stress were only 1.1 – 1.2 fold higher than its basal levels, compared to 6-7 fold higher levels in fibroblasts. This might have several reasons: 1) an impaired HSR in the brain might be relevant and disease-causing but not in neurons, 2) alterations of the HSR that were seen in patient-derived fibroblasts but not in cortical neurons are not disease-relevant, as the diseased cell type does not show any changes, or 3) the low HSR is an *in vitro* artifact of the monoculture and the culture conditions as the basal HSP70 level is already very high. As persistently high levels of HSP70 are detrimental to cells (Feder *et al.*, 1992; Volloch *et al.*, 1999), an additional induction of HSP70 upon stress might be prevented in iPSC-derived cortical neurons.

Considering the role of CHIP in this process, we observed only slightly lower HSP70 protein levels in patients but no difference in fold changes. Furthermore, the comparison of STUB1(-/-) with its isogenic control revealed very similar results as the comparison of patients and controls. This confirms our findings in patient lines and supports the limited effect of CHIP on the HSR in cortical neurons.

While the HSR is evolutionarily well conserved, tissue and cell variability of the chaperome in humans is prominent: Hageman and Kampinga (2009) analyzed the temporal and the spatial expression pattern of 45 tissues using the Unigene database and observed strong tissue specificity for the expression of HSPH, HSPA and DNAJ isoforms. Notably, the expression of *HSPA1A* is highly variable between tissues and developmental stages (embryoid body to adult). Focusing on the brain, histological analyses after heat hock in rodents showed the strongest HSP70 induction in the dentate gyrus, hypothalamus and cerebellum (Blake *et al.*, 1990; Li *et al.*, 1992). Of interest, comparison of HSR in neurons and glia *in vitro* revealed a higher induction of HSP70 in glial cells compared to neurons (Nishimura *et al.*, 1991; Marcuccilli *et al.*, 1996; Vogel *et al.*, 1997; Batulan *et al.*, 2003). This might be caused by differential co-chaperone levels: HSPBP1 expression in neurons is higher than in astrocytes and is directly linked to HSR inhibition (Zhao *et al.*, 2017), HSPB1/HSP27 levels are oppositely correlated (Satoh *et al.*, 1995). However, while HSP27 levels do not increase upon heat shock in astrocytes, this increase is observed in neurons (Satoh *et al.*, 1995). Other HSPs such as *DNAJB2A* (HSP70 family) and HSJ1a/b (HSP40 family) were reported to be highly enriched in neuronal tissue (Cheetham *et al.*, 1992; Chapple *et al.*, 2003). In our study, we additionally observed a strong cell specificity of HSPB1 and HSPB8, with higher expression under basal conditions in fibroblasts, but higher induction upon recovery of heat stress in neurons. This might point towards an important role of both small HSPs in stress coping in cortical neurons.

For a broader picture, proteomic analysis of control and patient CNs was performed. Comparisons point towards aberrations in protein folding and the ubiquitin system as well as

an increased oxidative stress level in unstressed patient cells. This is in line with reports that show that mutations alter CHIP's ability to ubiquitinate its substrates (Heimdal *et al.*, 2014; Ronnebaum *et al.*, 2014; Pakdaman *et al.*, 2017; Kanack *et al.*, 2018; Shi *et al.*, 2018). However, with more than 200 E3 ligases encoded in the human body, substrates are not exclusively ubiquitinated by one E3 ligase, but e.g. Parkin and CHIP act redundantly on some substrates (Morishima *et al.*, 2008). Furthermore, keeping in mind the function of CHIP in tagging misfolded proteins with ubiquitin for degradation, the importance of CHIP might only show up in a state with high abundancy of misfolded proteins.
In summary, our results question the role of impaired HSR in SCAR16 neuropathology and point to protein degradation and oxidative stress as potentially more critical factors in the pathogenesis of CHIP-related neurodegeneration. By the demonstration of major differences in the HSR of fibroblasts and induced cortical neurons of SCAR16 patients this study highlights the need for careful selection of proper cell types for modelling human diseases.

ACKNOWLEGDEMENTS

We are grateful to Jonathan Schisler for the recommendation of the specific CHIP antibody. We acknowledge to Melanie Kraft and Yvonne Schelling for their excellent technical assistance.

AUTHOR CONTRIBUTIONS

SS, SH and LS designed the study. SS, EH, AV and JA generated and collected data. SS, SH and LS drafted the manuscript. All authors were involved in interpretation of the data and critical revision of the manuscript. All authors gave their final approval.

REFERENCES

Abravaya, K., Phillips, B., Morimoto, R.I., 1991. Attenuation of the heat shock response in HeLa cells is mediated by the release of bound heat shock transcription factor and is modulated by changes in growth and in heat shock temperatures. Genes Dev. 5, 2117-27.
Acunzo, J., Katsogiannou, M., Rocchi, P., 2012. Small heat shock proteins HSP27 (HspB1), alphaB-crystallin (HspB5) and HSP22 (HspB8) as regulators of cell death. Int J Biochem Cell Biol. 44, 1622-31.
Anderson, L.G., *et al.*, 2010. Brain distribution of carboxy terminus of Hsc70-interacting protein (CHIP) and its nuclear translocation in cultured cortical neurons following heat stress or oxygen-glucose deprivation. Cell Stress Chaperones. 15, 487-95.
Baler, R., Welch, W.J., Voellmy, R., 1992. Heat shock gene regulation by nascent polypeptides and denatured proteins: hsp70 as a potential autoregulatory factor. J Cell Biol. 117, 1151-9.
Ballinger, C.A., *et al.*, 1999. Identification of CHIP, a novel tetratricopeptide repeat-containing protein that interacts with heat shock proteins and negatively regulates chaperone functions. Mol Cell Biol. 19, 4535-45.
Batulan, Z., *et al.*, 2003. High threshold for induction of the stress response in motor neurons is associated with failure to activate HSF1. J Neurosci. 23, 5789-98.
Bettencourt, C., *et al.*, 2015. Clinical and Neuropathological Features of Spastic Ataxia in a Spanish Family with Novel Compound Heterozygous Mutations in STUB1. Cerebellum. 14, 378-81.
Blake, M.J., Nowak, T.S., Jr., Holbrook, N.J., 1990. In vivo hyperthermia induces expression of HSP70 mRNA in brain regions controlling the neuroendocrine response to stress. Brain Res Mol Brain Res. 8, 89-92.
Borchert, N., *et al.*, 2010. Proteogenomics of Pristionchus pacificus reveals distinct proteome structure of nematode models. Genome Res. 20, 837-46.
Burdon, R.H., 1987. Thermotolerance and the heat shock proteins. Symp Soc Exp Biol. 41, 269-83.
Chapple, J.P., Cheetham, M.E., 2003. The chaperone environment at the cytoplasmic face of the endoplasmic reticulum can modulate rhodopsin processing and inclusion formation. J Biol Chem. 278, 19087-94.
Cheetham, M.E., Brion, J.P., Anderton, B.H., 1992. Human homologues of the bacterial heat-shock protein DnaJ are preferentially expressed in neurons. Biochem J. 284 (Pt 2), 469-76.
Cox, J., Mann, M., 2008. MaxQuant enables high peptide identification rates, individualized p.p.b.-range mass accuracies and proteome-wide protein quantification. Nat Biotechnol. 26, 1367-72.

Cox, J., *et al.*, 2011. Andromeda: a peptide search engine integrated into the MaxQuant environment. J Proteome Res. 10, 1794-805.
Dai, Q., *et al.*, 2003. CHIP activates HSF1 and confers protection against apoptosis and cellular stress. EMBO J. 22, 5446-58.
Ding, X., Goldberg, M.S., 2009. Regulation of LRRK2 stability by the E3 ubiquitin ligase CHIP. PLoS One. 4, e5949.
Elias, J.E., Gygi, S.P., 2007. Target-decoy search strategy for increased confidence in large-scale protein identifications by mass spectrometry. Nat Methods. 4, 207-14.
Feder, J.H., *et al.*, 1992. The consequences of expressing hsp70 in Drosophila cells at normal temperatures. Genes Dev. 6, 1402-13.
Ferreira, J.V., *et al.*, 2015. K63 linked ubiquitin chain formation is a signal for HIF1A degradation by Chaperone-Mediated Autophagy. Sci Rep. 5, 10210.
Franz-Wachtel, M., *et al.*, 2012. Global detection of protein kinase D-dependent phosphorylation events in nocodazole-treated human cells. Mol Cell Proteomics. 11, 160-70.
Gomez-Pastor, R., Burchfiel, E.T., Thiele, D.J., 2018. Regulation of heat shock transcription factors and their roles in physiology and disease. Nat Rev Mol Cell Biol. 19, 4-19.
Guo, D., *et al.*, 2015. Regulation of autophagic flux by CHIP. Neurosci Bull. 31, 469-79.
Haeussler, M., *et al.*, 2016. Evaluation of off-target and on-target scoring algorithms and integration into the guide RNA selection tool CRISPOR. Genome Biol. 17, 148.
Hageman, J., Kampinga, H.H., 2009. Computational analysis of the human HSPH/HSPA/DNAJ family and cloning of a human HSPH/HSPA/DNAJ expression library. Cell Stress Chaperones. 14, 1-21.
Hayer, S.N., *et al.*, 2017. STUB1/CHIP mutations cause Gordon Holmes syndrome as part of a widespread multisystemic neurodegeneration: evidence from four novel mutations. Orphanet J Rare Dis. 12, 31.
Heimdal, K., *et al.*, 2014. STUB1 mutations in autosomal recessive ataxias - evidence for mutation-specific clinical heterogeneity. Orphanet J Rare Dis. 9, 146.
Jana, N.R., *et al.*, 2005. Co-chaperone CHIP associates with expanded polyglutamine protein and promotes their degradation by proteasomes. J Biol Chem. 280, 11635-40.
Jiang, J., *et al.*, 2001. CHIP is a U-box-dependent E3 ubiquitin ligase: identification of Hsc70 as a target for ubiquitylation. J Biol Chem. 276, 42938-44.
Joshi, V., *et al.*, 2016. A Decade of Boon or Burden: What Has the CHIP Ever Done for Cellular Protein Quality Control Mechanism Implicated in Neurodegeneration and Aging? Front Mol Neurosci. 9, 93.
Kanack, A.J., Newsom, O.J., Scaglione, K.M., 2018. Most mutations that cause spinocerebellar ataxia autosomal recessive type 16 (SCAR16) destabilize the protein quality-control E3 ligase CHIP. J Biol Chem. 293, 2735-2743.
Kim, S.A., *et al.*, 2005. CHIP interacts with heat shock factor 1 during heat stress. FEBS Lett. 579, 6559-63.
Kumar, P., *et al.*, 2007. CHIP and HSPs interact with beta-APP in a proteasome-dependent manner and influence Abeta metabolism. Hum Mol Genet. 16, 848-64.
Li, Y., *et al.*, 1992. Distribution of 72-kDa heat-shock protein in rat brain after hyperthermia. Acta Neuropathol. 84, 94-9.
Liao, Y., *et al.*, 2019. WebGestalt 2019: gene set analysis toolkit with revamped UIs and APIs. Nucleic Acids Res. 47, W199-W205.
Lizama, B.N., *et al.*, 2018. Neuronal Preconditioning Requires the Mitophagic Activity of C-terminus of HSC70-Interacting Protein. J Neurosci. 38, 6825-6840.
Luber, C.A., *et al.*, 2010. Quantitative proteomics reveals subset-specific viral recognition in dendritic cells. Immunity. 32, 279-89.
Marcuccilli, C.J., *et al.*, 1996. Regulatory differences in the stress response of hippocampal neurons and glial cells after heat shock. J Neurosci. 16, 478-85.
Miller, V.M., *et al.*, 2005. CHIP suppresses polyglutamine aggregation and toxicity in vitro and in vivo. J Neurosci. 25, 9152-61.
Min, J.N., *et al.*, 2008. CHIP deficiency decreases longevity, with accelerated aging phenotypes accompanied by altered protein quality control. Mol Cell Biol. 28, 4018-25.
Morishima, Y., *et al.*, 2008. CHIP deletion reveals functional redundancy of E3 ligases in promoting degradation of both signaling proteins and expanded glutamine proteins. Hum Mol Genet. 17, 3942-52.
Murata, S., Chiba, T., Tanaka, K., 2003. CHIP: a quality-control E3 ligase collaborating with molecular chaperones. Int J Biochem Cell Biol. 35, 572-8.
Nishimura, R.N., *et al.*, 1991. Comparison of the heat shock response in cultured cortical neurons and astrocytes. Brain Res Mol Brain Res. 9, 39-45.
Okita, K., *et al.*, 2011. A more efficient method to generate integration-free human iPS cells. Nat Methods. 8, 409-12.
Pakdaman, Y., *et al.*, 2017. In vitro characterization of six STUB1 variants in spinocerebellar ataxia 16 reveals altered structural properties for the encoded CHIP proteins. Biosci Rep. 37.
Qian, S.B., *et al.*, 2006. CHIP-mediated stress recovery by sequential ubiquitination of substrates and Hsp70. Nature. 440, 551-5.
Ravi, S., *et al.*, 2018. Adverse Effects of Fenofibrate in Mice Deficient in the Protein Quality Control Regulator, CHIP. J Cardiovasc Dev Dis. 5.

Rehbach, K., *et al.*, 2019. Multiparametric rapid screening of neuronal process pathology for drug target identification in HSP patient-specific neurons. Sci Rep. 9, 9615.
Richter, K., Haslbeck, M., Buchner, J., 2010. The heat shock response: life on the verge of death. Mol Cell. 40, 253-66.
Rinaldi, L., *et al.*, 2019. Feedback inhibition of cAMP effector signaling by a chaperone-assisted ubiquitin system. Nat Commun. 10, 2572.
Ronnebaum, S.M., Patterson, C., Schisler, J.C., 2014. Emerging evidence of coding mutations in the ubiquitin-proteasome system associated with cerebellar ataxias. Hum Genome Var. 1, 14018.
Sahara, N., *et al.*, 2005. In vivo evidence of CHIP up-regulation attenuating tau aggregation. J Neurochem. 94, 1254-63.
San Gil, R., *et al.*, 2017. The heat shock response in neurons and astroglia and its role in neurodegenerative diseases. Mol Neurodegener. 12, 65.
Santoro, M.G., 2000. Heat shock factors and the control of the stress response. Biochem Pharmacol. 59, 55-63.
Sarge, K.D., Murphy, S.P., Morimoto, R.I., 1993. Activation of heat shock gene transcription by heat shock factor 1 involves oligomerization, acquisition of DNA-binding activity, and nuclear localization and can occur in the absence of stress. Mol Cell Biol. 13, 1392-407.
Satoh, J.I., Kim, S.U., 1995. Differential expression of heat shock protein HSP27 in human neurons and glial cells in culture. J Neurosci Res. 41, 805-18.
Schindelin, J., *et al.*, 2012. Fiji: an open-source platform for biological-image analysis. Nat Methods. 9, 676-82.
Schisler, J.C., *et al.*, 2013. CHIP protects against cardiac pressure overload through regulation of AMPK. J Clin Invest. 123, 3588-99.
Schuster, S., *et al.*, 2018. Establishment of STUB1/CHIP mutant induced pluripotent stem cells (iPSCs) from a patient with Gordon Holmes syndrome/SCAR16. Stem Cell Res. 29, 166-169.
Schuster, S., *et al.*, 2019. Generation of a homozygous CRISPR/Cas9-mediated knockout human iPSC line for the STUB1 locus. Stem Cell Res. 34, 101378.
Seo, J., *et al.*, 2016. CHIP controls necroptosis through ubiquitylation- and lysosome-dependent degradation of RIPK3. Nat Cell Biol. 18, 291-302.
Sha, Y., *et al.*, 2017. STUB1 regulates TFEB-induced autophagy-lysosome pathway. EMBO J. 36, 2544-2552.
Shi, C.H., *et al.*, 2014. Ataxia and hypogonadism caused by the loss of ubiquitin ligase activity of the U box protein CHIP. Hum Mol Genet. 23, 1013-24.
Shi, C.H., *et al.*, 2018. Disrupted structure and aberrant function of CHIP mediates the loss of motor and cognitive function in preclinical models of SCAR16. PLoS Genet. 14, e1007664.
Shi, Y., Kirwan, P., Livesey, F.J., 2012. Directed differentiation of human pluripotent stem cells to cerebral cortex neurons and neural networks. Nat Protoc. 7, 1836-46.
Shi, Y., *et al.*, 2013. Identification of CHIP as a novel causative gene for autosomal recessive cerebellar ataxia. PLoS One. 8, e81884.
Shin, Y., *et al.*, 2005. The co-chaperone carboxyl terminus of Hsp70-interacting protein (CHIP) mediates alpha-synuclein degradation decisions between proteasomal and lysosomal pathways. J Biol Chem. 280, 23727-34.
Singh, A.K., Pati, U., 2015. CHIP stabilizes amyloid precursor protein via proteasomal degradation and p53-mediated trans-repression of beta-secretase. Aging Cell. 14, 595-604.
Synofzik, M., *et al.*, 2014. Phenotype and frequency of STUB1 mutations: next-generation screenings in Caucasian ataxia and spastic paraplegia cohorts. Orphanet J Rare Dis. 9, 57.
Tang, M.B., *et al.*, 2018. Anisomycin prevents OGD-induced necroptosis by regulating the E3 ligase CHIP. Sci Rep. 8, 6379.
Tetzlaff, J.E., *et al.*, 2008. CHIP targets toxic alpha-Synuclein oligomers for degradation. J Biol Chem. 283, 17962-8.
Vjestica, A., *et al.*, 2013. Hsp70-Hsp40 chaperone complex functions in controlling polarized growth by repressing Hsf1-driven heat stress-associated transcription. PLoS Genet. 9, e1003886.
Vogel, P., Dux, E., Wiessner, C., 1997. Effect of heat shock on neuronal cultures: importance of protein synthesis and HSP72 induction for induced tolerance and survival. Metab Brain Dis. 12, 203-17.
Volloch, V.Z., Sherman, M.Y., 1999. Oncogenic potential of Hsp72. Oncogene. 18, 3648-51.
Yao, T.P., 2010. The role of ubiquitin in autophagy-dependent protein aggregate processing. Genes Cancer. 1, 779-786.
Zhang, M., *et al.*, 2005. Chaperoned ubiquitylation--crystal structures of the CHIP U box E3 ubiquitin ligase and a CHIP-Ubc13-Uev1a complex. Mol Cell. 20, 525-38.
Zhang, W., *et al.*, 2015. CHIP Knockdown Reduced Heat Shock Response and Protein Quality Control Capacity in Lens Epithelial Cells. Curr Mol Med. 15, 652-62.
Zhao, T., *et al.*, 2017. Differential HspBP1 expression accounts for the greater vulnerability of neurons than astrocytes to misfolded proteins. Proc Natl Acad Sci U S A. 114, E7803-E7811.

FIGURES

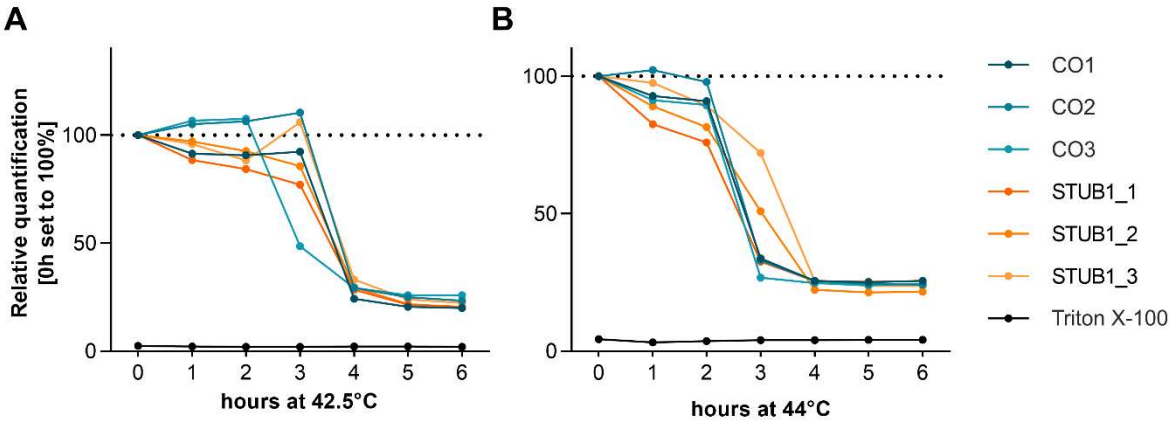

Figure 1 | Cell viability of fibroblasts upon heat stress is not impaired by dysfunctional CHIP. Viability of fibroblasts in percent during prolonged heat stress at **(A)** 42.5°C and **(B)** 44°C for 6h of 3 controls and 3 *STUB1* patients. Values are given as mean of triplicates. Triton X-100 was used as negative control for cell viability.

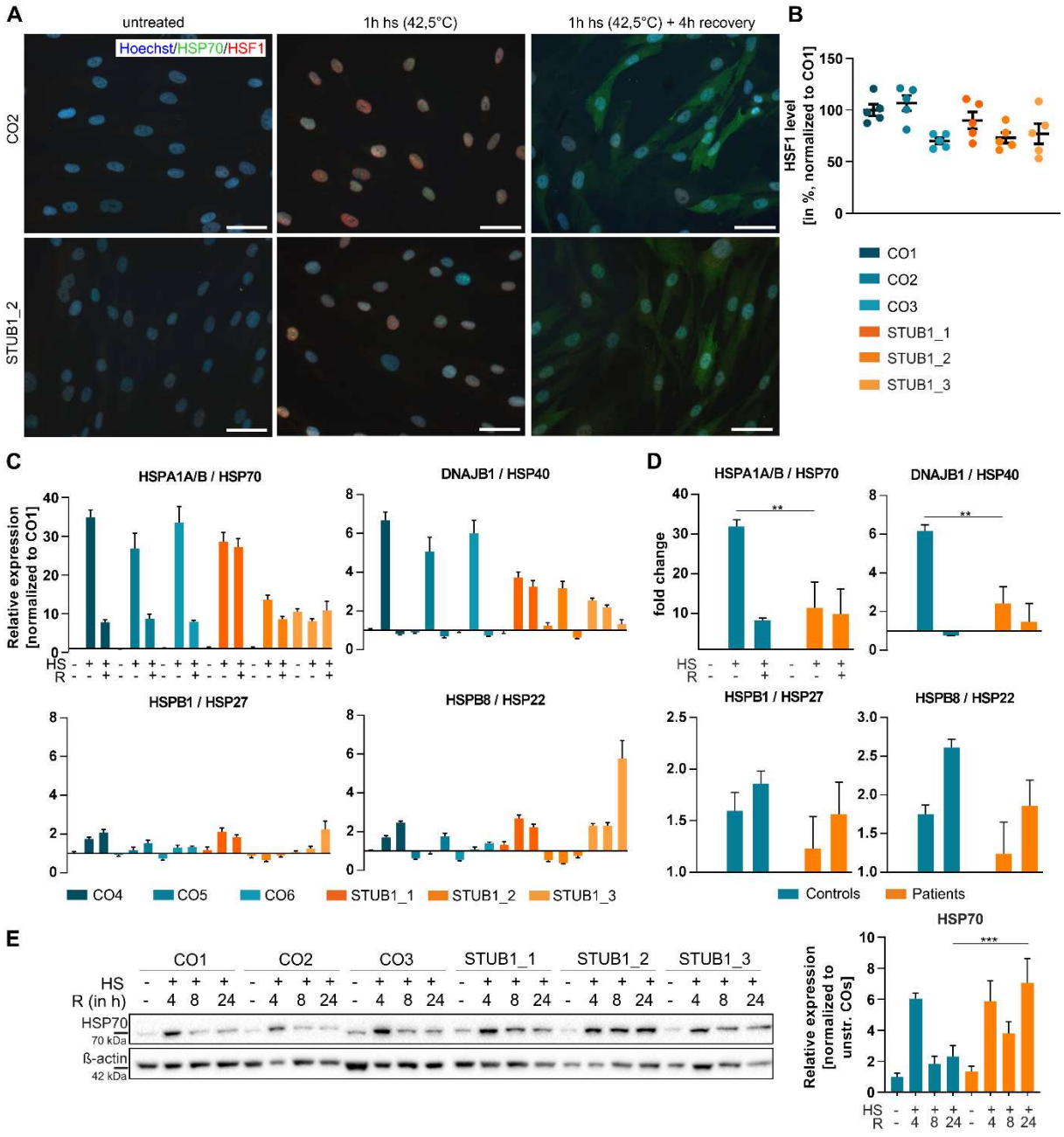

Figure 2 | Mutant CHIP impairs HSR induction and recovery in fibroblasts. (A) Immunocytochemical staining of HSF1 (red), HSP70 (green) and Hoechst (blue) of fibroblasts without stress, after heat shock (1h, 42.5°C) and after recovery (4h 37°C). Exemplary images of 1 control and 1 patient are shown. Scale bar 50 µm. **(B)** Quantification of HSF1 levels in nuclei of heat shocked fibroblasts, given in percent normalized to CO1. **(C)** Transcript analysis by qRT-PCR of *HSPA1A/B*, *DNAJB1*, *HSPB1* and *HSPB8* in unstressed, heat shocked (HS) and recovered (R) samples. Values are normalized to CO1 and the housekeeping genes *GAPDH* and *TBP*. N=3 replicates (mean ± SEM). **(D)** Pooled analysis of 3 controls and 3 patients. Transcript levels were normalized to the respective basal levels. ** p<0.01, One-way ANOVA. **(E)** Western blot analysis of HSP70 protein levels of fibroblasts without stress, after 1h HS and up to 24 h of recovery with ß-actin as the loading control. One representative image out of three experiments is shown. Quantification is based on the normalization to unstressed controls, 3 controls and 3 patients were pooled. *** p<0.001, One-way ANOVA.

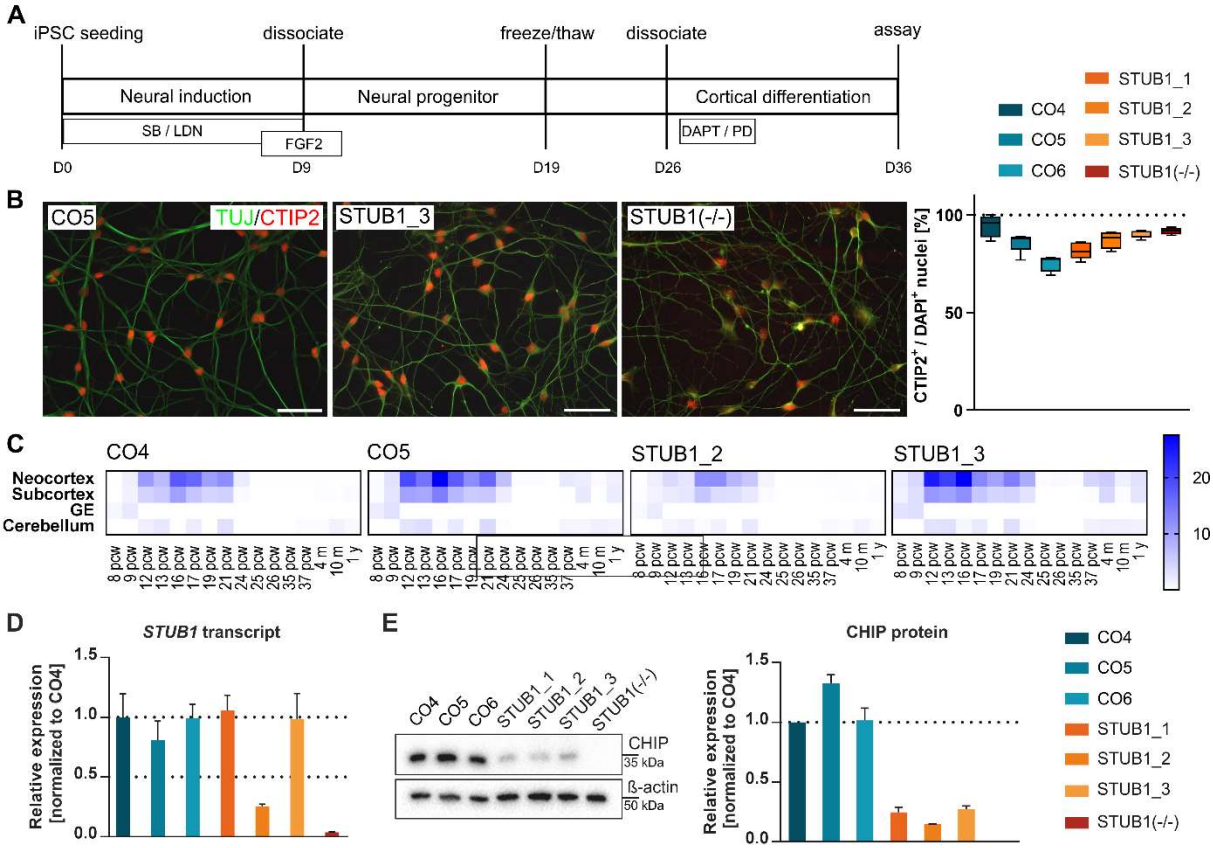

Figure 3 | Characterization of iPSC-derived neurons. (A) Schematic representation of the experimental procedure of the differentiation of induced pluripotent stem cell (iPSCs) into iPSC-derived cortical neurons (CNs). **(B)** Immunocytochemical stainings of CNs on D36 for TUJ (green) and CTIP2 (red). Scale bar: 50 µm. Exemplary stainings of 3 lines are shown here. Quantification of percentage of $CTIP2^+/DAPI^+$ cells in controls, patients and STUB1(-/-) was performed for 4-5 fields per cell line. Values are given as Boxplots showing Min to Max, with the mean indicated by a line. **(C)** Transcript expression in CNs match best expression found in neocortical tissue at post conception week 16. Heatmaps were produced for 2 controls (CO_4, CO_5) and 2 patients (STUB1_2; STUB1_3) by Wilcoxon's rank-sum comparisons of CN transcripts to the BrainSpan Atlas. All 4 generated lines display a similar expression pattern. **(D)** Transcript level of *STUB1* in 3 controls, 3 patients and the homozygous knockout line. Levels are normalized to CO_4. Values are given as mean ± SEM. Dotted lines indicate full level and 50% reduced transcript levels. **(E)** CHIP protein expression level was analyzed by Western Blotting. One representative blot is shown. Bands are quantified densitometrically and normalized to ß-actin and CO_4. Values are given as mean ± SEM. N=3. iPSC: induced pluripotent stem cells; CN: iPSC-derived cortical neurons; GE: ganglionic eminence; pcw: post conception week.

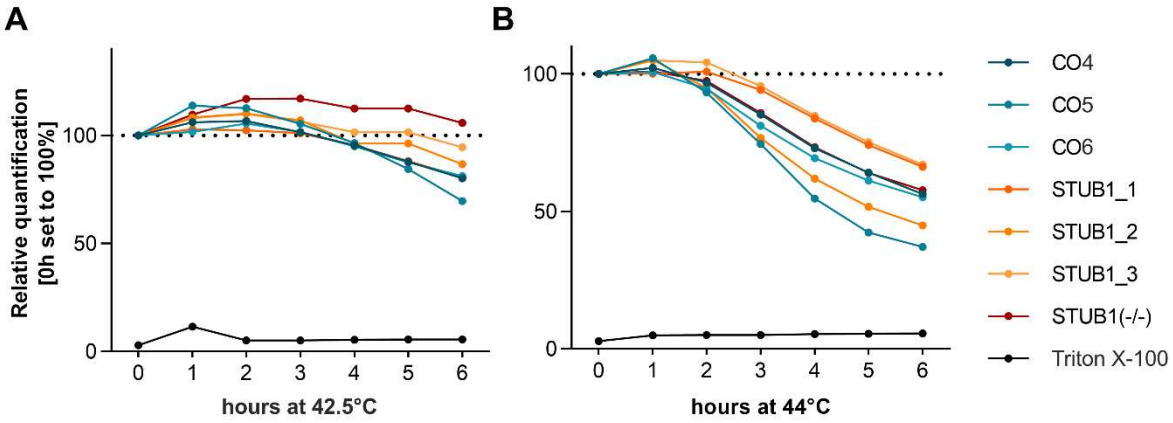

Figure 4 | Viability of cortical neurons upon heat shock is not impaired by dysfunctional CHIP. Cell viability [in %] during prolonged heat shock at **(A)** 42.5°C and **(B)** 44°C has been investigated in 3 control, 3 *STUB1* patient and a STUB1(-/-) line. Values are given as mean of triplicates. Triton X-100 was used as negative control for cell viability.

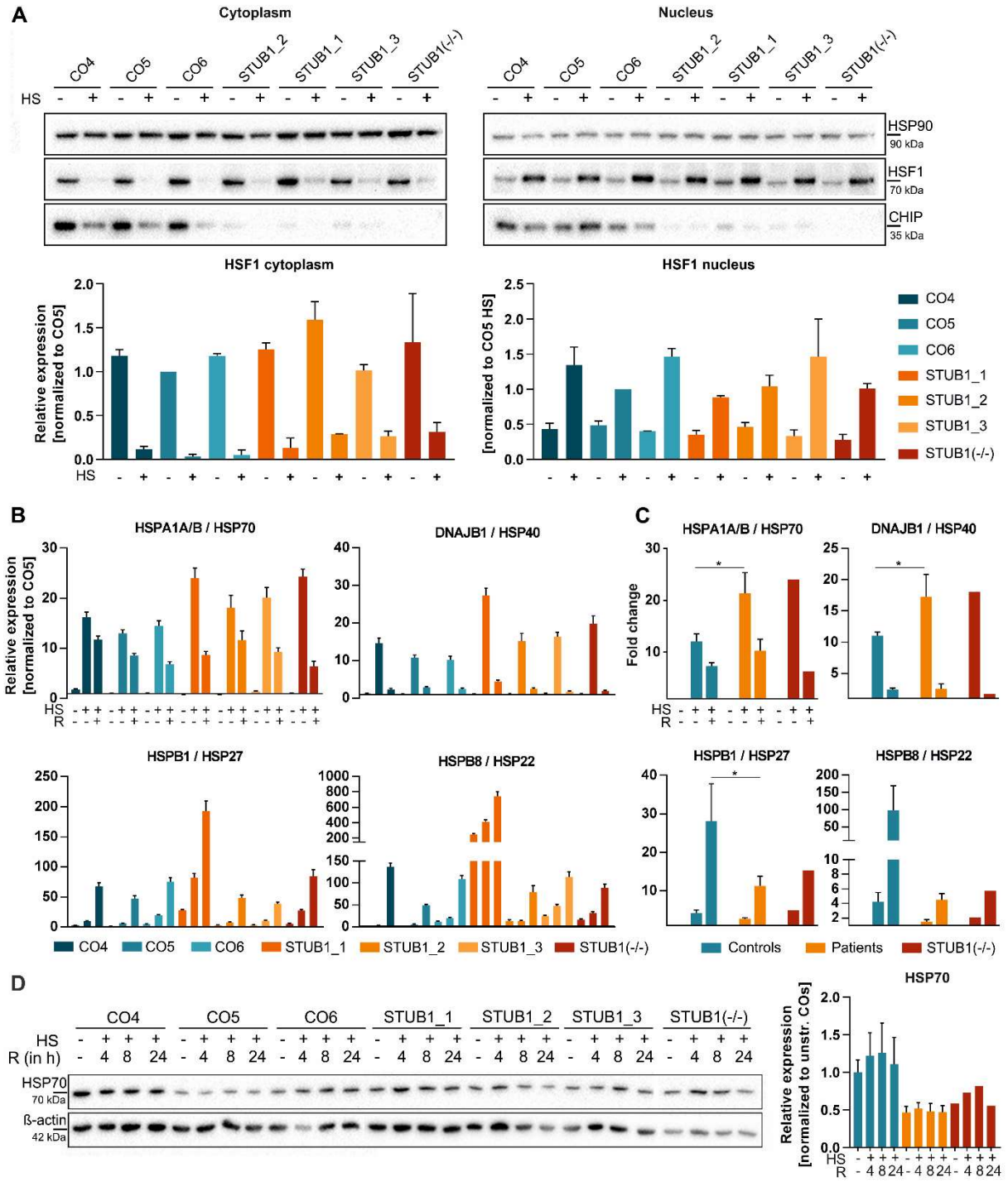

Figure 5 | Mutant CHIP does not impair the HSR in iPSC-derived cortical neurons (CNs). (A) Cytoplasmic and nuclear fractions of HSP90, HSF1 and CHIP before and after heat shock (HS, 1h, 42.5°C) in CNs of 3 controls, 3 patients and STUB1(-/-). HSP90, HSF1 levels were quantified densitometrically and normalized to HSP90 and to CO5 / CO5 HS. **(B)** Transcript analysis of *HSPA1A/B*, *DNAJB1*, *HSPB1* and *HSPB8* was performed by qRT-PCR. Values are normalized to CO5 and the housekeeping genes *GAPDH* and *TBP*. Each bar represents a triplicate with mean ± SEM. **(C)** Fold change of HSPs compared to baseline. Transcript levels of (B) were pooled for controls and patients. *: $P<0.05$; One-way ANOVA. **(D)** Western blot analysis of HSP70 levels of unstressed and heat shocked (HS) CNs with various times of recovery (R, in hours). HSP70 levels were quantified densitometrically and normalized to ß-actin. N=3 Western blots were performed as technical replicates.

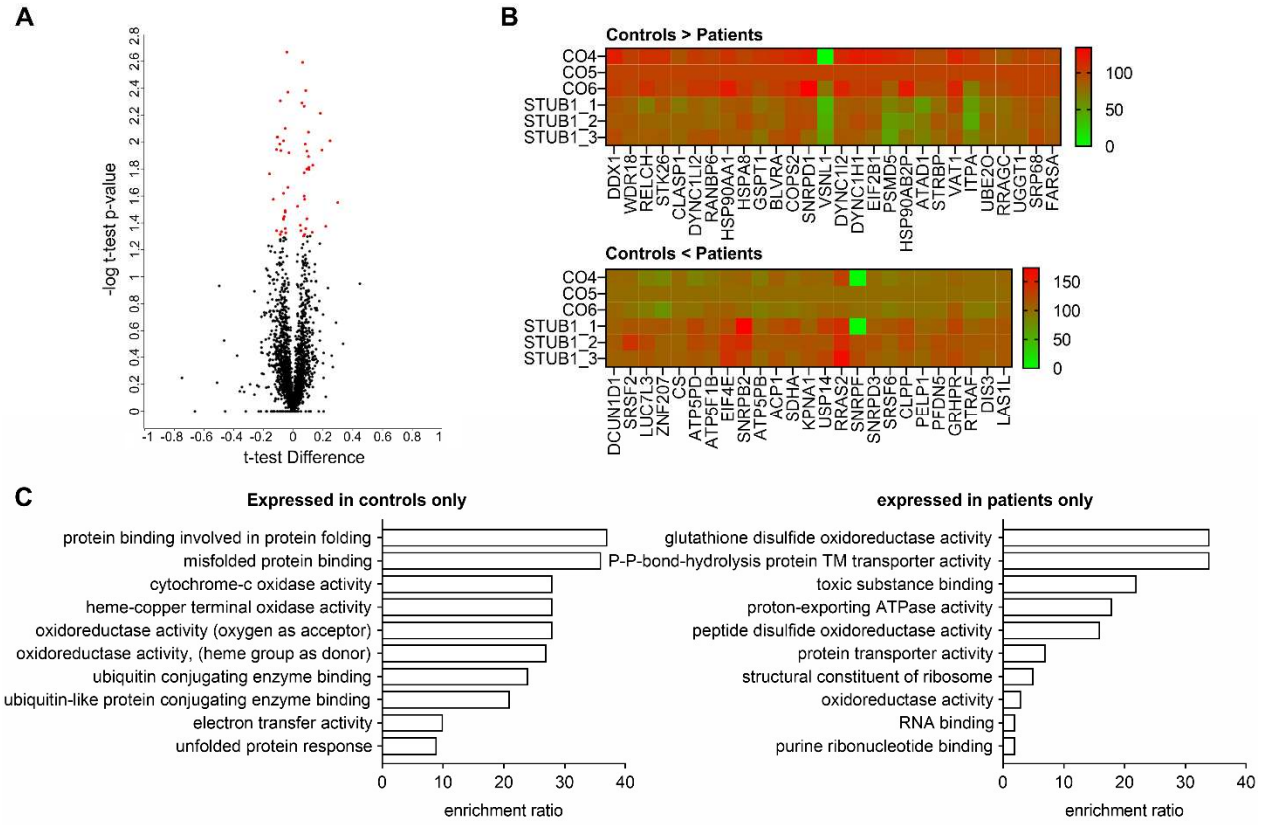

Figure 6 | Proteome analysis of cortical neurons from 3 controls and 3 STUB1 patients revealed protein (re)folding disturbances and increased oxidative stress in patients. (A) The volcano plot illustrates significantly differentially expressed proteins in patients vs. controls. The –log10 t-test p-value is plotted against the t-test difference controls vs patients. The significance threshold is set to $P = 0.05 / 1.30$ (-log10). **(B)** Heat map displaying significantly dysregulated proteins, for proteins downregulated (upper panel) and upregulated in patients (lower panel). Values are given as LOG10 LFQ intensity, CO5 is set to 100%. **(C)** Gene ontology (GO) analysis with Webgestalt of proteins expressed in at least 2 of 3 controls but not in patients (left panel) and in at least 2 of 3 patients but not in controls (right panel). Proteins were subjected to GO classification in terms of molecular function. A threshold of 5 proteins per classification was set. Enrichment ratios of GO terms are shown. GO: gene ontology.

SUPPLEMENTARY FIGURES AND TABLES

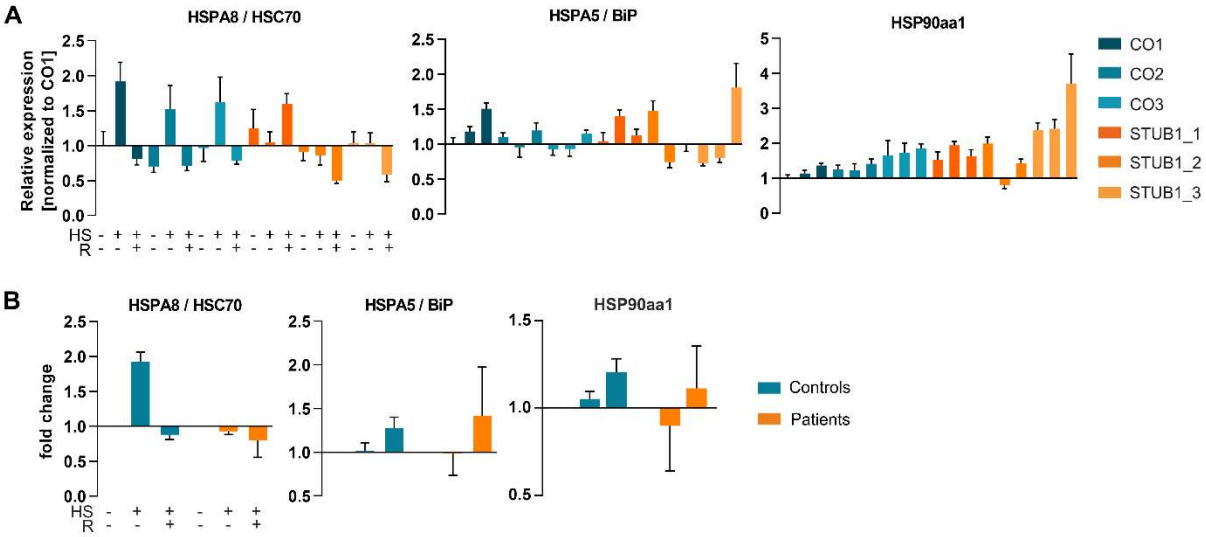

Suppl. Fig. S1: Transcript analysis of fibroblasts. (A) Transcript analysis of *HSPA8, HSPA5 and HSP90aa1* was performed by qRT-PCR. Values are normalized to CO1 and the housekeeping genes *GAPDH* and *TBP*. Each bar represents a triplicate with mean ± SEM. **(B)** Fold change of HSPs compared to baseline. Transcript levels of (B) were pooled for controls and patients.

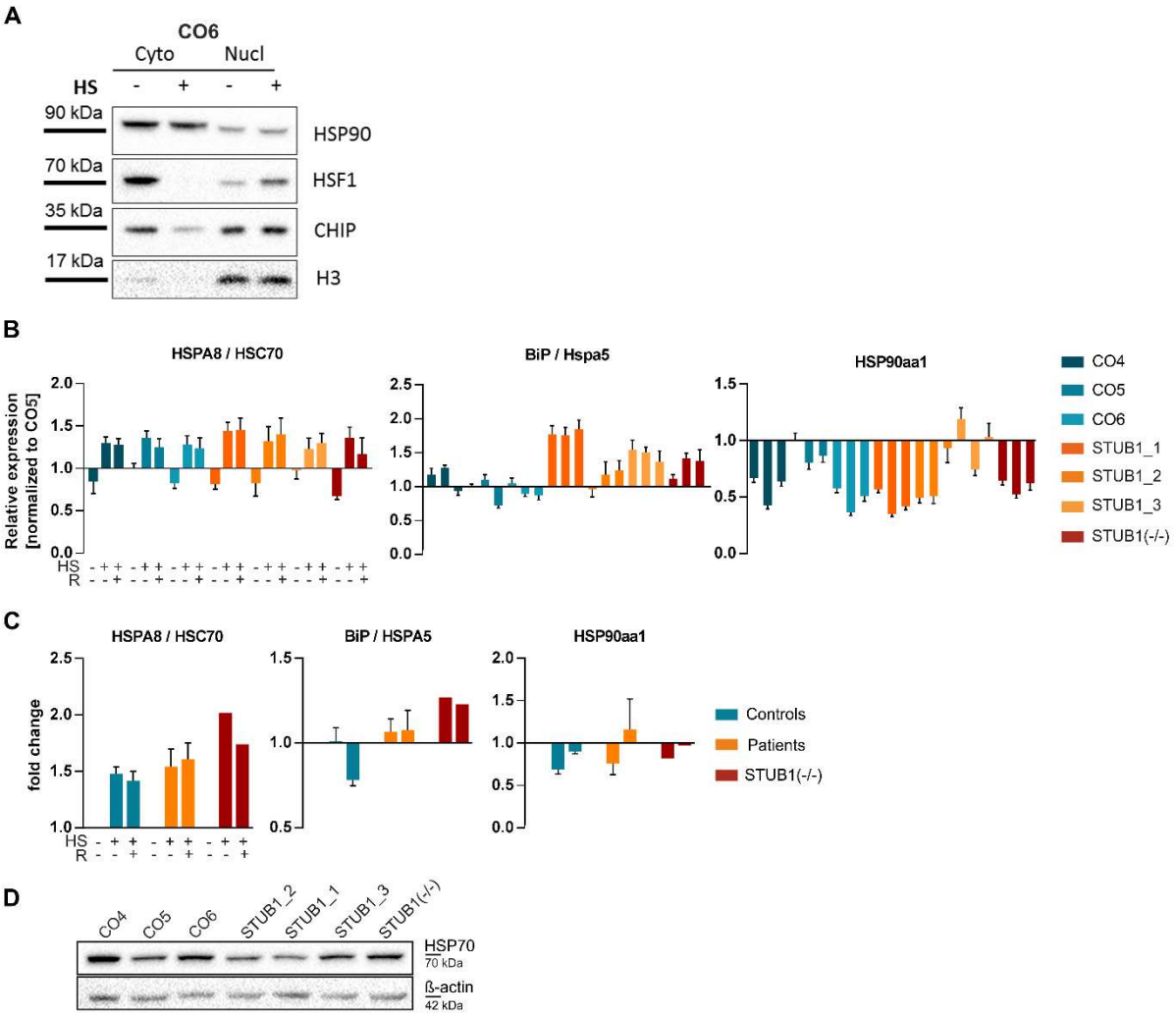

Suppl. Fig. S2 | Mutant CHIP does not impair the HSR in iPSC-derived neurons. **(A)** Representative Western blot of cortical neurons derived from iPSC of CO6 demonstrating shift of HSF1 and HSP70 but not HSP90 from the cytoplasm to the nucleus upon heat shock (HS). Proper fractionation was verified for absence or presence of histone 3 (H3) as a nuclear marker. **(B)** Transcript analysis of *HSPA8, HSPA5 and HSP90aa1* was performed by qRT-PCR. Values are normalized to CO5 and the housekeeping genes *GAPDH* and *TBP*. Each bar represents a triplicate with mean ± SEM. **(C)** Fold change of HSPs compared to baseline. Transcript levels of (B) were pooled for controls and patients. **(D)** HSP70 protein expression was assessed in unstressed cells of 3 controls, 3 patients and STUB1(-/-). ß-actin was used as loading control. Cyto: cytoplasm; Nucl: nucleus.

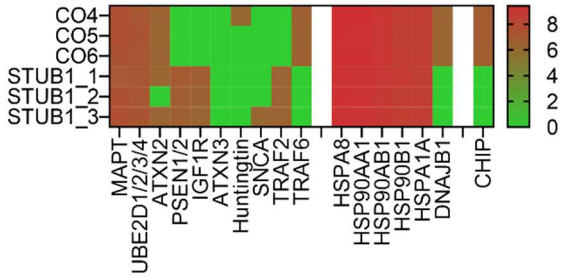

Suppl. Fig. S3 | Expression of selected CHIP interaction partners by proteomic analysis of iPSC-derived neurons. Protein of cortical neurons of 3 Controls and 3 *STUB1* patients was analyzed by LC-MS/MS and analyzed with Perseus. Values are given as –LOG10 LFQ values.

Suppl. Table S1 | Genetic characterization of SCAR16 patients, controls and generated homozygous knockout.
Controls: CO1, CO2, CO3, CO4, CO5, CO6; Patients: STUB1_1, STUB1_2, STUB1_3; f: female; m: male; F: fibroblasts; iPSC: induced pluripotent stem cells; CN: iPSC-derived cortical neurons.

Cell line	Cell type used	Age at skin biopsy, sex	Described mutations in *STUB1*	Annotations
CO1	F	28, m	None	None
CO2	F	24, f	None	None
CO3	F	22, m	None	None
CO4	iPSC, CN	46, f	None	None
CO5	iPSC, CN	37, f	None	None
CO6	iPSC, CN	46, m	None	None
STUB1_1	F, iPSC, CN	17, m	c.367C>G, p.L123V (homozygous)	symptoms: ataxia, spasticity
STUB1_2	F, iPSC, CN	32, m	c.355C>T, p.R119*; c.880A>T, p.I294T	symptoms: ataxia, spasticity, dementia, epilepsy, hypogonadism
STUB1_3	F, iPSC, CN	20, f	c.433A>C, p.K145Q; c.728C>T, p.P243L	symptoms: ataxia, spasticity, dementia, epilepsy
STUB1(-/-)	iPSC, CN	37, f	c.283-438del, p.V94Afs*5 (homozygous)	CRISPR/Cas9 induced homozygous knockout of *STUB1* isogenic to CO5

Suppl. Table S2 | qRT-PCR Primer

Target gene	Forward sequence	Reverse sequence
HSP90aa1	GCCCAGAGTGCTGAATACCC	TTAACAGGTGCCCTGCTTCT
HSPA1A/B	GGTGCTGACCAAGATGAAG	CTGCGAGTCGTTGAAGTAG
HSPA8	CCCTTTATGGTGGTGAATGA	GTAACAGTCTTCCCAAGGTAG
HSPB1	AAGCTAGCCACGCAGTCCAA	CGGCAGTCTCATCGGATTTT
HSPB8	GCTTCAAGCCAGAGGAGTTGA	ACAATGCCACCTTCTTGCTGT
HSPA5/BiP	CCCGAGAACACGGTCTTTGA	TTCAACCACCTTGAACGGCA
DNAJB1	CTGTCTTCTCTTTGGCCATCTC	CTGCTGGAACGAGAGGTATTG
STUB1	TCAAGGAGCAGGGCAATCGT	CAGCGGGTTCCGGGTGAT
GAPDH	TCACCAGGGCTGCTTTTAAC	GACAAGCTTCCCGTTCTCAG
TBP	CTTCGGAGAGTTCTGGGATTG	CACGAAGTGCAATGGTCTTTAG

Suppl. Table S3 | Proteins expressed in at least 2 control CNs and no patient CNs. Values are given in Log10 LFQ intensity.

Protein name	CO4	CO5	CO6	STUB1_1	STUB1_2	STUB1_3
AUP1	7,18	7,22	7,19	0	0	0
EBF1/2/3	6,88	7,41	7,04	0	0	0
SEC61A1	7,15	7,11	7,13	0	0	0
FMNL2	7,02	6,99	7,12	0	0	0
EML1	7,05	7,04	6,95	0	0	0
CKMT1A	6,94	7,17	6,85	0	0	0
SMPD3	6,80	7,10	7,04	0	0	0
NDUFC2;NDUFC2-KCTD14	6,92	6,98	7,04	0	0	0

FN3KRP	6,99	7,00	6,89	0	0	0
GABARAPL2	6,98	6,89	6,93	0	0	0
MUC2;MLP	6,83	6,99	6,96	0	0	0
ACTN4	6,94	6,95	6,89	0	0	0
RPS10;RPS10P5	6,81	6,80	6,99	0	0	0
TFAM	6,85	6,87	6,88	0	0	0
STAT5B;STAT5A	6,85	6,78	6,81	0	0	0
EVI5L	6,78	6,93	6,69	0	0	0
STUB1	6,83	6,82	6,73	0	0	0
STX1A	6,78	6,89	6,64	0	0	0
CMIP	6,83	6,82	6,66	0	0	0
TPPP	6,96	6,65	6,57	0	0	0
PSMD9	6,85	6,72	6,67	0	0	0
CELF3	6,69	6,86	6,63	0	0	0
LGALSL	6,67	6,90	6,60	0	0	0
RELN	6,73	6,57	6,86	0	0	0
TMEM65	6,59	6,94	6,52	0	0	0
PTP4A1/2	6,74	6,69	6,72	0	0	0
HSPE1-MOB4;MOB4	6,76	6,77	6,60	0	0	0
LPPR1	6,96	6,49	6,54	0	0	0
MTOR	6,72	6,59	6,80	0	0	0
IMPAD1	6,68	6,70	6,73	0	0	0
BACH2	6,27	7,03	6,36	0	0	0
LSM4	6,74	6,69	6,58	0	0	0
REM2	6,60	6,71	6,69	0	0	0
VPS11	6,65	6,72	6,63	0	0	0
KIAA1279	6,72	6,50	6,74	0	0	0
ASAP1	6,60	6,62	6,73	0	0	0
LUC7L	6,65	6,65	6,66	0	0	0
ARHGAP32	6,67	6,71	6,57	0	0	0
RAP2A/B/C	6,61	6,61	6,61	0	0	0
POU3F1/2/3	6,69	6,50	6,59	0	0	0
PAK7	6,50	6,76	6,46	0	0	0
KALRN	6,53	6,62	6,58	0	0	0
PIK3C2B	6,59	6,63	6,51	0	0	0
INTS1	6,49	6,51	6,69	0	0	0
MAVS	6,68	6,39	6,60	0	0	0
GMPPB	6,64	6,64	6,37	0	0	0
RABL6	6,48	6,61	6,56	0	0	0
EIF3K	6,56	6,55	6,55	0	0	0
CA2	6,48	6,42	6,70	0	0	0
CELSR3	6,49	6,56	6,54	0	0	0

EXOC3	6,50	6,57	6,51	0	0	0
WDR7	6,52	6,59	6,43	0	0	0
CEP97	6,55	6,51	6,48	0	0	0
NDUFA12	6,56	6,55	6,40	0	0	0
CBX1	6,44	6,50	6,55	0	0	0
RPRD2	6,52	6,43	6,49	0	0	0
NACAD	6,51	6,45	6,48	0	0	0
TRAF6	6,51	6,40	6,50	0	0	0
ACSS2	6,61	6,39	6,39	0	0	0
IK	6,37	6,54	6,49	0	0	0
STAU2	6,50	6,53	6,37	0	0	0
ARVCF	6,48	6,54	6,38	0	0	0
STAMBP	6,44	6,49	6,46	0	0	0
AIDA	6,46	6,44	6,43	0	0	0
HSPA14	6,38	6,44	6,50	0	0	0
TIGD4;APBB1	6,44	6,42	6,44	0	0	0
CNOT10	6,40	6,46	6,44	0	0	0
NARS2	6,46	6,43	6,41	0	0	0
INPP5F	6,36	6,36	6,50	0	0	0
SLC35A4	6,38	6,43	6,43	0	0	0
CHERP	6,40	6,41	6,38	0	0	0
C10orf76	6,40	6,45	6,32	0	0	0
AMER2	6,50	6,30	6,31	0	0	0
FAM188A	6,54	6,24	6,29	0	0	0
ARFIP2	6,29	6,43	6,40	0	0	0
PPP1R12A	6,35	6,37	6,40	0	0	0
FMR1	6,46	6,20	6,40	0	0	0
MRE11A	6,35	6,26	6,45	0	0	0
TRAPPC1	6,39	6,40	6,27	0	0	0
POGLUT1	6,33	6,30	6,41	0	0	0
DCK	6,26	6,54	6,15	0	0	0
GABBR1	6,32	6,44	6,26	0	0	0
TTYH1	6,27	6,19	6,51	0	0	0
PML	6,28	6,17	6,51	0	0	0
EXOC6B	6,45	6,28	6,26	0	0	0
CNTNAP5	6,29	6,32	6,36	0	0	0
DIS3L2	6,42	6,23	6,18	0	0	0
CRBN	6,33	6,24	6,19	0	0	0
FYTTD1	6,26	6,35	6,10	0	0	0
DNAJB1	6,30	6,24	6,18	0	0	0
NPC1	6,19	6,15	6,32	0	0	0
TRAPPC9	6,12	6,28	6,13	0	0	0
METTL13	6,27	6,14	6,11	0	0	0

GEMIN5	6,17	6,11	6,21	0	0	0
ACTBL2	9,07	0	7,39	0	0	0
SRSF7	0	7,10	7,10	0	0	0
PCNT	7,13	7,03	0	0	0	0
TMEM35	7,08	0	6,96	0	0	0
ATR	0	6,99	6,98	0	0	0
KIAA1211	7,03	0	6,88	0	0	0
RPL29	6,88	0	7,02	0	0	0
NUDT1	0	7,05	6,80	0	0	0
FAF1	6,93	6,86	0	0	0	0
THG1L	7,04	0	6,68	0	0	0
RPS15A	6,84	6,88	0	0	0	0
NKIRAS2	0	6,91	6,75	0	0	0
PFDN2	6,88	0	6,79	0	0	0
COX5B	6,68	6,89	0	0	0	0
ERCC4	6,73	6,81	0	0	0	0
DNAJC7	6,68	0	6,77	0	0	0
RAP1GAP	6,42	6,88	0	0	0	0
COX5A	6,69	0	6,72	0	0	0
SREK1	0	6,64	6,72	0	0	0
CLVS1	6,83	6,44	0	0	0	0
DAZAP1	0	6,65	6,69	0	0	0
RASAL2	6,58	6,73	0	0	0	0
DHX38	6,56	6,73	0	0	0	0
KCTD15	6,72	0	6,56	0	0	0
SORBS2	6,72	0	6,54	0	0	0
TAB1	6,60	0	6,66	0	0	0
SMAP2	6,66	6,59	0	0	0	0
NR1I2	6,75	0	6,43	0	0	0
GNB4	0	6,79	6,31	0	0	0
SCAPER	6,64	6,59	0	0	0	0
FOXP2	6,76	6,37	0	0	0	0
EPHB1	0	6,68	6,52	0	0	0
PREPL	6,46	6,67	0	0	0	0
CLPB	0	6,60	6,56	0	0	0
SIRPA	0	6,62	6,48	0	0	0
UQCRQ	6,51	0	6,60	0	0	0
RABL2A/B	6,51	6,60	0	0	0	0
RABGEF1	6,54	6,54	0	0	0	0
QTRTD1	6,41	0	6,63	0	0	0
KIAA0930	6,55	0	6,50	0	0	0
AKT3	6,51	0	6,53	0	0	0
SKIV2L	6,42	0	6,60	0	0	0

PPIL4	0	6,52	6,49	0	0	0
RAD23A	6,53	0	6,45	0	0	0
EFNB2	6,53	6,44	0	0	0	0
ZYG11B	6,51	6,46	0	0	0	0
ERI3	6,48	6,49	0	0	0	0
CEND1	6,47	0	6,47	0	0	0
NME7	6,53	6,39	0	0	0	0
SELENBP1	6,58	0	6,29	0	0	0
DIAPH1	6,46	6,45	0	0	0	0
TRMT10C	0	6,44	6,45	0	0	0
TMEM163	6,42	0	6,46	0	0	0
KATNAL1	0	6,32	6,53	0	0	0
DDX39A	0	6,32	6,52	0	0	0
DTX3	6,46	6,40	0	0	0	0
VCPIP1	6,38	6,46	0	0	0	0
DCHS1	6,44	0	6,39	0	0	0
ARMC1	0	6,44	6,36	0	0	0
NDN	0	6,45	6,34	0	0	0
UBR7	0	6,32	6,47	0	0	0
BCS1L	0	6,50	6,26	0	0	0
FECH	6,47	0	6,26	0	0	0
GCLC	6,24	0	6,43	0	0	0
QTRT1	0	6,43	6,22	0	0	0
NAA30	6,25	6,40	0	0	0	0
SMG8	6,29	6,36	0	0	0	0
CHCHD6	0	6,44	6,15	0	0	0
EIF2B2	6,34	0	6,30	0	0	0
PCID2	0	6,23	6,39	0	0	0
MYCBP2	6,28	6,34	0	0	0	0
SLC25A29	6,27	6,33	0	0	0	0
NCOA5	6,20	6,34	0	0	0	0
CBWD1/2/3/5/6/7	6,17	6,36	0	0	0	0
RDH14	0	6,45	5,97	0	0	0
RPS6KA4/5	6,24	6,29	0	0	0	0
PRPF4	6,28	6,24	0	0	0	0
APPL2	6,19	0	6,31	0	0	0
ERCC2	6,29	0	6,21	0	0	0
ELP3	6,21	6,28	0	0	0	0
NAGLU	6,25	6,20	0	0	0	0
ZFYVE20	6,28	0	6,15	0	0	0
KIAA1033	6,01	6,35	0	0	0	0
GAK	0	6,33	6,03	0	0	0
CDH10	6,29	0	6,08	0	0	0

C18orf8	6,21	0	6,19	0	0	0
DOCK3	6,06	6,28	0	0	0	0
CCNY;CCNYL1/2	6,11	0	6,17	0	0	0
IP6K1	6,08	6,14	0	0	0	0
CAND2	0	6,06	6,11	0	0	0
LZTS1	5,97	6,17	0	0	0	0

Suppl. Table S4 | Proteins expressed in at least 2 patient CNs and no control CNs. Values are given in Log10 LFQ intensity.

Protein name	**CO4**	**CO5**	**CO6**	**STU B1_1**	**STU B1_2**	**STU B1_3**
VPS18	0	0	0	6,04	6,06	6,13
SUPV3L1	0	0	0	6,23	6,09	6,07
CPT1C	0	0	0	6,24	6,14	6,17
PTPRO	0	0	0	6,21	6,20	6,18
TARBP2	0	0	0	6,19	6,16	6,25
ADAM10	0	0	0	6,37	6,12	6,06
PRPS2	0	0	0	6,25	6,13	6,23
PIGU	0	0	0	6,43	6,06	6,02
WDR26	0	0	0	6,27	6,18	6,29
DHX16	0	0	0	6,26	6,20	6,32
NUDCD2	0	0	0	6,18	6,35	6,27
STAM2	0	0	0	6,25	6,32	6,28
USP48	0	0	0	6,25	6,29	6,34
FBXO21	0	0	0	6,21	6,33	6,38
MRPS9	0	0	0	6,46	6,20	6,24
CNTN2	0	0	0	6,39	6,41	6,11
TRAF2	0	0	0	6,32	6,37	6,31
THNSL1	0	0	0	6,35	6,32	6,34
FAHD2A/B	0	0	0	6,42	6,29	6,29
SMYD3	0	0	0	6,31	6,17	6,50
Mar-05	0	0	0	6,45	6,26	6,31
CHTOP	0	0	0	6,28	6,39	6,40
UROD	0	0	0	6,45	6,28	6,33
FAR1	0	0	0	6,51	6,23	6,31
DTNA;DTNB	0	0	0	6,52	6,27	6,28
KDM3B	0	0	0	6,42	6,46	6,20
TRAPPC4	0	0	0	6,37	6,42	6,36
ZC3HC1	0	0	0	6,43	6,40	6,32
TOM1L2	0	0	0	6,37	6,34	6,44
MOCS3	0	0	0	6,31	6,45	6,40
MID1	0	0	0	6,66	6,21	6,15
PITPNM1	0	0	0	6,46	6,31	6,45

RELA	0	0	0	6,41	6,43	6,41
SNRPG;SNRPGP15	0	0	0	6,42	6,39	6,44
CNOT2	0	0	0	6,37	6,44	6,44
SLC8A2	0	0	0	6,15	6,58	6,44
ALG9	0	0	0	6,55	6,37	6,33
SRPK2	0	0	0	6,36	6,44	6,49
ACSL1	0	0	0	6,54	6,38	6,36
FAM120B	0	0	0	6,44	6,46	6,41
PTCD3	0	0	0	6,58	6,38	6,30
WASF3	0	0	0	6,23	6,59	6,48
RSRC2	0	0	0	6,41	6,60	6,36
PUM2	0	0	0	6,36	6,59	6,44
GMPPA	0	0	0	6,56	6,42	6,45
HMOX2	0	0	0	6,55	6,42	6,50
YARS2	0	0	0	6,64	6,38	6,41
SUMF2	0	0	0	6,63	6,41	6,41
DNAJC9	0	0	0	6,60	6,45	6,44
UBE4A	0	0	0	6,46	6,49	6,55
NPC2	0	0	0	6,72	6,34	6,34
TUBGCP2	0	0	0	6,48	6,50	6,54
CYTH1/2/3	0	0	0	6,47	6,57	6,49
CRAT	0	0	0	6,47	6,51	6,55
C8orf82	0	0	0	6,65	6,45	6,40
PFDN4	0	0	0	6,45	6,56	6,54
NOSIP	0	0	0	6,60	6,48	6,47
CNOT11	0	0	0	6,56	6,56	6,46
TMEM11	0	0	0	6,59	6,54	6,44
PACSIN2	0	0	0	6,54	6,48	6,57
ANKRD28	0	0	0	6,30	6,71	6,49
SPTLC1	0	0	0	6,77	6,30	6,39
CYFIP1	0	0	0	6,53	6,47	6,59
RALB	0	0	0	6,51	6,57	6,56
CHID1	0	0	0	6,69	6,45	6,46
ESYT2	0	0	0	6,72	6,41	6,46
C11orf73	0	0	0	6,40	6,46	6,75
CARS2	0	0	0	6,67	6,40	6,60
IGF1R	0	0	0	6,75	6,48	6,40
SELT	0	0	0	6,59	6,57	6,59
BLVRB	0	0	0	6,58	6,67	6,51
SLC35F6	0	0	0	6,82	6,43	6,40
NUP35	0	0	0	6,68	6,54	6,57
TMOD3	0	0	0	6,81	6,42	6,46
ABI1	0	0	0	6,52	6,68	6,59

LIG3	0	0	0	6,65	6,62	6,55
MAP7D1	0	0	0	6,51	6,67	6,63
TMEM256	0	0	0	6,78	6,49	6,48
HRSP12	0	0	0	6,73	6,54	6,54
NME4	0	0	0	6,93	6,36	6,16
DST	0	0	0	6,69	6,60	6,54
DVL2/3	0	0	0	6,69	6,56	6,60
CDK9	0	0	0	6,66	6,58	6,63
FAM171A2	0	0	0	6,54	6,69	6,65
DDI2	0	0	0	6,81	6,49	6,52
UBXN6	0	0	0	6,58	6,67	6,65
AP3B1	0	0	0	6,91	6,42	6,35
COLGALT1	0	0	0	6,92	6,36	6,40
SNX3	0	0	0	6,69	6,59	6,68
HPCAL4	0	0	0	6,47	6,78	6,69
TRAPPC3	0	0	0	6,57	6,67	6,74
C4orf27	0	0	0	6,63	6,67	6,72
AVIL	0	0	0	6,59	6,76	6,66
MOB1A/B	0	0	0	6,94	6,51	6,42
STK4	0	0	0	6,69	6,64	6,73
RBBP7	0	0	0	6,58	6,53	6,88
DENR	0	0	0	6,66	6,77	6,65
WRNIP1	0	0	0	6,65	6,63	6,80
TMCO1	0	0	0	6,74	6,71	6,67
PPP1R8	0	0	0	6,69	6,70	6,75
GOLGA4	0	0	0	6,60	6,62	6,89
LRPAP1	0	0	0	6,99	6,53	6,44
M6PR	0	0	0	6,80	6,66	6,74
SERINC1	0	0	0	6,86	6,68	6,65
TIGAR	0	0	0	6,77	6,70	6,76
RER1	0	0	0	6,93	6,62	6,61
PCYOX1L	0	0	0	6,71	6,77	6,78
GPC6	0	0	0	6,98	6,56	6,59
TIMM23;TIMM23B	0	0	0	6,73	6,79	6,78
PSEN1/2	0	0	0	6,95	6,68	6,66
MBOAT7	0	0	0	6,94	6,70	6,67
PPAPDC2	0	0	0	6,69	6,93	6,72
SYNE1	0	0	0	6,88	6,72	6,76
PEX11B	0	0	0	6,88	6,77	6,79
PHPT1	0	0	0	6,79	6,81	6,87
CARHSP1	0	0	0	6,84	6,86	6,85
NDUFS7	0	0	0	6,97	6,80	6,81
BDH2	0	0	0	6,92	6,85	6,83

PDPK1/2	0	0	0	6,76	6,99	6,83
REEP5	0	0	0	6,96	6,84	6,81
ITGB1	0	0	0	7,22	6,62	6,56
UNC119B	0	0	0	6,93	6,84	6,97
MMAB	0	0	0	7,11	6,94	6,73
NELFA	0	0	0	6,77	7,05	7,01
POFUT1	0	0	0	7,23	6,71	6,74
CISD2	0	0	0	6,95	6,91	7,03
RBM8A	0	0	0	6,97	7,01	6,96
C21orf33	0	0	0	7,06	7,05	7,06
SSR4	0	0	0	7,23	7,02	6,91
SEC61B	0	0	0	7,17	7,09	6,99
ARSB	0	0	0	7,32	6,94	7,03
PAPSS1	0	0	0	7,33	7,11	7,05
NR2F1	0	0	0	7,70	7,20	6,85
RTN1	0	0	0	7,31	7,67	7,53
LMNA	0	0	0	8,02	6,58	6,39
ACTB	0	0	0	8,12	8,18	8,14
MRPS34	0	0	0	0	6,08	6,01
KATNB1	0	0	0	5,99	0	6,12
PI4K2A	0	0	0	6,23	5,79	0
C7orf26	0	0	0	6,10	6,11	0
PICK1	0	0	0	0	6,10	6,17
NDC1	0	0	0	6,24	0	6,21
EFHD1/2	0	0	0	0	6,33	6,11
FOXRED1	0	0	0	6,26	6,21	0
IQSEC1	0	0	0	6,11	6,36	0
UBE4B	0	0	0	0	6,16	6,34
MPP6	0	0	0	6,17	6,34	0
PTPRD	0	0	0	0	6,29	6,23
TMEM68	0	0	0	6,35	6,18	0
RBM17	0	0	0	6,29	0	6,27
EI24	0	0	0	6,28	6,31	0
PLCD1	0	0	0	6,37	0	6,21
TPD52L2	0	0	0	6,43	0	6,18
GTF3C5	0	0	0	6,36	6,28	0
ARMC10	0	0	0	6,35	6,31	0
AASS	0	0	0	6,46	6,18	0
TAOK1	0	0	0	0	6,39	6,36
EXOSC7	0	0	0	6,35	0	6,40
RFX3	0	0	0	6,28	6,45	0
PEX14	0	0	0	6,34	0	6,42
MRPL48	0	0	0	6,52	6,21	0

ABCF2	0	0	0	6,49	6,29	0
MYT1	0	0	0	0	6,32	6,47
TRMT1;SEMA4B	0	0	0	6,49	0	6,30
AGL	0	0	0	0	6,50	6,30
H6PD	0	0	0	6,50	0	6,31
RNF214	0	0	0	0	6,43	6,40
GMPR2	0	0	0	6,27	0	6,53
DAGLB	0	0	0	6,61	0	6,08
ARRB2	0	0	0	0	6,46	6,39
MRPL4	0	0	0	6,49	6,36	0
EIF4G3	0	0	0	6,44	0	6,42
ARHGAP21	0	0	0	0	6,42	6,45
MTPAP	0	0	0	6,60	0	6,19
NUBP2	0	0	0	6,33	0	6,53
CPOX	0	0	0	6,46	0	6,43
RAB3B	0	0	0	6,55	6,32	0
MPI	0	0	0	6,36	0	6,55
TMEM214	0	0	0	6,67	0	6,06
RMDN1	0	0	0	6,56	0	6,37
HIBADH	0	0	0	6,67	6,12	0
SEH1L	0	0	0	6,57	6,36	0
MRPL43	0	0	0	0	6,44	6,51
NOL4L	0	0	0	0	6,43	6,52
PJA2	0	0	0	6,54	6,42	0
CELF4	0	0	0	0	6,45	6,51
ERLIN1	0	0	0	6,62	0	6,30
DNMT1	0	0	0	6,59	0	6,40
TSPAN6	0	0	0	6,69	0	6,21
SGSH	0	0	0	6,69	6,22	0
RAP1A/B	0	0	0	6,49	0	6,57
FDXR	0	0	0	6,70	6,29	0
CHL1	0	0	0	6,71	6,32	0
MACROD2	0	0	0	0	6,55	6,60
GUCY1B3	0	0	0	0	6,52	6,64
SPCS1	0	0	0	0	6,62	6,59
TMEM30A	0	0	0	0	6,70	6,51
PPP4R1	0	0	0	0	6,59	6,68
EIF2B5	0	0	0	6,58	0	6,69
RPS15	0	0	0	0	6,72	6,56
CCDC132	0	0	0	0	6,62	6,67
PRNP	0	0	0	0	6,62	6,71
PLOD3	0	0	0	6,88	6,22	0
RAB33A	0	0	0	0	6,72	6,64

TOMM20	0	0	0	0	6,77	6,58
ITGAV	0	0	0	6,90	0	6,28
SF3B4	0	0	0	6,68	0	6,73
CTSA	0	0	0	6,84	6,59	0
CPVL	0	0	0	6,92	0	6,47
RBX1	0	0	0	0	6,83	6,67
FAT1	0	0	0	6,92	0	6,55
EIF1;EIF1B	0	0	0	6,78	6,77	0
BTF3L4	0	0	0	6,73	6,82	0
PVRL2	0	0	0	6,97	0	6,50
BSCL2	0	0	0	6,90	6,67	0
VPS52	0	0	0	6,83	0	6,91
EPHA7	0	0	0	7,05	6,69	0
GPM6B	0	0	0	6,87	7,12	0
SCGN	0	0	0	0	6,60	7,28
MGST1	0	0	0	7,30	0	6,75
DBI	0	0	0	0	7,12	7,14
PDPR	0	0	0	0	7,07	7,19
UBTF	0	0	0	7,19	0	7,22
P4HA1	0	0	0	7,50	6,28	0
TP53I11	0	0	0	0	7,41	7,09
SWAP70	0	0	0	7,46	7,29	0
CALB1	0	0	0	7,80	6,78	0
TTN	0	0	0	7,99	8,04	0

Establishment of SPAST mutant induced pluripotent stem cells (iPSCs) from a hereditary spastic paraplegia (HSP) patient.

Hauser S, Erzler M, Theurer Y, **Schuster S**, Schüle R, Schöls L (2016). Establishment of SPAST mutant induced pluripotent stem cells (iPSCs) from a hereditary spastic paraplegia (HSP) patient. *Stem Cell Res,* 17(3):485-488.

Stem Cell Research 17 (2016) 485–488

Contents lists available at ScienceDirect

Stem Cell Research

journal homepage: www.elsevier.com/locate/scr

Lab Resource: Stem Cell Line

Establishment of SPAST mutant induced pluripotent stem cells (iPSCs) from a hereditary spastic paraplegia (HSP) patient

Stefan Hauser [a], Melanie Erzler [a], Yvonne Theurer [a], Stefanie Schuster [b,c], Rebecca Schüle [a,b], Ludger Schöls [a,b,*]

[a] German Center for Neurodegenerative Diseases (DZNE), Tuebingen, Germany
[b] Department of Neurology and Hertie Institute for Clinical Brain Research, University of Tuebingen, Tuebingen, Germany
[c] Graduate School of Cellular and Molecular Neuroscience, University of Tuebingen, Tuebingen, Germany

ARTICLE INFO

Article history:
Received 12 September 2016
Accepted 22 September 2016
Available online 26 September 2016

ABSTRACT

Human skin fibroblasts were isolated from a 40-year-old hereditary spastic paraplegia patient carrying an intronic splice site mutation (c.1687 + 2 T > A) in *SPAST*, leading to hereditary spastic paraplegia type 4 (SPG4). Fibroblasts were reprogrammed using episomal plasmids carrying *hOCT4*, *hSOX2*, *hKLF4*, *hL-MYC* and *hLIN28*. The generated transgene-free line iPS-SPG4-splice retained the specific mutation with no additional genomic aberrations, expressed pluripotency markers and was able to differentiate into cells of all germ layers *in vitro*. The generated iPS-SPG4-splice line might be a useful platform to study the pathomechanism of SPG4.

Resource table:

Name of Stem Cell line	iPS-SPG4-splice
Institution	German Center for Neurodegenerative Diseases (DZNE), Tuebingen, Germany
Person who created resource	Stefan Hauser, Melanie Erzler, Yvonne Theurer, Stefanie Schuster
Contact person and email	Ludger Schöls; Ludger.Schoels@uni-tuebingen.de
Date archived/stock date	July 2015
Origin	Human skin fibroblasts
Type of resource	Biological reagent: induced pluripotent stem cell (iPSCs); derived from a SPG4 patient carrying a heterozygous c.1687 + 2 T > A splice site mutation
Sub-type	Induced pluripotent stem cells (iPSCs)
Key transcription factors	*hOCT4*, *hSOX2*, *hKLF4*, *hL-MYC*, *hLIN28* (Addgene plasmids 27,076, 27,078 and 27,080; Okita et al., 2011)
Authentication	Identity and purity of iPS-SPG4-splice line confirmed by analysis of plasmid integration, mutation sequencing, SNP array analysis, pluripotency markers and *in vitro* differentiation potential
Link to related literature	N/A
Information in public databases	N/A
Ethics	Patient informed consent obtained/ Ethics Review Board-competent authority approval obtained

1. Resource details

Hereditary spastic paraplegia (HSP) is a neurodegenerative disorder characterised by lower limb spasticity and weakness due to axonal degeneration in the corticospinal tract. The most common form of HSP is the autosomal dominantly inherited spastic paraplegia type 4 (SPG4) which is caused by mutations within the *SPAST* gene encoding for the microtubule-severing enzyme spastin (Schule et al., 2016). To study the underlying disease mechanisms, the iPSC line iPS-SPG4-splice was generated by delivery of episomal plasmids encoding human *OCT4*, *SOX2*, *KLF4*, *L-MYC* and *LIN28* in skin fibroblasts from a 40-year-old patient with a phenotype of pure HSP (Okita et al., 2011). Gait difficulties developed early in childhood with a slowly progressive course of disease. The quality of the generated iPSCs was investigated by genotypic and functional assays. Genomic integrity was analysed by comparative SNP analysis of fibroblasts and the generated iPSCs (Fig. 1A), resequencing of the mutation-site (Fig. 1B) and exclusion of genomic integration of episomal plasmids (Fig. 1C). The expression of pluripotency markers on protein and RNA level was assessed by alkaline phosphatase staining (ALP) (Fig. 2A), immunocytochemical stainings of OCT4, TRA-

* Corresponding author at: German Center for Neurodegenerative Diseases (DZNE), Tuebingen, Germany.
E-mail address: ludger.schoels@uni-tuebingen.de (L. Schöls).

http://dx.doi.org/10.1016/j.scr.2016.09.022

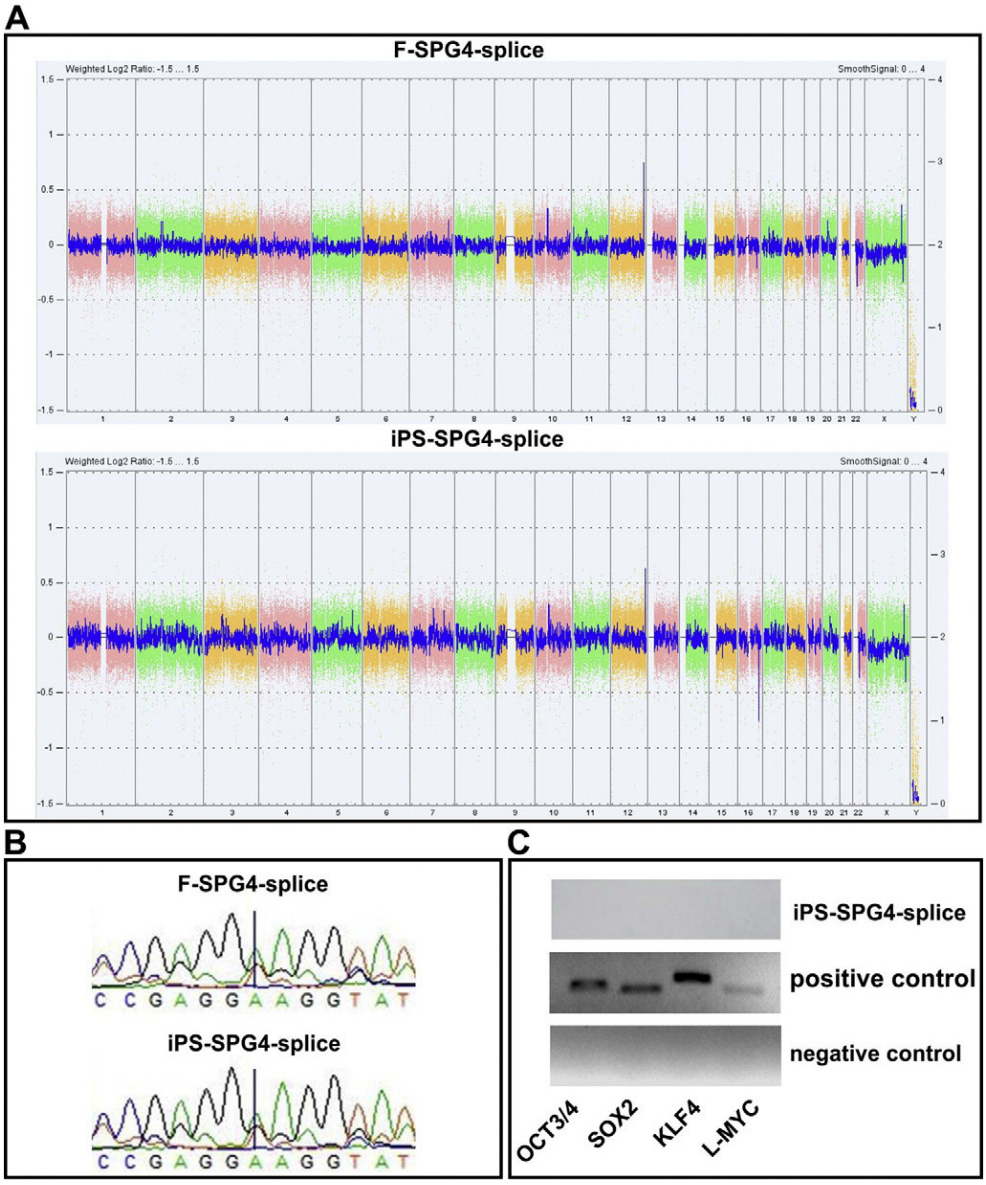

Fig. 1. Genomic characterisation of generated iPS-SPG4-splice. (A) SNP array analysis of fibroblast (F-SPG4-splice) and generated iPSCs (iPS-SPG4-splice) reveal genomic integrity. Data is shown in whole genome view (WGV) and expressed as the weighted log2 ratio of the copy number on the left Y-axis (blue line), and the chromosome number on the X-axis. (B) Sanger sequencing of the region containing the heterozygous splice site mutation c.1687 + 2 T > A in F-SPG4-splice and iPS-SPG4-splice. (C) RT-PCR verification of the absence of plasmid integration in iPS-SPG4-splice. Plasmid-specific primer for hOCT3/4, SOX2, KLF4, and L-MYC with DNA from iPS-SPG4-splice, plasmid samples as positive control, and ddH_2O as negative control were used.

1-81, NANOG and SSEA-4 (Fig. 2B) as well as qRT-PCR analysis of OCT4, NANOG, KLF4, c-MYC, SOX2, REX1, DNMT3B and TDGF1 in comparison to human embryonic stem cell lines (HuES-H6 / HuES—H9) and fibroblasts (Fig. 2C). Additionally, the potential of generated iPSCs to differentiate into cells of all three germ layers was investigated. iPSCs were able to differentiate into neurons expressing β-III-tubulin, muscle cells positive for α-smooth muscle actin (SMA), and early endodermal cells positive for α-fetoprotein (AFP) (Fig. 2D).

2. Materials and methods

2.1. Reprogramming of fibroblast to iPSCs

Patient fibroblasts carrying a heterozygous splice site mutation (c.1687 + 2 T > A) in *SPAST* were derived from skin biopsies by dissection and cultivation in fibroblast medium consisting of Dulbecco's modified eagle's medium (DMEM) high glucose (Life technologies) with 10% fetal bovine serum (FBS, Life technologies). After approx. 10 days of cultivation at 37 °C and 5% CO_2 fibroblasts were collected and expanded by medium change every 2–3 days. Reprogramming was achieved by nucleofection of 1×10^5 cells with 1 μg of each plasmid (*hOCT4*, *hSOX2*, *hKLF4*, *hL-MYC* and *hLIN28* (Okita et al., 2011)) using the Nucleofector 2D system (Lonza). After reprogramming, cells were replaced in one well of a 6-well plate and cultivated for 1 day in fibroblast medium. After a period of 2 days in fibroblast medium supplemented with 2 ng/ml FGF-2 (Peprotech) cells were transferred to Essential 8 (E8) medium containing 100 μM NaB (Sigma-Aldrich). 3–4 weeks after reprogramming, iPSC colonies were picked manually and further cultivated on Matrigel-coated 6-well dishes using E8 medium. IPSCs were split in a ratio of 1:6–1:12 by adding PBS/EDTA (0.02% EDTA in

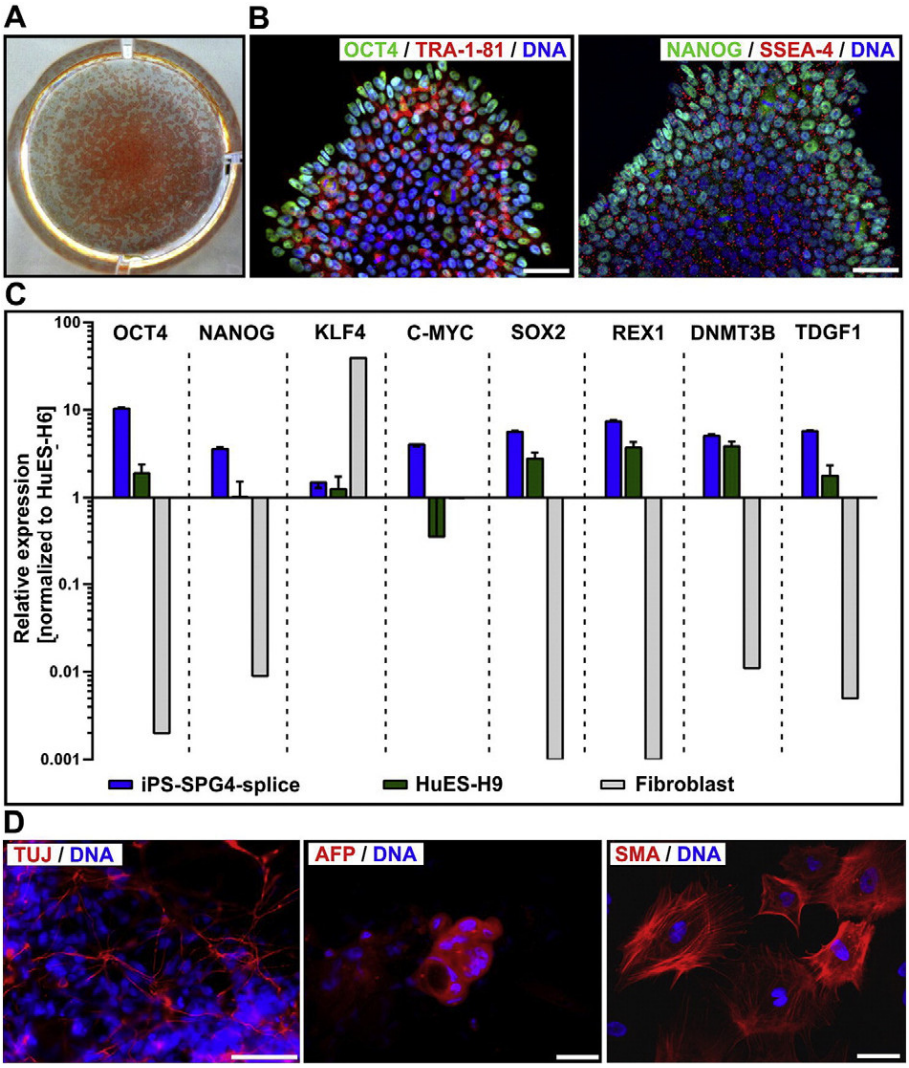

Fig. 2. Functional characterisation of generated iPS-SPG4-splice by (A) alkaline phosphatase (ALP) activity and the expression of specific pluripotency marker identified *via* (B) immunocytochemical staining of OCT4 (green), TRA1–81 (red) as well as NANOG (green) and SSEA-4 (red). Nuclei are counterstained with DAPI (blue). Scale bar = 50 μm. (C) qRT-PCR with cDNA from iPS-SPG4-splice, HuES—H6, HuES-H9 and fibroblasts and pluripotency specific primers OCT4, NANOG, KLF4, C-MYC, SOX2, REX1, DNMT3B and TDGF1 normalized to the housekeeping gene GAPDH and the hESCs HuES—H6. (D) Immunostainings of ectodermal (β-III-tubulin (TUJ), scale bar = 100 μm), endodermal (α-fetoprotein (AFP), scale bar = 50 μm) and mesodermal (α-smooth-muscle-actin (SMA), scale bar = 50 μm) markers reveal the differentiation potential of iPS-SPG4-splice. Nuclei are counterstained with DAPI (blue).

PBS). Between passage 5 and 10, cells were analysed and frozen in E8 medium with 40% KOSR (Life technologies), 10% DMSO (Sigma-Aldrich) and 1 μM Y-27632 (Abcam Biochemicals).

2.2. SNP array analysis

DNA was isolated using the DNeasy blood & tissue kit (Qiagen) according to the manufacturer's guidelines. Using the Affymetrix CytoScan HD technology (Affymetrix) SNP array analysis was performed by using 2 μg of DNA of the iPSC line as well as the original fibroblast line. Raw data was processed using Affymetrix Chromsome Analysis Suite (ChAS) 2.0 software.

Table 1
Primers (Okita et al., 2011) used for integration analysis by PCR.

	Forward sequence	Reverse sequence
KLF4	CCACCTCGCCTTACACATGAAG	TAGCGTAAAAGGAGCAACATAG
L-MYC	GGCTGAGAAGAGGATGGCTAC	TTTGTTTGACAGGAGCGACAAT
OCT3/4	CATTCAAACTGAGGTAAGGG	TAGCGTAAAAGGAGCAACATAG
SOX2	TTCACATGTCCCAGCACTACCAG	TTTGTTTGACAGGAGCGACAAT

2.3. Sequencing of mutation site

Using the 3130xl Genetic Analyzer (Applied Biosystems) and a primer set flanking the mutation (c.1687 + 2 T > A) in *SPAST*, the mutation site was analysed by applying standard procedures and visualization with Staden 2.0.0b10 software (Staden Sourceforge).

Table 2
Primers used for validation of pluripotency genes.

	Forward sequence	Reverse sequence
c-MYC	ATTCTCTGCTCTCCTCGACG	CTGTGAGGAGGTTTGCTGTG
DNMT3	ACGACACAGAGGACACACAT	AAGCCCTTGATCTTTCCCCA
GAPDH	AGGTCGGAGTCAACGGATTT	ATCTCGCTCCTGGAAGATGG
KLF4	CCATCTTTCTCCACGTTCGC	CGTTGAACTCCTCGGTCTCT
NANOG	CAAAGGCAAACAACCCACTT	TGCGTCACACCATTGCTATT
OCT4	GGAAGGTATTCAGCCAAACG	CTCCAGGTTGCCTCTCACTC
REX1	AACGGGCAAAGACAAGACAC	AACTCACCCCTTATGACGCA
SOX2	TGATGGAGACGGAGCTGAAG	GCTTGCTGATCTCCGAGTTG
TDGF1	GGTCTGTGCCCCATGACA	AGTTCTGGAGTCCTGGAAGC

Table 3
Antibodies used for validation of pluripotency genes and *in vitro* differentiation potential.

	Antibody	Dilution	Manufacturer
Pluripotency	rabbit *anti*-NANOG	1:50	Stemgent
	goat anti-OCT4	1:100	Santa-Cruz
	mouse anti-SSEA4	1:500	Abcam
	mouse anti-TRA-1-80	1:500	Merck-Millipore
In vitro differentiation	mouse anti-AFP	1:200	Sigma-Aldrich
	mouse anti-SMA	1:100	Dako
	mouse anti-TUJ	1:1000	Sigma-Aldrich

2.4. Non-integration of transgenes

DNA was isolated as described before. Using plasmid specific primers (see Table 1) as well as the three episomal plasmids (pCXLE-hUL, pCXLE-hSK and pCXLE-hOCT4) as positive control the integration was analysed. Therefore, RT-PCR reactions were performed using GoTaq G2 DNA Polymerase (Promega) according to the manufacturer's instruction. PCR products were separated on a 2.0% agarose gel and visualized with Midori Green.

2.5. Alkaline phosphatase staining

For ALP staining iPSCs were cultivated on 12-well plates and fixed in 4% paraformaldehyde (PFA) for 1 minute. After 3 times washing in PBS staining solution (40 μl Naphthol AS-MX phosphate alkaline solution (Sigma-Aldrich) and 1 ml Fast Red (1 mg/ml, Sigma Aldrich)) was added for 30 min. ALP-positive colonies were stained dark red.

2.6. Immunocytochemical staining

iPSCs were cultivated on 24-well plates on coverslips until confluency of 60–80%. After fixation in 4% paraformaldehyde (PFA) for 15 min cells were washed 3 times with PBS and incubated in blocking buffer (PBS, 1% FCS, 0.1% Triton X-100) for 45 min. Cells were stained for 1 h at room temperature (RT) with the primary antibody (see Table 3). After 3 washes in PBS, cells were incubated with the secondary antibody (Alexa488 or Alexa568 diluted 1:300 (Life technologies)) in the dark at RT for 1 h. Nuclear counterstaining was achieved by addition of DAPI (1:10,000) for 15 min at RT in the dark. After embedding in ProLong Diamond Antifade Mountant cells were analysed with Axio Imager Z1 with ApoTome (Zeiss).

2.7. qRT-PCR of pluripotency marker

RNA was isolated using the High Pure RNA Isolation Kit (Roche) according to the manufacturer's guidelines. Reverse transcription was performed using the Transcriptor High Fidelity cDNA Synthesis Kit (Roche). Using Light Cycler 480 SYBR Green I Master (Roche) and specific pluripotency gene primers (see Table 2) qRT-PCR was performed. Runs were performed as triplicates and C_T-values were normalized using the $2^{-\Delta\Delta Ct}$ method with the hESC line HuES-H6 as reference and GAPDH as housekeeping gene.

2.8. In vitro differentiation potential

For embryonic body (EB) generation iPSCs were cultivated in EB medium consisting of 80% DMEM/F12 (Life technologies), 20% KOSR, 1× NEAA, 1× Pen/Strep, 2 mM L-Glutamine and 0.1 mM 2-Mercaptoethanol on AggreWell 800 plates (Stemcell Technologies) with medium change at day 2. EBs were collected on day 4 and plated on 0.1% gelatine (Sigma-Aldrich) coated coverslips. Cells were cultivated for additional 2–3 weeks with medium change every other day and analysed by immunocytochemical staining using antibodies against AFP (α-fetoprotein), SMA (α-smooth muscle actin) and TUJ (β-III-tubulin) (see Table 3).

Acknowledgements

This study was supported by the European Union within the 7th European Community Framework Programme through funding for the NEUROMICS network (F5-2012-305121 to L.S.), the Marie Curie International Outgoing Fellowship (grant PIOF-GA-2012-326681 to R.S. and L.S.), and the DZNE intersite project (grant to L.S.). We thank the patient for participation.

References

Okita, K., Matsumura, Y., Sato, Y., Okada, A., Morizane, A., Okamoto, S., ... Yamanaka, S., 2011. A more efficient method to generate integration-free human iPS cells. Nat. Methods 8 (5), 409–412.

Schule, R., Wiethoff, S., Martus, P., Karle, K.N., Otto, S., Klebe, S., ... Schols, L., 2016. Hereditary spastic paraplegia: Clinicogenetic lessons from 608 patients. Ann. Neurol. 79 (4), 646–658.

Comparative transcriptional profiling of motor neuron disorder-associated genes in various human cell culture models.

Hauser S, **Schuster S**, Heuten E, Höflinger P, Admard J, Schelling Y, Ossowski S, Schöls L (2020). Comparative transcriptional profiling of motor neuron disorder-associated genes in various human cell culture models. In preparation.

Comparative transcriptional profiling of motor neuron disorder-associated genes in various human cell culture models

Stefan Hauser[1,2], Stefanie Schuster[1,2,3], Elena Heuten[1], Philip Höflinger[1,2,3], Jakob Admard[4], Yvonne Schelling[1,2], Stephan Ossowski[4,5], Ludger Schöls[1,2,5]

[1] German Center for Neurodegenerative Diseases (DZNE), Tübingen, Germany.
[2] Department of Neurology and Hertie Institute for Clinical Brain Research, University of Tübingen, Tübingen, Germany.
[3] Graduate School of Cellular and Molecular Neuroscience, University of Tübingen, Tübingen, Germany.
[4] Institute of Medical Genetics and Applied Genomics, University of Tübingen, Tübingen, Germany.
[5] Center of Rare Diseases, University of Tübingen, Tübingen, Germany.

Keywords:

Motor neuron disorders, Hereditary spastic paraplegia, Amyotrophic lateral sclerosis, Spinal muscular atrophy, Gene expression, iPSCs, Neurons, Disease modelling

Abstract

Disease modelling requires appropriate cellular models that best mimic the underlying pathophysiology. Human origin and an adequate expression of the disease protein are pre-requisites that support information from a model to be meaningful. In this study we investigated expression profiles of (i) PBMCs and (ii) fibroblasts as patient derived cells as well as (iii) lymphoblasts and (iv) induced pluripotent stem cells (iPSC) as immortalized sources and (v) iPSC-derived cortical neurons to assess its aptitude to model motor neuron diseases (MNDs) including hereditary spastic paraplegia (HSP), amyotrophic lateral sclerosis (ALS) and spinal muscular atrophy (SMA). We generated all five cell lines from two healthy donors and performed RNA sequencing to display expression patterns in MND-related genes. For the ten most common HSP genotypes we proved gene expression by qPCR. Depending on the specific MND gene we found largely different expression patterns. Out of 168 MND-related genes, 50 had their highest expression in iPSC-derived cortical neurons, 41 were most strongly expressed in fibroblasts, 26 in lymphoblasts, 22 in iPSCs and 14 in PBMCs. 15 MND-related genes were not detectable in any of the analyzed cell types. This study provides comprehensive information on expression of genes associated with a large spectrum of MNDs. Expression profiles can be used to inform on appropriate cell models for genotype specific motor neuron research.

Introduction

Studies on pathophysiology of human disease and the development of new therapeutics are essentially dependent on suitable disease models. This is particularly difficult in neurological disease as often only the nervous system is affected and access to human neuronal tissue is limited to nerve and brain biopsies or post-mortem material that are notoriously rare with very limited access.

Primary patient cells like peripheral blood mononuclear cells (PBMCs) isolated from blood or fibroblasts isolated from skin biopsies are easily accessible but not primarily affected by the disease and therefore might represent pathophysiological processes only to a limited and often unknown extend. Additionally, primary patient cells possess limited growth capacity which hampers its use in large-scale screening approaches. To overcome this limitation strategies of immortalizing primary patient cells have been developed early on, e.g. the transformation of PBMCs (mainly B lymphocytes) to lymphoblasts by using the Epstein-Barr virus (Miller, 1982). With the discovery of induced pluripotent stem cells (iPSCs) a novel and promising technique to generate disease-relevant and patient-specific cell types arose (Takahashi and Yamanaka, 2006). Over the last years iPSCs became a widespread tool to generate neuronal cell types that are genetically identical with patients suffering from the neurological disease of interest. iPSCs can be reprogrammed from easily accessible cell types like fibroblasts, PBMCs or keratinocytes according to well standardized procedures (Okita *et al.*, 2013; Hauser *et al.*, 2016a). iPSC-derived neurons have been used to model many human neurological diseases including motor neuron diseases (MNDs).

MNDs comprise three major groups of rare neurodegenerative diseases including (i) hereditary spastic paraplegia (HSP) involving primarily upper motor neurons, (ii) spinal muscular atrophy (SMA) with lower motor neuron affection and (iii) amyotrophic lateral sclerosis (ALS) with rapid degeneration of upper and lower motor neurons. All three MNDs are genetically highly heterogeneous and split up into more than 80 genotypes of HSP, at least 30 genes causing ALS and 18 genes associated with SMA (Adam *et al.*; Kinsley and Siddique, 2015; Hedera, 2018). Further, MNDs show a substantial overlap with other disease groups like cerebellar ataxias, leukoencephalopathies and hereditary peripheral neuropathies (Synofzik and Schüle, 2017). In total more than 160 genes related to motor neuron impairment are known to date.

Till the discovery of iPSCs, research on MND mostly focused on mouse models and cell culture models using immortalized murine and human cell lines. Animal models are advantageous in providing an *in vivo* system with its whole complexity but differences between species are huge and transferability to human disease is difficult. This is especially true in the context of neurological disorders. The hope that mouse models mimic human disease pathology has been disappointing in particular for MNDs (reviewed in Genc *et al.*, 2019).

The potential of iPSC to generate a patient-specific cell model that represents the cell type affected by the disease of interest opened new possibilities to study MND in a human neuronal

cell culture model (reviewed in Denton *et al.*, 2016). For example, analysis of SPAST-deficient neurons generated from SPG4 patients revealed pathophysiological axonal defects like axonal swellings, a hallmark of HSP disease pathology, in human iPSC-derived neurons (Havlicek *et al.*, 2013; Denton *et al.*, 2014). Further, in a study of SPG5, iPSC-derived neurons were employed to decipher the neurotoxic role of oxysterols that is likely to drive pathogenesis in this subtype of HSP (Schöls *et al.*, 2017). Additionally, iPSC-derived neurons have been used for pharmacological screens to identify novel targets for the treatment of MNDs e.g. in SPG4 and SPG11 (Pozner *et al.*, 2018; Rehbach *et al.*, 2019). iPSC-derived motor neurons and cortical neurons have also been used to mimic familial as well as sporadic forms of ALS. Observed phenotypes range from e.g. cytoskeletal defects, impaired axonal transport, cell death and vulnerability, ER stress and mitochondrial dysfunction (reviewed in: Guo *et al.*, 2017).

To choose an adequate disease model is of utmost importance for medical research. The expression of disease-related molecules is a pre-requisite of meaningful cell models. Using RNA-Sequencing (RNA-Seq) analyses we here compared the transcript expression profiles of more than 160 MND-related genes including all spastic paraplegia genes (SPGs), SMA genes and ALS genes known so far in biosamples of two independent healthy individuals including (i) PBMCs and (ii) fibroblasts as primary cells, (iii) lymphoblasts and (iv) iPSCs as immortalized cell lines as well as (v) iPSC-derived cortical projection neurons representing a cell type predominantly affected in HSP and ALS. This dataset may help to inform about the ideal source of human cell culture to model the disease of interest.

Results

To analyze MND-related gene expression in different cell types of the same individual peripheral blood mononuclear cells (PBMC) as well as fibroblasts (F) from two healthy donors were isolated from whole blood and skin biopsies. An immortalized lymphoblast cell line (LB) was generated by infection of PBMCs using the Epstein-Barr-Virus (EBV). Fibroblast were reprogrammed to induced pluripotent stem cells (iPSCs) and further differentiated to cortical projection neurons (CN) (Fig. 1A). By this, we were able to compare various cell types ranging from easily-accessible primary cells over immortalized cell lines to cell types affected by MNDs.

By comparing the global RNA-Sequencing profile of the various cell types we found a highly different and cell type-specific gene expression profile (Fig. 1B). As expected PBMCs and lymphoblasts closely clustered together while the other analyzed cell types showed very divergent and unique global transcript profiles as shown by principal component analysis. Of interest, there was high similarity between the same cell types of different individuals. This is also represented by the expression of cell type-specific markers (Fig. 1C). PBMCs and lymphoblasts exclusively expressed the marker HLA-DRA (HLA class II histocompatibility antigen, DR alpha chain) and CD74 (HLA class II histocompatibility antigen gamma chain), while fibroblast could be discriminated by expression of ELN (elastin) and LOX (lysyl oxidase). Pluripotency markers like OCT4 (octamer-binding transcription factor 4) and LIN28 (lin-28 homolog A) were exclusively detectable in iPSCs, whereas MAP2 (microtubule-associated protein 2) and NSG2 (neuronal

vesicle trafficking-associated protein 2) were highly expressed solely in iPSC-derived cortical neurons. This highlights the purity of our cell culture systems and supports the validity of this analysis.

To compare the gene expression profile in the different cell types a list of 168 MND-related genes was generated. This list covered all hereditary spastic paraplegia genes (SPGs) known at the time of study including 65 HSP genes (SPG1 – SPG80; SPGs with defined chromosomal loci but unknown genes could not be analyzed), 30 ALS-related genes, 18 SMA-related genes and 55 spasticity-related genes. To normalize for sequencing depth we divided the total reads per sample by 1,000,000 (RPM – reads per million) and further normalized for gene length by dividing the RPM values of each gene by the length of the gene in kilobases (RPKM – reads per kilobase million).

A summary of all analyzed MND-related genes in an alphabetic order can be seen in figure 2. RPKM values ranged from 0 – 538 depending on cell type and gene of interest. For a better visualization genes with RPKMs > 105 were separately visualized (Fig. 2B). We observed high variability in gene expression between cell types of the same donor and low variability between the same cell type of different donors.

For a clearer presentation and easier comparison of the different gene expression patterns the relative expression values for each gene and disease were determined. Therefore, the mean value of both donors per gene and cell type were calculated and the highest value of each gene was set to 100% (Fig. 3). Afterwards genes were classified per disease (HSP, ALS and SMA) and grouped according to its highest expression per cell type from high to low RPKMs.

Out of 65 HSP-related genes, 26 had their highest expression in iPSC-derived cortical neurons ranging from 2 – 328 RPKMs. 2 were most strongly expressed in iPSCs (range: 21 – 294 RPKMs), 19 in fibroblasts (range: 1 – 65 RPKMs), 10 in lymphoblasts (range: 6 – 63 RPKMs) and 3 in PBMCs (range: 2 – 16 RPKMs). 5 of 65 HSP-related genes were not detectable in any of the analyzed cell types.

Concerning the 30 ALS-causing genes, 9 were expressed highest in neurons (range: 4 – 90 RPKMs) whereas, 5 showed higher expression in iPSCs (range: 5 – 538 RPKMs), 5 in fibroblasts (range: 2 – 148 RPKMs), 6 in lymphoblasts (range: 3 – 511 RPKMs) and 3 in PBMCs (range: 16 – 30 RPKMs). ANG and UBQLN2 were not detectable at all.

Out of the 18 analysed SMA-related genes, 5 were most abundant in neurons (range: 4 – 62 RPKMs), 2 in iPSCs (range: 2 – 5 RPKMs), 3 in fibroblasts (range: 2 – 41 RPKMs), 4 in lymphoblasts (range: 9 – 38 RPKMs), 1 in PBMCs (1 RPKM). 3 genes (AR, ATP7A and UBA1) were not detected in any of these cell types.

To validate and replicate the results of the RNA-Seq analysis, the 10 most common HSP genes according to a large representative HSP cohort (Schüle *et al.* 2016) were selected for further qRT-PCR determination and validation (Fig. 4). Two of these genes (KIF5A, SPG11) are also associated with ALS. In general, expression profiles were found to be largely similar in RNA-Seq data and qRT-PCR for SPG3 (ATL1), SPG4 (SPAST), SPG5 (CYP7B1), SPG7 (SPG7), SPG10 (KIF5A), SPG11 (SPG11), SPG15 (ZFYVE26), SPG17 (BSCL2), SPG31 (REEP1) and SPG35 (FA2H) (Fig. 4B-K). For example, REEP1 was almost exclusively expressed in iPSC-derived cortical neurons (CNs) while

SPAST was approximately 10 times lower expressed in PBMCs, LBs, Fs and iPSCs compared to CNs. Again, a very low variability of qRT-PCR data was observed between the same cell types of two independent donors.

Discussion

This study presents a comparative data set of the expression of >160 MND-related genes in patient-derived primary biosamples (PBMCs and fibroblasts), immortalized cell lines (lymphoblasts, iPSCs) as well as cortical neurons reflecting the cell type affected by the disease. In general, the direct comparison of the expression data of two independent healthy individuals showed large similarity in expression profiles for a given cell type (e.g. fibroblasts) between individuals but a huge variability within the same individual across different cell types. Figures 2 and 3 provide an overview on expression profiles to inform on suitable cell types that express the RNA of interest of >160 MND-related transcripts. Cells with highest expression are recommended for further studies to compare differences in protein expression between patients and controls and its pathophysiological relevance.

The highest expression of MND-related genes varied largely between the five cell types on analysis in this study. 8.3% of MND genes were most abundant in PBMCs, 15.5% in lymphoblasts, 24.4% in fibroblasts, 13.1% in iPSCs and 29.8% are expressed highest in CNs, while 8.9% of all MND-related genes could not be identified in any of the analyzed cell types. Comparable distributions could also be seen for all three groups of MND with CNs being the most commonly represented cell type (HSP: 40%, ALS: 30%, SMA: 28%). An overview of all HSP, SMA and ALS genes and the respective cell type with the highest expression is provided in figure 5. This clearly shows that a general statement of an ideal cell type for disease modelling of MNDs is not valid. Nevertheless, iPSC-derived cortical neurons and/or fibroblasts are in most cases more suitable cell types compared to PBMCs or lymphoblasts.

We selected projection neurons of cortical layer V/VI for this study as they can be differentiated with high purity from iPSC and motor neurons constitute a specific subtype of projection neurons originating from cortical layer V/VI. Our differentiation protocol allowed for a reproducible generation of a largely homogeneous neuronal cell population with 100% of cells expressing ß-III-tubulin as neuronal marker and >85% of cells being positive for CTIP-2 expression indicating cortical projection neurons of layer V/VI (Rehbach *et al.*, 2019). This allows to perform RNA-Seq analysis of neurons without cross-contamination of cells of glial origin as demonstrated by the non-detection of glial markers like GFAP. Established motor neuron protocols do not reach such an extent of purity and represent lower (rather than upper) motor neurons that are not affected in HSP (reviewed in: Sances *et al.*, 2016).

The intuitive notion that the expression of MND genes is highest in cortical neurons as the primary affected cell type in HSP and ALS is only true in ~30% of all MND genes. This may reflect that the function of a motor neuron and especially its extremely long axons require additional functionality of supporting cells including oligodendrocytes, microglia, astrocytes as well as

peripheral Schwann cells and is further influenced by more general systemic metabolic pathways and changes. In extreme cases, especially when gene products play a role in general metabolic pathways like ARSI (SPG66) or CYP27A1 (CTX), the expression of the RNA is absent in iPSC-derived cortical neurons but is highest in fibroblasts or PBMCs (Fig. 2 and Fig. 3). The other way round, more easily available patient-derived cell types like fibroblasts and PBMCs do not express several relevant MND genes like SPG10 (KIF5A), SPG26 (B4GALNT1), SPG31 (REEP1), ERBB4 and PLEKHG5 and therefore disqualify as cellular models for pathogenic studies in these MNDs.
Studying the expression profiles by looking at specific clusters that share a similar cellular function as summarized by Blackstone and colleagues (2018), some pathophysiologically related HSPs show similar expression profiles. HSPs associated with axonal transport deficits like SPG4 (SPAST), SPG10 (KIF5A), SPG30 (KIF1A), SPG31 (REEP1) and SPG72 (REEP2) share highest expression in cortical neurons as their primary side of action and are only low expressed or absent in all other analyzed cell types. Interestingly, some RNAs including L1CAM (SPG1), PLP1 (SPG2), MAG (SPG75) and GFAP (Alexander disease) are expressed in none of the cell types studied here. These genes define subtypes of MNDs with primary myelin or glial dysfunction. For example PLP1 (proteolipid protein) is the primary constituent of myelin in the central nervous system (Diehl *et al.*, 1986). In this specific subset of MND-related genes a suitable cell culture model probably requires different approaches and cell types like iPSC-derived oligodendrocytes, Schwann cells and/or astrocytes or even a co-culture or 3-dimensional *in vitro* culture system to obtain meaningful and disease-relevant results (Shaltouki *et al.*, 2013; Douvaras *et al.*, 2014; Kim *et al.*, 2017; reviewed in: McComish and Caldwell, 2018).
In summary we provide a valuable dataset of more than 160 MND-related transcripts of different patient-derived biosamples, which can be employed to preselect a proper cellular model to potentially decipher molecular mechanism with pathophysiological relevance and screening for novel therapeutic targets in various types of MNDs.

Material and Methods

Isolation of primary cells

The study has been approved by the Ethics Committee of the University of Tübingen (598/2011BO1). Informed consent was obtained from all participants.
Fibroblasts were obtained from skin biopsies of two healthy individuals (Donor 1: age: 46, gender: female / Donor 2: age: 37 gender: female). Skin tissue was dissected and cultivated in a 25 cm^2 tissue culture flask containing Dulbecco's modified eagle's medium (DMEM) high glucose (Life technologies) with 10% fetal bovine serum (FBS, Life technologies) (fibroblast medium) for 10 days at 37 °C and 5% CO_2. Fibroblast expansion was achieved by medium change every 2-3 days. PBMCs were isolated from whole blood of the same healthy donors as fibroblasts using a classical density gradient centrifugation with Ficoll (Ficoll Paque-PLUS, GE Healthcare) according to manufacturer’s guidelines.

Transformation of PBMCs to lymphoblasts

Immortalized lymphoblast cell lines were generated by infection of PBMCs (mainly B lymphocytes) using the EBV (Pelloquin *et al.*, 1986). In brief, separated PBMCs were resuspended in 2 ml sterile EBV-containing supernatant of B95-8 cells and incubated for 30 min at 40°C. EBV-transformed lymphocytes (lymphoblasts) were cultivated in RPMI medium (Sigma-Aldrich) containing 20% FBS, 1% Penicillin/Streptomycin (Biochrom), 1 µg/ml Cyclosporin A (Sigma-Aldrich), 1mM sodium pyruvate (Sigma-Aldrich), 20mM HEPES (Sigma-Aldrich) and 1% L-glutamine (Merck). Lymphoblasts were frozen in cryopreservation medium containing of 90% FBS supplemented with 10% DMSO (Sigma-Aldrich).

Reprogramming of fibroblasts to iPSCs

Reprogramming was achieved by electroporation of $1x10^5$ fibroblasts with 1µg of episomal plasmids (pCXLE-hUL, pCXLE-hSK and pCXLE-hOCT4) as described by (Okita *et al.*, 2011). 1 day after electroporation fibroblast growth factor-2 (FGF-2, 2 ng/mL, Peprotech) was supplemented to the fibroblast media. The following day cells were cultivated in Essential 8 (E8) medium supplemented with 100 µM sodium butyrate (Sigma-Aldrich) with media change every other day. Approx. 3-4 weeks after electroporation iPSC colonies were manually picked and further expanded on Matrigel-coated well plates. Splitting and replating of iPSCs was achieved by adding PBS/EDTA (0.02% EDTA in PBS). iPSCs were genomically and functionally analyzed according to (Hauser *et al.*, 2016b).

Differentiation of iPSCs to cortical neurons

iPSCs were differentiated to neurons of cortical layer V and VI according to published protocols with minor modifications (Shi *et al.*, 2012; Rehbach *et al.*, 2019). Briefly, iPSCs were seeded at a density of 3 x 10^5 cells per cm^2 in E8 medium supplemented with 10 µM Y-27632 (Selleckchem). Neural induction was obtained by supplementation of dual SMAD inhibitors (10 µM SB431542 (Sigma-Aldrich) and 500 nM LDN-193189 (Sigma-Aldrich)) to 3N medium for 10 days. On day 10, cells were split in a 1:3 ratio and further expanded in 3N medium including 20 ng/ml FGF-2 for 2 days. Until day 27, cells were cultivated in 3N medium with media change every other day. On day 27, cells were dissociated using Accutase (Sigma-Aldrich) and replated at a density of ~ 8 x 10^5 cells per cm^2. The following day, 10 µM PD0325901 (Tocris) and 10 µM DAPT (Sigma Aldrich) was added to 3N medium with an additional media change at day 30. From day 32 onwards 3N medium was changed every other day and RNA of cortical neurons was isolated at day 37 of differentiation.

RNA-Sequencing analysis

RNA isolation of cells (PBMCs, lymphoblasts, fibroblasts, iPSCs, iPSC-derived cortical neurons) was performed by using the RNeasy Mini Kit (Qiagen) according to the manufacturer's guidelines. Further purification of isolated RNA was achieved with TruSeq mRNA v2Kit (polyA) (Illumina). RNA samples were sequenced on a HiSeq2500 (Illumina) by DeCODE genetics (Reykjavik, Iceland).

For further expression analysis and to calculate the sample similarity a multi-dimensional scaling (MDS) plot of all RNA-Seq samples was prepared. For comparison of 138 spasticity-related genes, RPKMs (Reads Per Kilobase Million) for each transcript and cell type were calculated. Images were generated by using GraphPad Prism.

qRT-PCR validation

500 ng isolated RNA of each sample was reverse-transcribed to cDNA by using the RevertAid First Strand cDNA Synthesis Kit (Thermo Fisher Scientific) according to manufacturer's instructions. Real-time qPCR was performed in triplicates by adding 2 µl primer pairs (2 µM) and 5 µl SYBR Green Select Master Mix (Applied Biosystems) to 3 µl cDNA (1.25 ng/µl).

For amplification the following primers were used:

Primer	**Forward sequence**	**Reverse sequence**
ATL-1 / SPG3	CAGTCCAAGTCCTCATTGTC	AATCAACTGATTCCTGGTTGTA
BSCL2 / SPG17	TTCTACTACAGGACCGACTG	CAGCTCAAGCTCTAAGGTAAC
CYP7B1 / SPG5	CAGTTCTTCTTGGTGGAAAGTA	TGCAACTGACTGATGCTAAA
FA2H / SPG35	TGGGAGAGAAGTACGATGAG	GGGACACTGTACCAGACA
GAPDH	TCACCAGGGCTGCTTTTAAC	GACAAGCTTCCCGTTCTCAG
KIF5A / SPG10	GTCACCAACATGAATGAACAC	CCAGGTCCACCAGATACA
REEP1 / SPG31	CCTTTGTTGGTTTCCATTCTAT	CAGACAATCATCGATTTCCTTT
SPAST / SPG4	ATAGTTACAGGACAAGGTGAAC	ACGTCCGTTTGTGACTTG
SPG7 / SPG7	CAGGATTCTTTGGAAATGCC	CCATCTTCCCATCCACAAT
SPG11 / SPG11	GTATTTCAGGCAACACCCA	GGCTTTCCAAGACCTATCAAT
TBP	CTTCGGAGAGTTCTGGGATTG	CACGAAGTGCAATGGTCTTTAG
ZFYVE26 / SPG15	ATACAGCAGAGCAGCAAC	TCTGTAAGAGCTTGAGAACATC

Real-time qPCR was performed on the Viia7 Real-Time PCR System (Applied Biosystems) applying the following qRT-PCR program: 50°C for 2min, 95°C for 2min, 40 cycles of 95°C for 1s, 60°C for 30s and 72°C for 5s, followed by 95°C for 15s, 60°C for 1min and 95°C for 15s. Melting curve analysis confirmed the specificity of the PCR products. Further analysis was performed with QuantStudio Software V1.3 (Thermo Fisher Scientific) and visualized using GraphPad Prism.

Acknowledgments

This work was supported by an EC funded Neuromics project (F5-2012-305121) to L.S. L.S. is member of the European Reference Network for Rare Neurological Diseases - Project ID No 739510.

Author contribution

Conceptualization, S.H., and L.S.; Methodology, S.H., S.S., and J.A.; Software, J.A, and S.O.; Formal Analysis, S.H., S.S., and J.A.; Investigation, S.H., S.S., E.H., P.H., J.A., and Y.S.; Resources, S.O.;

Writing – Original Draft, S.H.; Writing – Review & Editing, S.S., E.H., P.H., J.A., S.O., and L.S.; Visualization, S.H.; Supervision, S.H., S.O., and L.S.; Project Administration, S.H. and L.S.; Funding Acquisition, L.S.

References

Adam M, Ardinger H, Pagon R, Wallace S, Bean L, Stephens K*, et al.* Spinal Muscular Atrophy--GeneReviews®.

Denton KR, Lei L, Grenier J, Rodionov V, Blackstone C, Li XJ. Loss of spastin function results in disease-specific axonal defects in human pluripotent stem cell-based models of hereditary spastic paraplegia. Stem cells 2014; 32(2): 414-23.

Denton KR, Xu C, Shah H, Li X-J. Modeling axonal defects in hereditary spastic paraplegia with human pluripotent stem cells. Frontiers in biology 2016; 11(5): 339-54.

Diehl H-J, Schaich M, Budzinski R-M, Stoffel W. Individual exons encode the integral membrane domains of human myelin proteolipid protein. Proceedings of the National Academy of Sciences 1986; 83(24): 9807-11.

Douvaras P, Wang J, Zimmer M, Hanchuk S, O'Bara MA, Sadiq S*, et al.* Efficient generation of myelinating oligodendrocytes from primary progressive multiple sclerosis patients by induced pluripotent stem cells. Stem cell reports 2014; 3(2): 250-9.

Genc B, Gozutok O, Ozdinler PH. Complexity of Generating Mouse Models to Study the Upper Motor Neurons: Let Us Shift Focus from Mice to Neurons. International journal of molecular sciences 2019; 20(16): 3848.

Guo W, Fumagalli L, Prior R, Van Den Bosch L. Current advances and limitations in modeling ALS/FTD in a dish using induced pluripotent stem cells. Frontiers in neuroscience 2017; 11: 671.

Hauser S, Erzler M, Theurer Y, Schuster S, Schüle R, Schöls L. Establishment of SPAST mutant induced pluripotent stem cells (iPSCs) from a hereditary spastic paraplegia (HSP) patient. Stem cell research 2016a; 17(3): 485-8.

Hauser S, Hoflinger P, Theurer Y, Rattay TW, Schols L. Generation of induced pluripotent stem cells (iPSCs) from a hereditary spastic paraplegia patient carrying a homozygous Y275X mutation in CYP7B1 (SPG5). Stem cell research 2016b; 17(2): 437-40.

Havlicek S, Kohl Z, Mishra HK, Prots I, Eberhardt E, Denguir N*, et al.* Gene dosage-dependent rescue of HSP neurite defects in SPG4 patients' neurons. Human molecular genetics 2013; 23(10): 2527-41.

Hedera P. Hereditary spastic paraplegia overview. GeneReviews®[Internet]: University of Washington, Seattle; 2018.

Kim H-S, Lee J, Lee DY, Kim Y-D, Kim JY, Lim HJ*, et al.* Schwann cell precursors from human pluripotent stem cells as a potential therapeutic target for myelin repair. Stem cell reports 2017; 8(6): 1714-26.

Kinsley L, Siddique T. Amyotrophic lateral sclerosis overview. GeneReviews®[Internet]: University of Washington, Seattle; 2015.

McComish SF, Caldwell MA. Generation of defined neural populations from pluripotent stem cells. Philosophical Transactions of the Royal Society B: Biological Sciences 2018; 373(1750): 20170214.

Miller G. Immortalization of human lymphocytes by Epstein-Barr virus. The Yale journal of biology and medicine 1982; 55(3-4): 305.

Okita K, Matsumura Y, Sato Y, Okada A, Morizane A, Okamoto S*, et al.* A more efficient method to generate integration-free human iPS cells. Nature methods 2011; 8(5): 409-12.

Okita K, Yamakawa T, Matsumura Y, Sato Y, Amano N, Watanabe A*, et al.* An efficient nonviral method to generate integration-free human-induced pluripotent stem cells from cord blood and peripheral blood cells. Stem cells 2013; 31(3): 458-66.
Pelloquin F, Lamelin J, Lenoir G. Human blymphocytes immortalization by epstein-barr virus in the presence of cyclosporin a. In vitro cellular & developmental biology 1986; 22(12): 689-94.
Pozner T, Schray A, Regensburger M, Lie DC, Schlötzer-Schrehard U, Winkler J*, et al.* Tideglusib rescues neurite pathology of SPG11 iPSC derived cortical neurons. Frontiers in neuroscience 2018; 12: 914.
Rehbach K, Kesavan J, Hauser S, Ritzenhofen S, Jungverdorben J, Schüle R*, et al.* Multiparametric rapid screening of neuronal process pathology for drug target identification in HSP patient-specific neurons. Scientific reports 2019; 9(1): 1-13.
Sances S, Bruijn LI, Chandran S, Eggan K, Ho R, Klim JR*, et al.* Modeling ALS with motor neurons derived from human induced pluripotent stem cells. Nat Neurosci 2016; 19(4): 542-53.
Schöls L, Rattay TW, Martus P, Meisner C, Baets J, Fischer I*, et al.* Hereditary spastic paraplegia type 5: natural history, biomarkers and a randomized controlled trial. Brain 2017; 140(12): 3112-27.
Shaltouki A, Peng J, Liu Q, Rao MS, Zeng X. Efficient generation of astrocytes from human pluripotent stem cells in defined conditions. Stem cells 2013; 31(5): 941-52.
Shi Y, Kirwan P, Livesey FJ. Directed differentiation of human pluripotent stem cells to cerebral cortex neurons and neural networks. Nature protocols 2012; 7(10): 1836.
Synofzik M, Schüle R. Overcoming the divide between ataxias and spastic paraplegias: shared phenotypes, genes, and pathways. Movement Disorders 2017; 32(3): 332-45.
Takahashi K, Yamanaka S. Induction of pluripotent stem cells from mouse embryonic and adult fibroblast cultures by defined factors. cell 2006; 126(4): 663-76.

Figures

Figure 1

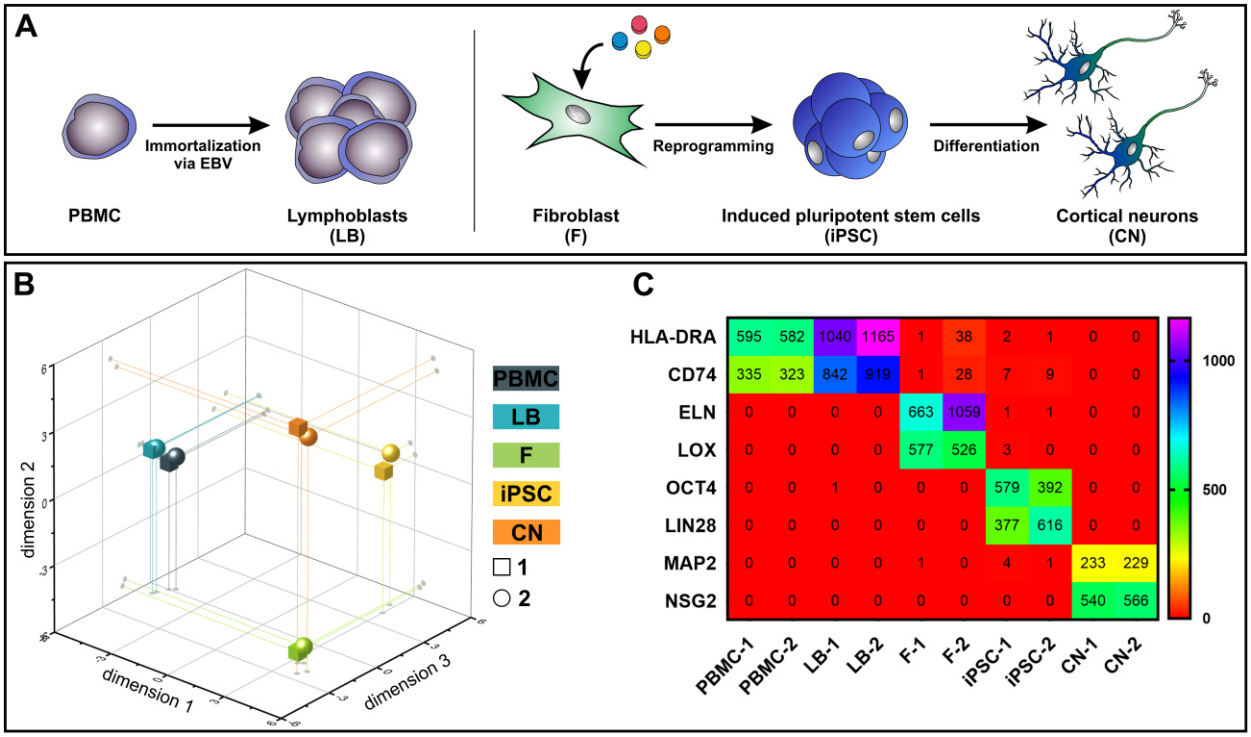

Fig. 1. Overview of patient-relevant cell types used for RNA-Sequencing profiling. **(A)** Peripheral blood mononuclear cells (PBMC) were isolated from whole blood and immortalized to lymphoblasts (LB) by EBV (Epstein-Barr Virus)-transformation. Fibroblasts (F) were isolated from skin biopsies, reprogrammed to induced pluripotent stem cells (iPSCs) and further differentiated to cortical neurons (CN). **(B)** Multidimensional scaling plot (MDS, 3-dimensional) of all analyzed RNA-Seq samples. **(C)** RPKM (reads per kilobase million) values of cell type-specific markers of the two healthy donors (1 and 2).

Figure 2

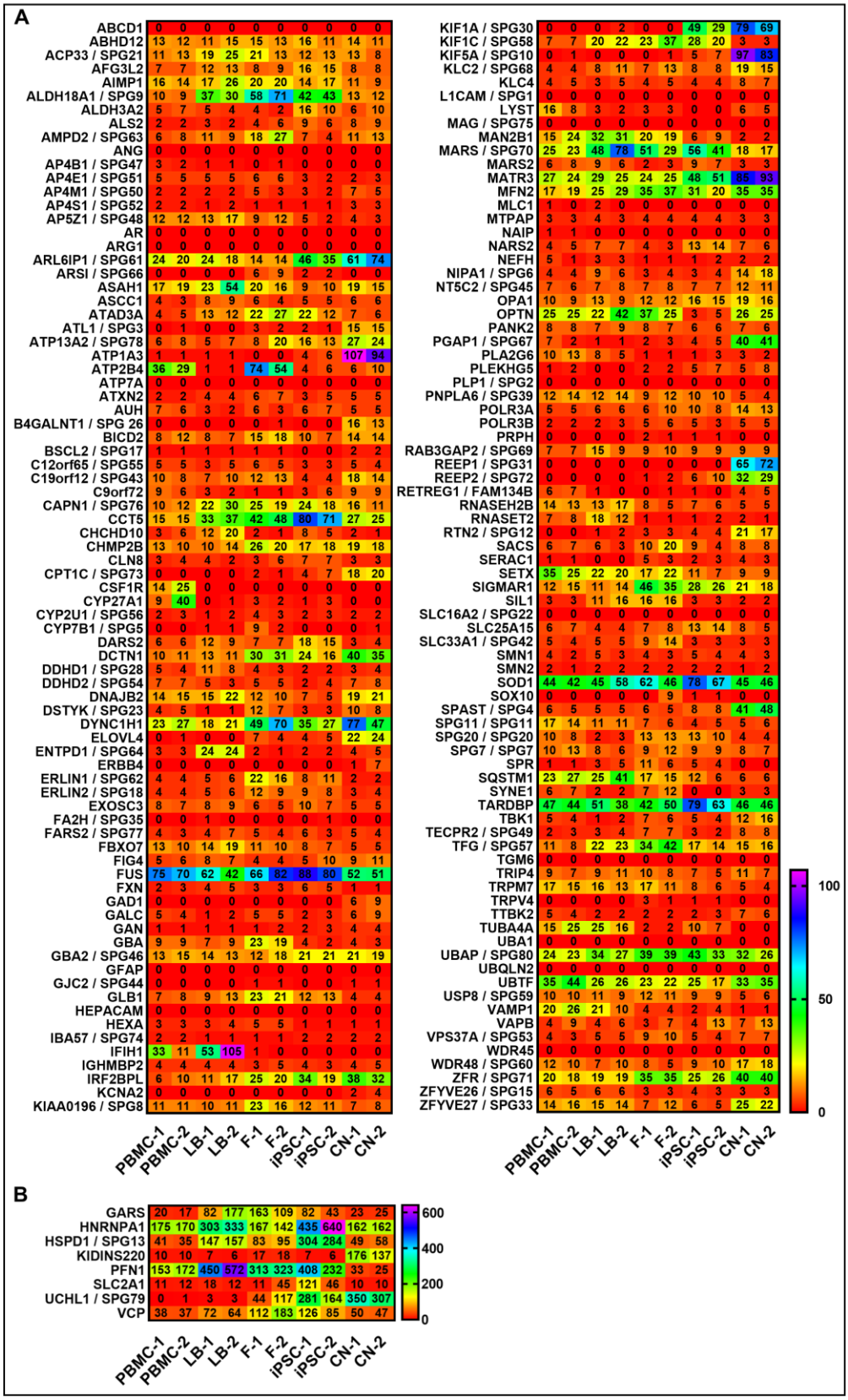
A
ABCD1 0 0 0 0 0 0 0 0 0 0
ABHD12 13 12 11 15 15 13 16 11 14 11
ACP33 / SPG21 11 13 19 25 21 13 12 13 13 8
AFG3L2 7 7 12 13 8 9 16 15 8 8
AIMP1 16 14 17 26 20 20 14 17 11 9
ALDH18A1 / SPG9 10 9 37 30 58 71 42 43 13 12
ALDH3A2 5 7 5 4 4 2 16 10 6 10
ALS2 2 2 3 2 4 6 9 6 8 9
AMPD2 / SPG63 6 8 11 9 18 27 7 4 11 13
ANG 0 0 0 0 0 0 0 0 0 0
AP4B1 / SPG47 3 2 1 1 0 1 0 0 0 0
AP4E1 / SPG51 5 5 5 5 6 6 3 2 2 3
AP4M1 / SPG50 2 2 2 2 5 3 3 2 7 5
AP4S1 / SPG52 2 2 1 2 1 1 1 1 3 3
AP5Z1 / SPG48 12 12 13 17 9 12 5 2 4 3
AR 0 0 0 0 0 0 0 0 0 0
ARG1 0 0 0 0 0 0 0 0 0 0
ARL6IP1 / SPG61 24 20 24 18 14 14 46 35 61 74
ARSI / SPG66 0 0 0 0 6 9 2 2 0 0
ASAH1 17 19 23 54 20 16 9 10 19 15
ASCC1 4 3 8 9 6 4 5 5 6 6
ATAD3A 4 5 13 12 22 27 22 12 7 6
ATL1 / SPG3 0 1 0 0 3 2 2 1 15 15
ATP13A2 / SPG78 6 8 5 7 8 20 16 13 27 24
ATP1A3 1 1 1 1 0 0 4 6 107 94
ATP2B4 36 29 1 1 74 54 4 6 6 10
ATP7A 0 0 0 0 0 0 0 0 0 0
ATXN2 2 2 4 4 6 7 3 5 5 5
AUH 7 6 3 2 6 3 6 7 5 5
B4GALNT1 / SPG 26 0 0 0 0 0 1 0 0 16 13
BICD2 8 12 8 7 15 18 10 7 14 14
BSCL2 / SPG17 1 1 1 1 1 1 0 0 2 2
C12orf65 / SPG55 5 5 3 5 6 5 3 3 5 4
C19orf12 / SPG43 10 8 7 10 12 13 4 4 18 14
C9orf72 9 6 3 2 1 1 3 6 9 9
CAPN1 / SPG76 10 12 22 30 25 19 24 18 16 11
CCT5 15 15 33 37 42 48 80 71 27 25
CHCHD10 3 6 12 20 2 1 8 5 2 1
CHMP2B 13 10 10 14 26 20 17 18 19 18
CLN8 3 4 4 2 3 6 7 7 3 3
CPT1C / SPG73 0 0 0 0 2 1 4 7 18 20
CSF1R 14 25 0 0 0 0 0 0 0 0
CYP27A1 9 40 0 1 3 2 1 3 0 0
CYP2U1 / SPG56 2 3 1 2 4 3 2 3 2 2
CYP7B1 / SPG5 0 0 1 1 9 2 0 0 0 1
DARS2 6 6 12 9 7 7 18 15 3 4
DCTN1 10 11 13 11 30 31 24 16 40 35
DDHD1 / SPG28 5 4 11 8 4 3 2 2 3 4
DDHD2 / SPG54 7 7 5 3 5 5 2 4 7 8
DNAJB2 14 15 15 22 12 10 7 5 19 21
DSTYK / SPG23 4 5 1 1 12 7 3 3 10 8
DYNC1H1 23 27 18 21 49 70 35 27 77 47
ELOVL4 0 1 0 0 7 4 4 5 22 24
ENTPD1 / SPG64 3 3 24 24 2 1 2 2 4 5
ERBB4 0 0 0 0 0 0 0 0 1 7
ERLIN1 / SPG62 4 4 5 6 22 16 8 11 2 2
ERLIN2 / SPG18 4 4 5 6 12 9 9 8 3 4
EXOSC3 8 7 8 9 6 5 10 7 5 5
FA2H / SPG35 0 0 1 0 0 0 0 1 0 0
FARS2 / SPG77 4 3 4 7 5 4 6 3 5 4
FBXO7 13 10 14 19 11 10 8 7 5 5
FIG4 5 6 8 7 4 4 5 10 9 11
FUS 75 70 62 42 66 82 88 80 52 51
FXN 2 3 4 5 3 3 6 5 1 1
GAD1 0 0 0 0 0 0 0 0 6 9
GALC 5 4 1 2 5 5 2 3 6 9
GAN 1 1 1 1 1 2 2 3 4 4
GBA 9 9 7 9 23 19 4 2 4 3
GBA2 / SPG46 13 15 14 13 12 18 21 21 21 19
GFAP 0 0 0 0 0 0 0 0 0 0
GJC2 / SPG44 0 0 0 0 1 1 0 0 1 1
GLB1 7 8 9 13 23 21 12 13 4 4
HEPACAM 0 0 0 0 0 0 0 0 0 0
HEXA 3 3 3 4 5 5 1 1 1 1
IBA57 / SPG74 2 2 1 1 1 1 2 2 2 2
IFIH1 33 11 53 105 1 0 0 0 0 0
IGHMBP2 4 4 4 4 3 5 4 3 4 5
IRF2BPL 6 10 11 17 25 20 34 19 38 32
KCNA2 0 0 0 0 0 0 0 0 2 4
KIAA0196 / SPG8 11 11 10 11 23 16 12 11 7 8
KIF1A / SPG30 0 0 0 2 0 0 49 29 79 69
KIF1C / SPG58 7 7 20 22 23 37 28 20 3 3
KIF5A / SPG10 0 1 0 0 0 1 5 7 97 83
KLC2 / SPG68 4 4 8 11 7 13 8 8 19 15
KLC4 4 5 3 5 4 5 4 4 8 7
L1CAM / SPG1 0 0 0 0 0 0 0 0 0 0
LYST 16 8 3 2 3 3 0 0 6 5
MAG / SPG75 0 0 0 0 0 0 0 0 0 0
MAN2B1 15 24 32 31 20 19 6 9 2 2
MARS / SPG70 25 23 48 78 51 29 56 41 18 17
MARS2 6 8 9 6 2 3 9 7 3 3
MATR3 27 24 29 25 24 25 48 51 85 93
MFN2 17 19 25 29 35 37 31 20 35 35
MLC1 1 0 2 0 0 0 0 0 0 0
MTPAP 3 3 4 3 4 4 4 4 3 3
NAIP 1 1 0 0 0 0 0 0 0 0
NARS2 4 5 7 7 4 3 13 14 7 6
NEFH 5 1 3 3 1 1 1 2 2 2
NIPA1 / SPG6 4 4 9 6 3 4 3 4 14 18
NT5C2 / SPG45 7 6 7 8 7 8 7 7 12 11
OPA1 10 9 13 9 12 12 16 15 19 16
OPTN 25 25 22 42 37 25 3 5 26 25
PANK2 8 8 7 9 8 7 6 6 7 6
PGAP1 / SPG67 7 2 1 1 2 3 4 5 40 41
PLA2G6 10 13 8 5 1 1 1 3 3 2
PLEKHG5 1 2 0 0 2 2 5 7 5 8
PLP1 / SPG2 0 0 0 0 0 0 0 0 0 0
PNPLA6 / SPG39 12 14 12 14 9 12 10 10 5 4
POLR3A 5 5 6 6 6 10 10 8 14 13
POLR3B 2 2 2 3 5 6 5 3 5 5
PRPH 0 0 0 0 2 1 1 1 0 0
RAB3GAP2 / SPG69 7 7 15 9 9 10 9 9 9 9
REEP1 / SPG31 0 0 0 0 0 0 0 0 65 72
REEP2 / SPG72 0 0 0 0 1 2 6 10 32 29
RETREG1 / FAM134B 6 7 1 0 0 1 1 0 4 5
RNASEH2B 14 13 13 17 8 5 7 6 5 5
RNASET2 7 8 18 12 1 1 1 2 2 1
RTN2 / SPG12 0 0 1 2 3 3 4 4 21 17
SACS 6 7 6 3 10 20 9 4 8 8
SERAC1 1 1 0 0 5 3 2 3 4 3
SETX 35 25 22 20 17 22 11 7 9 9
SIGMAR1 12 15 11 14 46 35 28 26 21 18
SIL1 3 3 11 16 16 16 3 3 2 2
SLC16A2 / SPG22 0 0 0 0 0 0 0 0 0 0
SLC25A15 6 7 4 4 7 8 13 14 8 5
SLC33A1 / SPG42 5 4 5 5 9 14 3 3 3 3
SMN1 4 2 5 3 4 3 5 4 4 3
SMN2 2 1 2 2 2 2 2 2 1 2
SOD1 44 42 45 58 62 46 78 67 45 46
SOX10 0 0 0 0 0 9 1 1 0 0
SPAST / SPG4 6 5 5 5 6 5 8 8 41 48
SPG11 / SPG11 17 14 11 11 7 6 4 5 5 6
SPG20 / SPG20 10 8 2 3 13 13 13 10 4 4
SPG7 / SPG7 10 13 8 6 9 12 9 9 8 7
SPR 1 1 3 5 11 6 5 4 0 0
SQSTM1 23 27 25 41 17 15 12 6 6 6
SYNE1 6 7 2 2 7 12 0 0 3 3
TARDBP 47 44 51 38 42 50 79 63 46 46
TBK1 5 4 1 2 7 6 5 4 12 16
TECPR2 / SPG49 2 3 3 4 7 7 3 2 8 8
TFG / SPG57 11 8 22 23 34 42 17 14 15 16
TGM6 0 0 0 0 0 0 0 0 0 0
TRIP4 9 7 9 11 10 8 7 5 11 7
TRPM7 17 15 16 13 17 11 8 6 5 4
TRPV4 0 0 0 0 3 1 1 1 0 0
TTBK2 5 4 2 2 2 2 2 3 7 6
TUBA4A 15 25 25 16 2 2 10 7 0 0
UBA1 0 0 0 0 0 0 0 0 0 0
UBAP / SPG80 24 23 34 27 39 39 43 33 32 26
UBQLN2 0 0 0 0 0 0 0 0 0 0
UBTF 35 44 26 26 23 22 25 17 33 35
USP8 / SPG59 10 10 11 9 12 11 9 9 5 6
VAMP1 20 26 21 10 4 4 2 4 1 1
VAPB 4 9 4 6 3 7 4 13 7 13
VPS37A / SPG53 4 3 5 5 9 10 5 4 7 7
WDR45 0 0 0 0 0 0 0 0 0 0
WDR48 / SPG60 12 10 7 10 8 5 9 10 17 18
ZFR / SPG71 20 18 19 19 35 35 25 26 40 40
ZFYVE26 / SPG15 6 5 6 6 3 3 4 3 3 3
ZFYVE27 / SPG33 14 16 15 14 7 12 6 5 25 22
100
50
0
PBMC-1 PBMC-2 LB-1 LB-2 F-1 F-2 iPSC-1 iPSC-2 CN-1 CN-2
B
GARS 20 17 82 177 163 109 82 43 23 25
HNRNPA1 175 170 303 333 167 142 435 640 162 162
HSPD1 / SPG13 41 35 147 157 83 95 304 284 49 58
KIDINS220 10 10 7 6 17 18 7 6 176 137
PFN1 153 172 450 572 313 323 408 232 33 25
SLC2A1 11 12 18 12 11 45 121 46 10 10
UCHL1 / SPG79 0 1 3 3 44 117 281 164 350 307
VCP 38 37 72 64 112 183 126 85 50 47
600
400
200
0
PBMC-1 PBMC-2 LB-1 LB-2 F-1 F-2 iPSC-1 iPSC-2 CN-1 CN-2

Fig. 2. Expression profiling of MND-related transcripts in RPKMs (reads per kilobase million) in five cell types derived from healthy donors (1 and 2). Alphabetic order of MND-related genes with **(A)** RPKMs ranging from 0 – 105 and with **(B)** RPKMs with at least one value > 105. HSP transcripts are encoded as: gene name / SPG type. Other MND-related transcripts are encoded as: gene name. RPKMs below 0.5 were set as 0. PBMC – peripheral blood mononuclear cells, LB – lymphoblasts, F – fibroblasts, iPSC – induced pluripotent stem cells, CN – iPSC-derived cortical neurons.

Figure 3

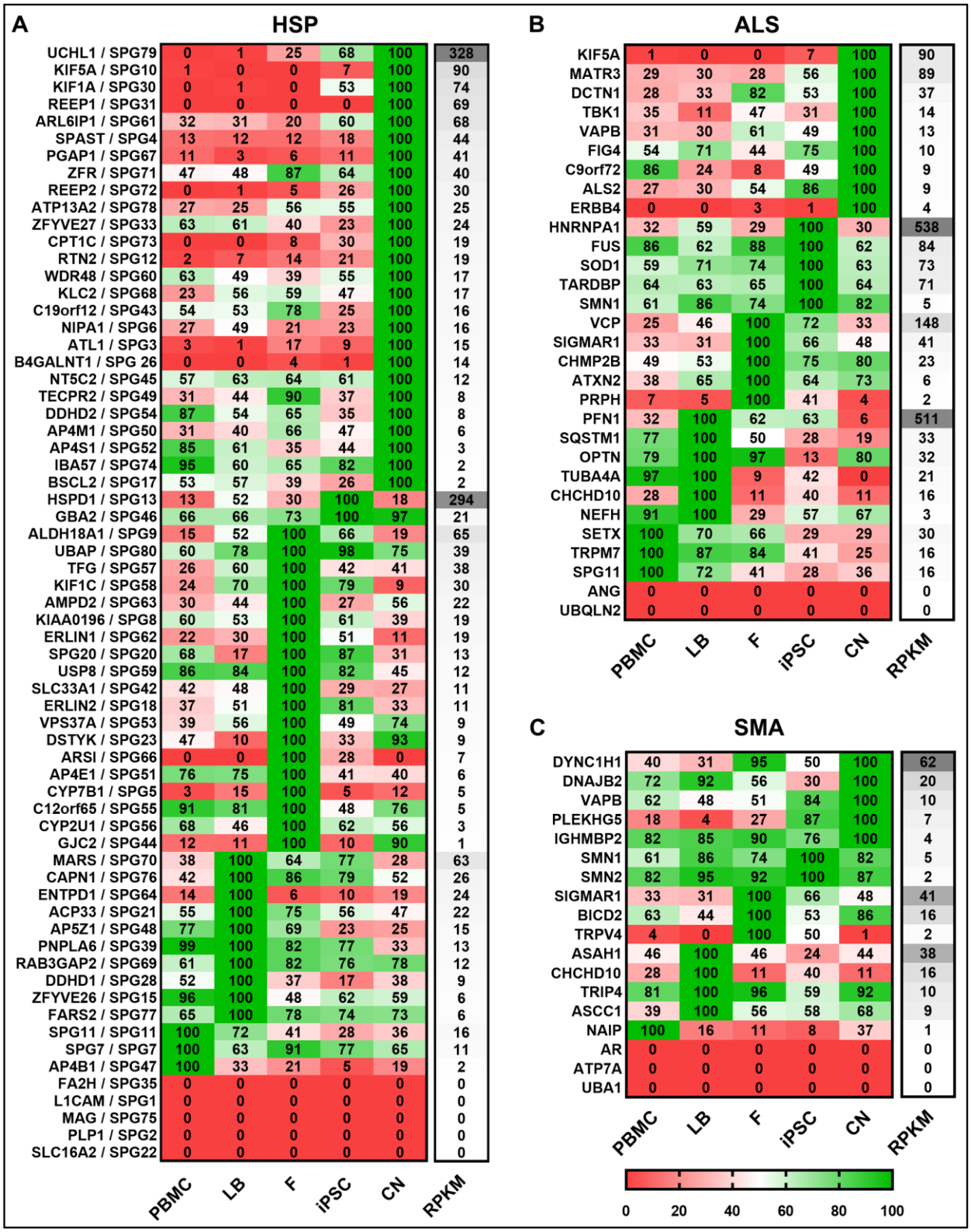
A
HSP
UCHL1 / SPG79 0 1 25 68 100 328
KIF5A / SPG10 1 0 0 7 100 90
KIF1A / SPG30 0 1 0 53 100 74
REEP1 / SPG31 0 0 0 0 100 69
ARL6IP1 / SPG61 32 31 20 60 100 68
SPAST / SPG4 13 12 12 18 100 44
PGAP1 / SPG67 11 3 6 11 100 41
ZFR / SPG71 47 48 87 64 100 40
REEP2 / SPG72 0 1 5 26 100 30
ATP13A2 / SPG78 27 25 56 55 100 25
ZFYVE27 / SPG33 63 61 40 23 100 24
CPT1C / SPG73 0 0 8 30 100 19
RTN2 / SPG12 2 7 14 21 100 19
WDR48 / SPG60 63 49 39 55 100 17
KLC2 / SPG68 23 56 59 47 100 17
C19orf12 / SPG43 54 53 78 25 100 16
NIPA1 / SPG6 27 49 21 23 100 16
ATL1 / SPG3 3 1 17 9 100 15
B4GALNT1 / SPG 26 0 0 4 1 100 14
NT5C2 / SPG45 57 63 64 61 100 12
TECPR2 / SPG49 31 44 90 37 100 8
DDHD2 / SPG54 87 54 65 35 100 8
AP4M1 / SPG50 31 40 66 47 100 6
AP4S1 / SPG52 85 61 35 44 100 3
IBA57 / SPG74 95 60 65 82 100 2
BSCL2 / SPG17 53 57 39 26 100 2
HSPD1 / SPG13 13 52 30 100 18 294
GBA2 / SPG46 66 66 73 100 97 21
ALDH18A1 / SPG9 15 52 100 66 19 65
UBAP / SPG80 60 78 100 98 75 39
TFG / SPG57 26 60 100 42 41 38
KIF1C / SPG58 24 70 100 79 9 30
AMPD2 / SPG63 30 44 100 27 56 22
KIAA0196 / SPG8 60 53 100 61 39 19
ERLIN1 / SPG62 22 30 100 51 11 19
SPG20 / SPG20 68 17 100 87 31 13
USP8 / SPG59 86 84 100 82 45 12
SLC33A1 / SPG42 42 48 100 29 27 11
ERLIN2 / SPG18 37 51 100 81 33 11
VPS37A / SPG53 39 56 100 49 74 9
DSTYK / SPG23 47 10 100 33 93 9
ARSI / SPG66 0 0 100 28 0 7
AP4E1 / SPG51 76 75 100 41 40 6
CYP7B1 / SPG5 3 15 100 5 12 5
C12orf65 / SPG55 91 81 100 48 76 5
CYP2U1 / SPG56 68 46 100 62 56 3
GJC2 / SPG44 12 11 100 10 90 1
MARS / SPG70 38 100 64 77 28 63
CAPN1 / SPG76 42 100 86 79 52 26
ENTPD1 / SPG64 14 100 6 10 19 24
ACP33 / SPG21 55 100 75 56 47 22
AP5Z1 / SPG48 77 100 69 23 25 15
PNPLA6 / SPG39 99 100 82 77 33 13
RAB3GAP2 / SPG69 61 100 82 76 78 12
DDHD1 / SPG28 52 100 37 17 38 9
ZFYVE26 / SPG15 96 100 48 62 59 6
FARS2 / SPG77 65 100 78 74 73 6
SPG11 / SPG11 100 72 41 28 36 16
SPG7 / SPG7 100 63 91 77 65 11
AP4B1 / SPG47 100 33 21 5 19 2
FA2H / SPG35 0 0 0 0 0 0
L1CAM / SPG1 0 0 0 0 0 0
MAG / SPG75 0 0 0 0 0 0
PLP1 / SPG2 0 0 0 0 0 0
SLC16A2 / SPG22 0 0 0 0 0 0
PBMC LB F iPSC CN RPKM
B
ALS
KIF5A 1 0 0 7 100 90
MATR3 29 30 28 56 100 89
DCTN1 28 33 82 53 100 37
TBK1 35 11 47 31 100 14
VAPB 31 30 61 49 100 13
FIG4 54 71 44 75 100 10
C9orf72 86 24 8 49 100 9
ALS2 27 30 54 86 100 9
ERBB4 0 0 3 1 100 4
HNRNPA1 32 59 29 100 30 538
FUS 86 62 88 100 62 84
SOD1 59 71 74 100 63 73
TARDBP 64 63 65 100 64 71
SMN1 61 86 74 100 82 5
VCP 25 46 100 72 33 148
SIGMAR1 33 31 100 66 48 41
CHMP2B 49 53 100 75 80 23
ATXN2 38 65 100 64 73 6
PRPH 7 5 100 41 4 2
PFN1 32 100 62 63 6 511
SQSTM1 77 100 50 28 19 33
OPTN 79 100 97 13 80 32
TUBA4A 97 100 9 42 0 21
CHCHD10 28 100 11 40 11 16
NEFH 91 100 29 57 67 3
SETX 100 70 66 29 29 30
TRPM7 100 87 84 41 25 16
SPG11 100 72 41 28 36 16
ANG 0 0 0 0 0 0
UBQLN2 0 0 0 0 0 0
PBMC LB F iPSC CN RPKM
C
SMA
DYNC1H1 40 31 95 50 100 62
DNAJB2 72 92 56 30 100 20
VAPB 62 48 51 84 100 10
PLEKHG5 18 4 27 87 100 7
IGHMBP2 82 85 90 76 100 4
SMN1 61 86 74 100 82 5
SMN2 82 95 92 100 87 2
SIGMAR1 33 31 100 66 48 41
BICD2 63 44 100 53 86 16
TRPV4 4 0 100 50 1 2
ASAH1 46 100 46 24 44 38
CHCHD10 28 100 11 40 11 16
TRIP4 81 100 96 59 92 10
ASCC1 39 100 56 58 68 9
NAIP 100 16 11 8 37 1
AR 0 0 0 0 0 0
ATP7A 0 0 0 0 0 0
UBA1 0 0 0 0 0 0
PBMC LB F iPSC CN RPKM
0 20 40 60 80 100

Fig. 3. Expression of **(A)** HSP-, **(B)** ALS- and **(C)** SMA-related transcripts classified according to the cell type showing the highest expression. Mean value of two donors were calculated for each gene, cell type and disease and the highest value of each gene was set to 100%. For each cell type relative values (in %) are given for the respective gene. Grouping per cell type is shown from high to low RPKMs. HSP transcripts are encoded as: gene name / SPG type. Other MND-related transcripts are encoded as: gene name. PBMC – peripheral blood mononuclear cells, LB – lymphoblasts, F – fibroblasts, iPSC – induced pluripotent stem cells, CN – iPSC-derived cortical neurons, RPKMs – reads per kilobase million.

Figure 4

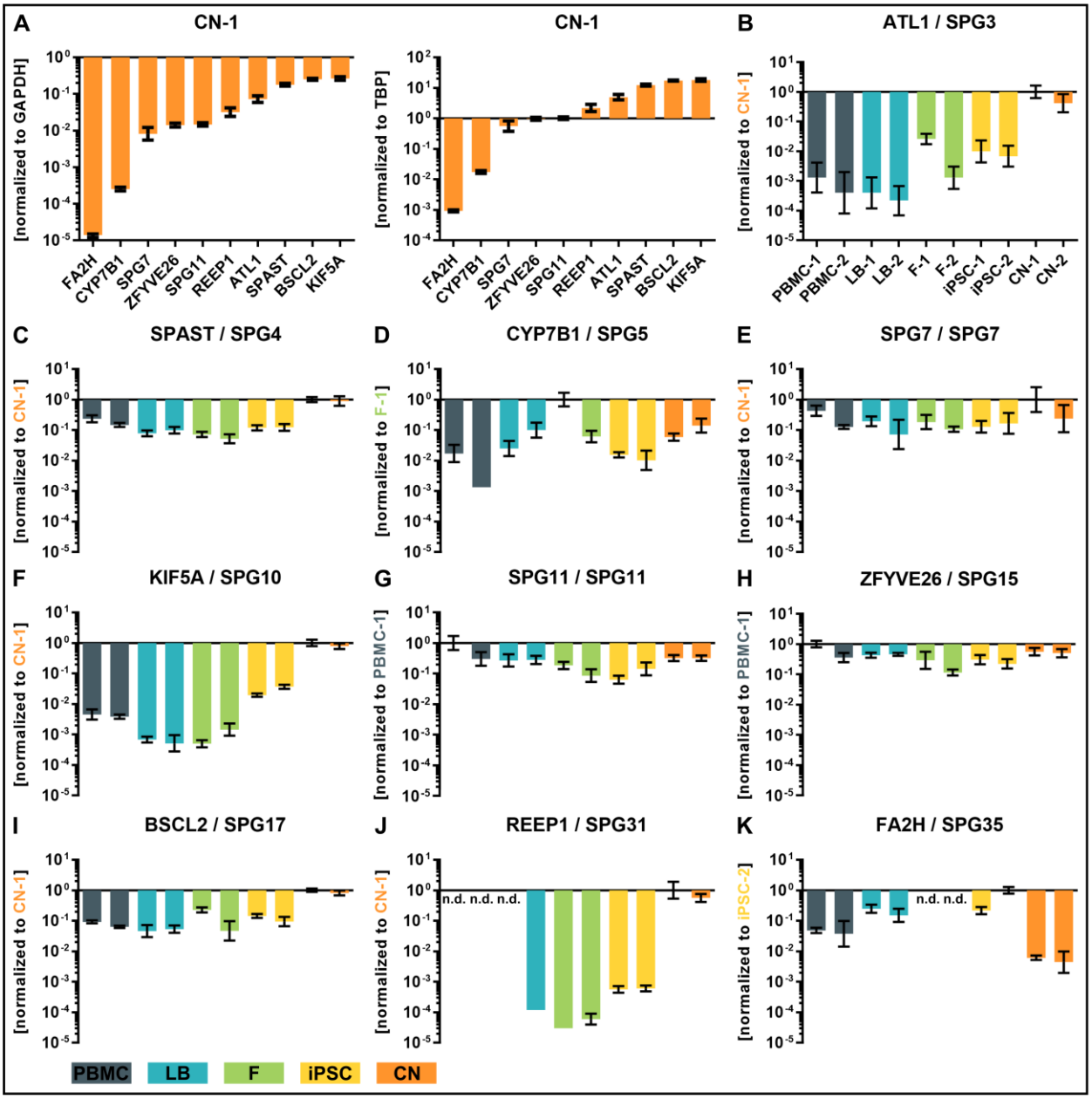

Fig. 4. qRT-PCR validation of transcripts of the 10 most common subtypes of HSP **(A).** ΔCT-values of iPSC-derived cortical neurons of donor 1 (CN-1) normalized to the housekeeping genes GAPDH and TBP **(B – K)** Relative values (ΔΔCT) of all analyzed cell types and transcripts normalized to the housekeeping genes GAPDH and TBP and to the cell line with highest transcript expression value (set to 1) n.d. – not detectable, PBMC – peripheral blood mononuclear cells, LB – lymphoblasts, F – fibroblasts, iPSC – induced pluripotent stem cells, CN – iPSC-derived cortical neurons.

Figure 5

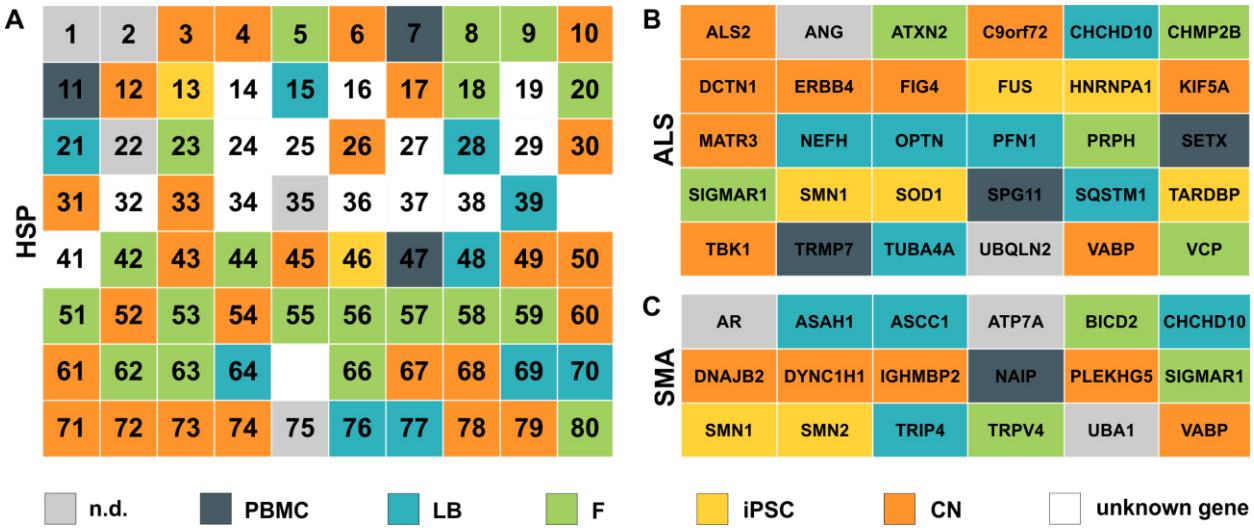

Fig. 5. Simplified overview of HSP, ALS and SMA analyzed disease genes. **(A)** HSP genes are listed according to their SPG number (1-80). **(B)** ALS and **(C)** SMA genes are ordered alphabetically. Color defines the cell type with the highest expression for each gene. n.d. – not detectable, PBMC – peripheral blood mononuclear cells, LB – lymphoblasts, F – fibroblasts, iPSC – induced pluripotent stem cells, CN – iPSC-derived cortical neurons, unknown gene – only loci identified.

Acknowledgements

I would like to express my sincere gratitude to Ludger Schöls for the possibility of performing my PhD thesis in his laboratory. Thank you for creating such a pleasant working atmosphere and for the freedom of doing my own research and creating my own ideas.
I want to thank my advisory board members Tassula Proikas-Cezanne and Peter Heutink for their help and suggestions on my project, and Peter for taking the role as a second examiner. I also want to thank Stefan Liebau for participating in my examination board.

My special thanks go to Stefan. Thank you for your help, your expertise, your motivating comments, your emotional support and your friendship. I really enjoyed working closely together with you and hope that I will find a similar colleague in my next jobs.

I am deeply grateful to all my colleagues that supported, helped, encouraged, suffered and laughed with me during this PhD - and who became friends. Thanks for all the fun in- and outside of the lab (at Besen, Wasen, Schokomarkt, Christmas parties or during Karaoke sessions). I want to thank Philip, Ulrike, Maike, Yvonne, Selina, Jenny, Melli, Elena, David, Ina and Milena, and thanks to many other colleagues at the Hertie Institute and the DZNE for their help and comments.

Thanks to my friends, to the ones in Tübingen especially for all the fun that we had here. I really enjoyed living in Tübingen for so many years (although it is really time for me to leave soon ;)), and this was mainly because of you. I also want to thank my friends who are further away, for all the supporting messages and calls, and for the great weekends and times that I spent with you.

I would like to thank my family for their support, their distractions, their love and for my adorable nieces and nephew ☺. You are such an important part of my life and I really couldn't have managed to get to this point without you!

Finally, I especially want to thank Jo for his unlimited support, for listening to endless stories of frustration but also for sharing my enthusiasm on interesting work and experiments. Thank you for distracting me and handling my moods during times when going to work was less pleasant for me. I am so looking forward to our next steps in life and I am so happy to share this with you!!!